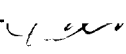


## AN ABSTRACT OF THE THESIS OF

Christopher W. Sinton for the degree of Master of Science in  
Oceanography presented on November 24, 1992

Title: The Evolution of the Galapagos Platform: Results  
from Radiometric Dating and Experimental Petrology

*Redacted for Privacy*

Abstract approved: 

David M. Christie

The Galápagos Islands are the subaerial portions of a broad platform that overlies young oceanic crust formed at the Galápagos Spreading Center (GSC). The platform, which is believed to be the most recent expression of the Galápagos hotspot, is the westernmost extension of the E-W trending Carnegie Ridge. The Galápagos Platform is distinct from other hotspot-generated platforms, such as Hawaii, by having a broader pattern of volcanism and a wide variety of lava compositions, including some more typical of mid-ocean ridge settings. K-Ar and  $^{40}\text{Ar}$ - $^{39}\text{Ar}$  radiometric dating of submarine samples from seamounts and fault scarps from the central platform and Carnegie Ridge show an increase in the age of volcanism to the east, extending the known age trend for the islands and supporting the hotspot generation model for these features. These age data indicate that the velocity of the Nazca plate over the hotspot has decreased over the past 11 Ma. Lavas from the Carnegie Ridge which are older than 5 Ma are systematically lower in  $\text{TiO}_2$  relative to lavas younger than 5 Ma. This is interpreted to indicate a decreasing influence of the GSC on Galápagos volcanism with time.

Radiometric ages from seamounts along the Wolf-Darwin volcanic lineament show no distinct age progression. This indicates that extensional faulting in the underlying lithosphere is controlling the localization of mantle melting. Similar lithospheric fractures may also control volcanism on the northern islands of Pinta, Marchena, and Genovesa. Lavas recovered from seamounts to the east and southeast of these islands are similar in composition to those of Genovesa, though some are more primitive. Plagioclase-phyric lavas are common to both the islands and the seamounts. Plagioclase phenocrysts are typically anorthitic and contain abundant, devitrified inclusions of magmatic glass. In order to determine the bulk composition of plagioclase-hosted melt inclusions in lavas from one of the seamounts on the northeastern edge of the platform (PL13), phenocrysts were heated to the liquidus temperature of the trapped melt. The inclusion compositions determined by this method are among the most primitive MORB compositions yet discovered and are close to being a primary basaltic magma. Minor element variations within the melt inclusions indicate that the host anorthite was exposed to discrete magma batches with different minor element compositions during crystallization.

The Evolution of the Galápagos Platform: Results from Radiometric  
Dating and Experimental Petrology

by

Christopher W. Sinton

A THESIS

submitted to

Oregon State University

in partial fulfillment of  
the requirements for the  
degree of

Master of Science

Completed November 24, 1992

Commencement June, 1993

*Redacted for Privacy*

APPROVED:

---

Professor of Oceanography in charge of major

*Redacted for Privacy*

---

Dean of College of Oceanography

*Redacted for Privacy*

---

Dean of Graduate School

Date thesis is presented November 24, 1992

Typed by Christopher W. Sinton

## ACKNOWLEDGEMENTS

I could not have completed this thesis without the unquestionable support from both my advisors, Dave Christie and Bob Duncan. Thanks also to Anita Grunder, who contributed thoughtful revisions to the text.

Doug, Lance, Randy, and Bill were excellent friends to have around for beer and coffee. Lew Hogan and Sue Pullen were always ready to help me when logistical problems reared their ugly heads.

My wife, Diana, was always there to scratch my back. Thanks also to the consistent, unconditional support from my family.

Many thanks to the coffee bean pickers world-wide, whose mountain-grown product, when roasted to perfection, provided a daily source of inspiration.

This research was supported by a grant from the National Science Foundation.

## TABLE OF CONTENTS

<b>CHAPTER I: Introduction .....</b>	<b>1</b>
<b>CHAPTER II: Geochronology of Submarine Basalts from the Galápagos Platform .....</b>	<b>5</b>
Abstract .....	6
Introduction .....	7
Previous Work.....	10
Sample Descriptions .....	11
Analytical Methods .....	12
Results .....	16
The Central Platform.....	16
Northeast Seamounts.....	21
Wolf-Darwin Lineament .....	21
Discussion .....	23
Central Platform and Carnegie Ridge .....	25
Wolf-Darwin Lineament .....	27
Northeastern Seamounts .....	29
Conclusions .....	31
References .....	33
<b>CHAPTER III: Near-Primary Melt Inclusions in Anorthite Phenocrysts from the Galápagos Platform .....</b>	<b>35</b>
Abstract .....	36
Preface.....	38
Introduction .....	39
Anorthite-ultraphyric basalts from the Galápagos Platform .....	39
Melt Inclusions in Galápagos Island Lavas .....	42
Results .....	42
Interpretation .....	44
Discussion .....	47
High CaO-Al <sub>2</sub> O <sub>3</sub> Magmas from Mid-Ocean Ridges .....	49
Possible mantle source .....	51
High CaO-Al <sub>2</sub> O <sub>3</sub> Magmas as a MORB End Member .....	51
Minor Element Variation in Melt Inclusions .....	52
Conclusions .....	53
References .....	54

<b>CHAPTER IV: Conclusion .....</b>	<b>57</b>
Bibliography.....	60
Appendices .....	65

## LIST OF FIGURES

<u>Figure</u>	<u>Page</u>
Fig. I.1 Local map of the Galápagos Platform and Galápagos Spreading Center.....	2
Fig. II.1 The Galápagos Platform.....	8
Fig. II.2 Calculated ages plotted on regional map .....	22
Fig. II.3 Graph showing the disparity between calculated K-Ar and $^{40}\text{Ar}$ - $^{39}\text{Ar}$ IH ages from the same samples.....	24
Fig. II.4 Plot of age vs. distance from the western edge of the platform for central platform and Carnegie Ridge samples from PLUME2 .....	26
Fig. II.5 Plot of MgO vs. $\text{TiO}_2$ for whole rock compositions of PLUME2 samples .....	28
Fig. III.1 Generalized map of the Galápagos region .....	40
Fig. III.2 Backscatter electron images of PL13 anorthite-hosted melt inclusions .....	43
Fig. III.3 $\text{Al}_2\text{O}_3$ vs. MgO of remelted inclusions from PL13-12 at 1240°C, 1250°C, 1260°C, 1270°C, and 1280°C .....	45
Fig. III.4 MgO vs. $\text{TiO}_2$ , $\text{Na}_2\text{O}$ , and $\text{P}_2\text{O}_5$ content of high $\text{TiO}_2$ and low $\text{TiO}_2$ 1270°C melt inclusions.....	48
Fig. III.5 Comparison of 1270° melt inclusions and PL13 pillow- rim glasses to primitive MORB glass compositions.....	50



## LIST OF TABLES

Table II.1	Sample location and analytical methods .....	14
Table II.2	K/Ar data for Galápagos Platform basalts.....	17
Table II.3	$^{40}\text{Ar}$ - $^{39}\text{Ar}$ total fusion ages for Galápagos Platform basalts.....	17
Table II.4	Isotopic data for $^{40}\text{Ar}$ - $^{39}\text{Ar}$ analyses.....	18
Table II.5	Plateau and isochron age calculations for Galápagos Platform basalts .....	20
Table III.1	Analyses of representative pillow-rim glasses.....	41
Table III.2	Average compositions for inclusions and calculated primary melt .....	47

# THE EVOLUTION OF THE GALÁPAGOS PLATFORM: RESULTS FROM RADIOMETRIC DATING AND EXPERIMENTAL PETROLOGY

## I. Introduction

The Galápagos hotspot is an example of a mantle plume that has in the past coincided with a spreading ridge, but now several hundred kilometers distance separates the two melting regimes (Fig. I.1). The evidence for a hotspot under the Galápagos archipelago is very strong. Excessive volcanism in an intraplate setting is often indicative of a hotspot. In addition, some of the lavas on the Galápagos islands have an unmistakable OIB composition. The Carnegie and Cocos ridges, two aseismic ridges on the Nazca and Cocos plates, respectively, radiate away from the Galápagos region in the direction of the respective plate motions and are age progressive away from the islands (White et al., 1992; Christie et al., 1992; Castillo et al., in prep). These observations indicate that there is a long-lived hotspot beneath the Galápagos archipelago. The older traces of volcanism have apparently been subducted under Central and South America, though the Coiba and Malpelo ridges may be older remnants of either the Cocos or Carnegie ridges that have been separated by transform faulting (Hey, 1977). The thickened oceanic crust that composes the core of the Caribbean seafloor could be an oceanic plateau that is the result of the initiation of the Galápagos hotspot (Duncan and Hargraves, 1984). This hypothesis is supported by plate reconstruction models (Duncan and Hargraves, 1984), the approximate uniformity of composition and age of circum-Caribbean ophiolites (Donnelly et al., 1990; Sinton and Duncan, 1992). The Galápagos platform is the most recent product of the hotspot and lies just south of the Galápagos Spreading Center (GSC) on the Nazca plate (Fig. I.1). The Carnegie and Cocos ridges indicate that the GSC has resided over the Galápagos hotspot, until 5 Ma, when the GSC migrated north to its present position (Hey, 1977).

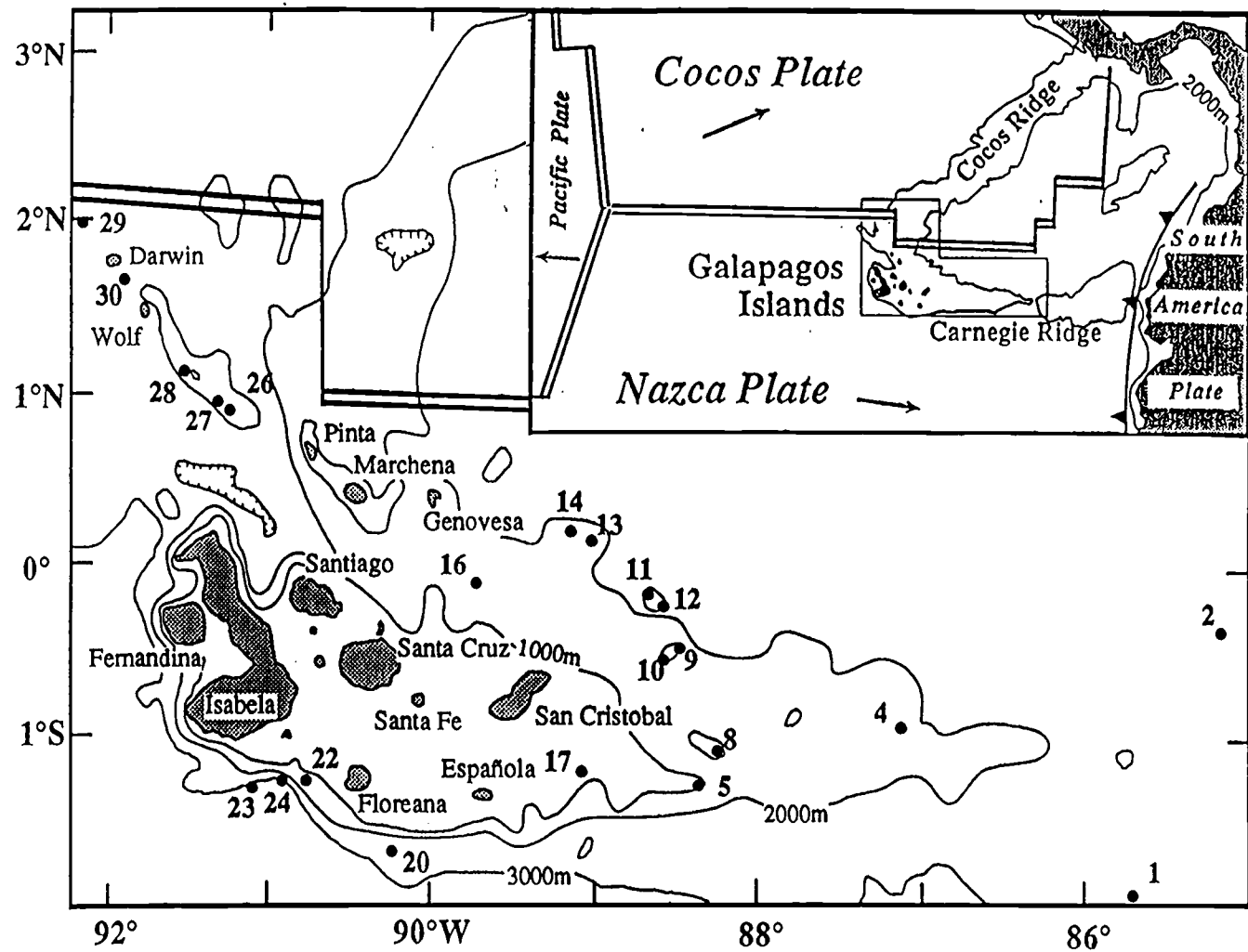


Figure I.1. Local map of the Galápagos Platform and Galápagos Spreading Center. The larger islands are named and the numbers represent dredge sites for the PLUME2 cruise that used in the thesis. Inset is a regional map of the Panama Basin.

The interaction between the Galápagos hotspot and the GSC did not end with the northward migration of the GSC and this is reflected in the geology of the Galápagos Islands. Many of the basalts from the northern and central islands are virtually indistinguishable from those erupted at mid-ocean ridges (Baitis and Swanson, 1976; White and Hoffman, 1978), in addition to lavas that are more typical of ocean islands. There is a consistent geographic arrangement to the isotopic and trace element compositions of the island lavas, describing a horseshoe pattern open to the northeast in which the more depleted lavas occur in the northeast and central parts of the archipelago while more enriched lavas are found on the south, west, and northwest periphery of the platform (White et al., 1992). Thus, the Galápagos archipelago provides an important example of a hotspot setting that is midway between a ridge-centered hotspot, such as Iceland, and an intraplate hotspot, like Hawaii. Study of the petrology, geochemistry, and temporal development of the Galápagos platform can provide insight into the dynamics of mixing of the mid-ocean ridge and hotspot mantle sources.

Current models based on existing data from the Galápagos islands invoke entrainment of upper asthenosphere material by the mantle plume (Geist et al., 1988; White et al., 1992) or remelting of the young lithosphere under the Galápagos platform by the plume (Feighner and Richards, 1992) to explain the compositional pattern. The interaction between the mantle plume and the GSC operates both ways, i.e., elevations in  $^{87}\text{Sr}/^{86}\text{Sr}$  and trace element concentrations at GSC segments near the platform indicate a hotspot influence (Schilling et al., 1982; Verma and Schilling, 1982). The process that moves plume material to this section of the GSC is not yet well understood.

Leg 2 of the PLUME expedition (R/V Thomas Washington) performed Seabeam mapping and dredged some of the submarine features of the Galápagos platform and western Carnegie Ridge in an effort to enhance our understanding of the Galápagos

hotspot. This thesis is part of a multidimensional study that resulted from this cruise. Chapter II (first manuscript) describes the temporal evolution of the platform based on K-Ar and  $^{40}\text{Ar}$ - $^{39}\text{Ar}$  dating of the submarine samples. The geochronology of the islands describes a pattern that is generally time progressive away from the hotspot in the direction of the Nazca plate, but with several complexities. Volcanism to the north of the main platform could not have formed at a hotspot location on the western edge of the platform. The new data are used in conjunction with the previous island data to provide a more complete picture of the timing of Galápagos volcanism.

Chapter III (second manuscript) reports the results of experimental work on lavas from a seamount on the northeastern edge of the platform (PL13). Glass analyses of the lavas from this and other northeastern seamounts show that they are relatively primitive liquids that have major element compositions similar to MORB liquids, i.e., they have low alkali and  $\text{TiO}_2$  abundances. Some of the lavas contain high modal percentages (30-40%) of high An plagioclase ( $\text{An}_{88-92}$ ) that bear inclusions of olivine, spinel, and devitrified glass. Heating of plagioclase phenocrysts from PL13 lavas to the liquidus temperature of the melt inclusions effectively rehomogenizes the inclusions, revealing a near-primary, high  $\text{CaO}$ - $\text{Al}_2\text{O}_3$  liquid. Glass compositions of this type are more common to mid-ocean ridges and near-axis seamounts than to ocean island basalts. In terms of Galápagos platform formation, this indicates that volcanism on the northeast seamounts is controlled predominantly by mid-ocean ridge processes rather than mantle plume processes. On a broader scale, the the inclusions represent near primary MORB liquids that provide a valuable window into the genesis of oceanic basalts.

## **II. Geochronology of Submarine Basalts from the Galápagos Platform**

## Abstract

The Galápagos Islands are the subaerial portions of a broad, volcanic platform that has been constructed on young oceanic lithosphere formed at the Galápagos Spreading Center (GSC). The platform, which is believed to be the most recent expression of the Galápagos hotspot, is the westernmost extension of the E-W trending Carnegie Ridge. K-Ar and  $^{40}\text{Ar}$ - $^{39}\text{Ar}$  radiometric ages of submarine samples from the central platform and Carnegie Ridge are generally older to the east, extending the trend seen in the island ages and supporting the hotspot model for the generation of these features. These age data indicate that the velocity of the Nazca plate over the hotspot has decreased over the past 11 Ma, from 75 mm/yr to 37 mm/yr. Lavas from the Carnegie Ridge which are older than 5 Ma are systematically lower in  $\text{TiO}_2$  content relative to lavas younger than 5 Ma. This is interpreted to indicate a decreasing influence of the GSC on the composition of Galápagos volcanism with time, compatible with migration of the spreading system away from the hotspot.

Radiometric ages from seamounts along the Wolf-Darwin lineament are closely grouped and show no distinct age progression. This indicates that extensional faulting in the underlying lithosphere is controlling volcanism along the lineament. Lithospheric faulting may also control the locality and timing of volcanism on the northern islands of Pinta, Marchena, and Genovesa. Lavas recovered from seamounts to the east and southeast of these islands are similar in composition to those of Genovesa. Back tracking one of the seamounts, Fitzroy, places its original eruptive position near Genovesa. This element of fixity of the melting region, coupled with the lack of a hotspot compositional signal in the lavas of Genovesa and the seamounts, suggests that heat from the plume may be contributing to melting in this area, but plume material is not.

## Introduction

The Galápagos Islands are the subaerial exposures of a large, shallow volcanic platform that lies just south of the Galápagos Spreading Center (GSC) in the eastern Pacific Ocean (Fig. II.1). The platform is thought to be the latest expression of a Galápagos hotspot (Morgan, 1971, 1972), though the islands display a broader, more diffuse pattern of prolonged volcanism than other Pacific island chains which cannot readily be explained by the simple hotspot model.

Ocean island basalts (OIB) usually have distinctively higher  $^{87}\text{Sr}/^{86}\text{Sr}$ , lower  $^{143}\text{Nd}/^{144}\text{Nd}$ , and light rare earth element (LREE) enrichment relative to mid-ocean ridge basalt (MORB). In this respect, the Galápagos Islands also deviate from the classic hotspot, displaying both OIB and MORB characteristics (Geist et al., 1988; White et al., 1992). White and Hoffman (1978) first noted a regional compositional horseshoe pattern open to the northeast such that  $^{87}\text{Sr}/^{86}\text{Sr} < 0.7030$  from the center to the northeastern platform and  $^{87}\text{Sr}/^{86}\text{Sr} > 0.7030$  progressively away from the central platform. Geist et al. (1988) suggested that this pattern was due to a thermally buoyant Galápagos mantle plume that had entrained depleted upper mantle material. White et al. (1992) have further refined this model, describing a laterally heterogeneous mantle plume undergoing shear by the motion of the overlying Nazca plate. Laboratory experiments indicate that a rising conduit of material that is sheared laterally will entrain some of the surrounding material (Richards and Griffiths, 1989).

Another model that is based on gravity observations (Feighner and Richards, 1992) suggests that the broad pattern of volcanism can be attributed to thinning of the young oceanic lithosphere over which the platform is constructed. They suggested that the thinning is caused by the mantle plume remelting the young, relatively warm (and



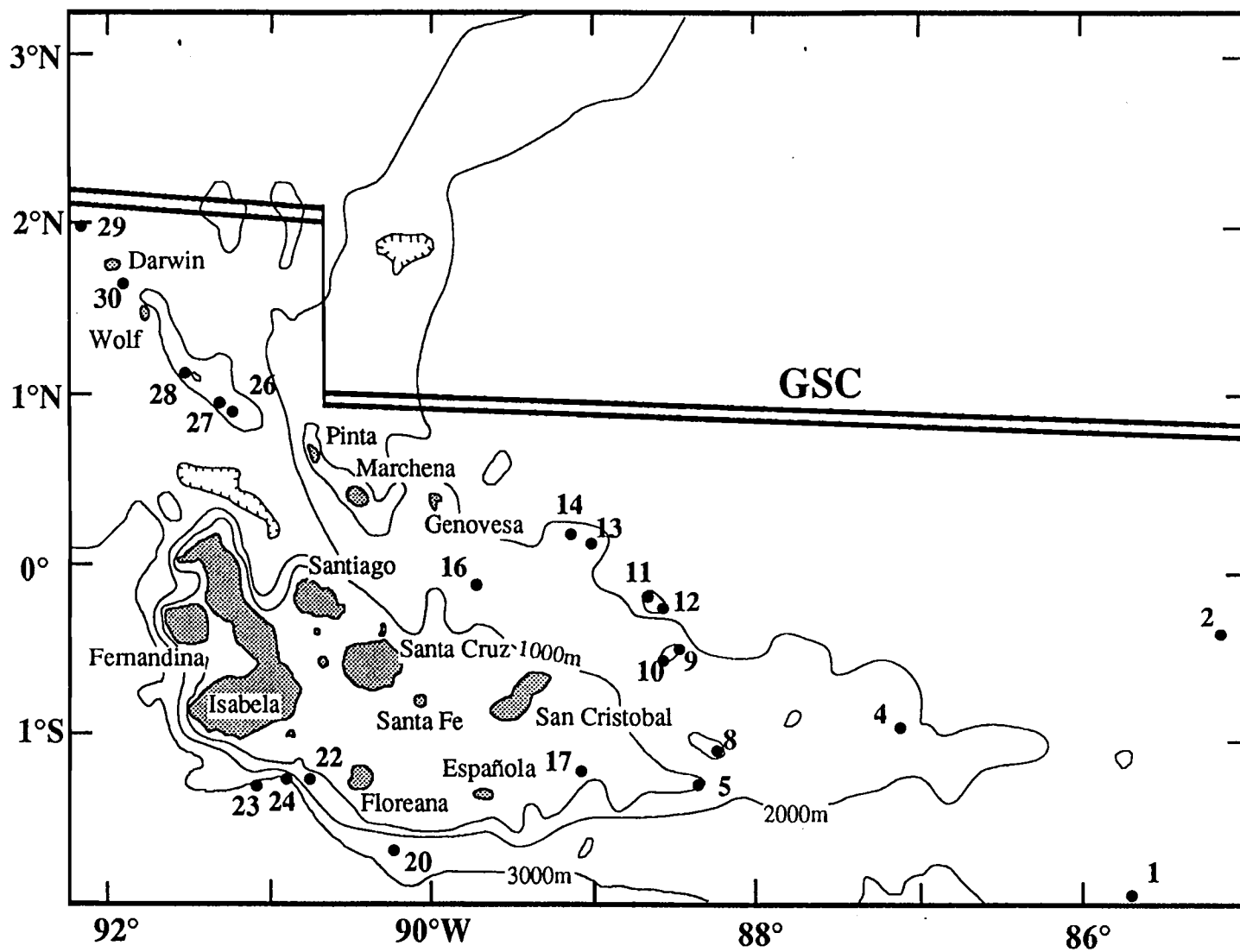


Figure II.1. The Galapagos platform. PLUME2 dredge sites are numbered

thin) lithosphere that underlies the platform. However, White et al. (1992) suggest that the plume would not provide sufficient heat for this process to occur and that the observed compositional patterns do not indicate significant assimilation of lithosphere by the plume.

Interaction between the hotspot and the GSC is evident on ridge segments between 89°W and 95.5°W and is manifested by elevated radiogenic isotopic ratios and incompatible elements (Verma and Schilling, 1982; Schilling et al., 1982). Morgan (1978) suggested that this anomaly is caused by the sub-lithospheric transfer of plume material beneath the Wolf-Darwin lineament, a NW-trending line of seamounts and islands (Wolf and Darwin) that runs from the northern platform to the GSC (Fig. II.1). However, isotopic data from the volcanoes along the lineament do not show a gradual decrease in a hotspot component toward the ridge crest (Harpp et al., 1990), as would be expected in the case of simple mixing between the magmas derived from the ridge and the plume were the case. Harpp et al. (1990) suggest much deeper flow and mixing between the ridge and the plume.

Recent dredging during leg 2 of the PLUME expedition of the R/V Thomas Washington (1990) sampled submarine features of the Galápagos Platform and western Carnegie Ridge. This has greatly expanded the sample coverage of the area, particularly in the northeastern and eastern sections of the platform. Thus, we have an opportunity to further examine the temporal and compositional variations of Galápagos volcanism. Some of the geochemical results from these samples are reported elsewhere (Harpp et al. 1990; Christie et al., 1992; Sinton et al., 1992). Here we report results from K-Ar and  $^{40}\text{Ar}$ - $^{39}\text{Ar}$  dating of these samples. The results are then used to better evaluate the temporal and compositional evolution of the Galápagos platform.

### Previous Work

The majority of the Galápagos Islands lie on the main portion of the platform, which is bounded by a steep escarpment to the south and west (Fig. II.1). Active volcanism is concentrated on, though not restricted to, the western platform on the islands of Isabela and Fernandina. The current position of the hotspot appears to be beneath Fernandina, the largest and most active volcano on the platform. The epicenters of recent earthquakes in the Galápagos cluster around Isabela and Fernandina, indicating the area of brittle deformation and extension associated with the hotspot.

The platform can be divided into two distinct regions, the central platform and the northern volcanoes. The central platform is surrounded by a 1000m isobath and encompasses all of the larger islands. The composition of the lavas from the central platform islands are highly variable in petrology and composition, ranging from MORB-like basalts to rhyolites (McBirney and Williams, 1969). K-Ar ages and paleomagnetic data from the central platform islands indicate a general age progression toward the east, consistent with the formation of the volcanoes over a fixed mantle plume near Fernandina (Cox and Dalrymple, 1966; White et al., 1992). Volcanism, it appears, can persist over considerable time on a single island. For instance, alkalic and tholeiitic lavas from San Cristobal have erupted continuously between 2.3 to 0.7 Ma without any obvious temporal pattern (Geist et al., 1986; White et al., 1992). This is unlike volcanism on the Hawaiian islands, which exhibit later stages of eruption of alkalic material, but the volume of lava is small compared to the initial shield building eruptions of tholeiitic basalt.

The northern islands of Pinta, Marchena, and Genovesa do not display the range of lava compositions that are seen on the central platform islands and are generally smaller. Pinta and Marchena are located on a NW-trending submarine scarp (McBirney and Williams, 1969) and are coincident with the intersection of NNW and ENE striking

fractures (Vicenzi et al., 1990). Pinta is an elongated shield made of enriched tholeiitic lavas erupted during two stages of volcanism, a shield building stage (~0.7 Ma) and a younger fissure stage (Cullen and McBirney, 1987). Marchena Island is a shield volcano with two recognizable series of lavas, both of which are composed of moderately evolved alkalic and tholeiitic basalts that are compositionally similar to lavas erupted from the GSC segment nearest Marchena (Vicenzi et al., 1990). The lavas from Genovesa that have been examined are remarkably MORB-like (Cullen et al., 1989; White et al., 1992). Lavas with as much as 40 % plagioclase phenocrysts and megacrysts (plagioclase-ultraphyric) are common to these three islands, but are uncommon on the central platform islands (Cullen et al., 1989). The compositional distinction between Pinta lavas and the more MORB-like lavas from Marchena and Genovesa coincides with a north-south transform fault that separates Pinta from Marchena and Genovesa (Fig. II.1). Pinta last erupted in 1928 and Marchena and Genovesa have both erupted in the past few years (White et al., 1992).

Darwin and Wolf Islands lie ~150 km north of Isabela along the NW-trending Wolf-Darwin lineament and have K-Ar ages of 0.4 Ma and 0.9-1.6 Ma, respectively (White et al., 1992). Plagioclase-ultraphyric lavas are also found on these islands (White et al., 1992). Given the east-southeast motion of the Nazca plate, the northwestern islands of Wolf and Darwin and the northeastern islands of Pinta, Marchena, and Genovesa could not have formed at a hotspot now located beneath Fernandina.

### Sample Descriptions

Figure II.1 shows the locations of all the dredge samples used in this study. Material recovered from the Carnegie Ridge (PL1 to PL8 and PL17) is composed of moderately to highly altered basalts notably lacking pillow rim glass. They are predominantly aphyric with some plagioclase-phyric lavas (PL4). Basalts from the

southern escarpment near Isabela (PL22, PL23, and PL24) are very fresh, plagioclase-olivine phyric alkali basalts with glassy rims. PL20 lies to the east of these dredges and provided variably altered, rounded, basalt pebbles. Five dredges from the Wolf-Darwin lineament (PL26 to PL30) recovered very fresh, aphyric and plagioclase-ultraphyric basalts with glassy pillow rims. Rocks recovered from seamounts on the northeastern edge of the platform (PL9 to PL16) range from slightly to moderately altered with glassy and non-glassy pillow rims. Some of the recovered rocks are rounded cobbles, indicating that some of the seamounts were at one time subaerial (Christie et al., 1992). Most samples from the northeastern seamounts are aphyric, though those that have more primitive glass compositions are either plagioclase-ultraphyric or olivine and spinel-phyric. The majority of these samples are rather primitive and have  $\text{MgO} > 8\%$  in glass and relatively low  $\text{K}_2\text{O}$  abundances.

#### Analytical Methods

Where possible, dated samples (1) came from the freshest and best crystallized material, generally taken as far from the pillow rim as possible, (2) were free of extensive alteration and weathered surfaces (i.e., cracks and fractures), and (3) had enough  $\text{K}_2\text{O}$  to generate measurable radiogenic Ar. For a suite of rocks from the same dredge, the most differentiated samples (highest  $\text{K}_2\text{O}$  contents) were used. Rocks from PL13 were extremely deficient in  $\text{K}_2\text{O}$  (0-0.06 wt. %) and radiometric dating was not attempted on these. Sample locations and analytical dating methods used are reported in Table II.1.

Two radiometric dating methods were employed in this study, conventional K-Ar and  $^{40}\text{Ar}$ - $^{39}\text{Ar}$  (total fusion [TF] and incremental heating [IH]). Both are based on the decay of  $^{40}\text{K}$  to  $^{40}\text{Ar}$ , which is assumed to occur at a constant rate over time (decay constant,  $\lambda_{\epsilon} + \lambda_{\beta} = 5.543 \times 10^{-10} \text{ yr}^{-1}$ ). It is also assumed in these methods that all radiogenic  $^{40}\text{Ar}$  has been retained in the sample and that the lava equilibrated with an

atmospheric Ar composition ( $^{40}\text{Ar}/^{36}\text{Ar} = 295.5$ ) at the time of crystallization.

Submarine basalts can be problematic in dating because rapid quenching of sea-floor basalt may prohibit the magma from equilibrating completely with atmospheric argon and leave  $^{40}\text{Ar}$  inherited from the mantle source in the sample. This, however, should not be a problem in these rocks because all of the samples were recovered from relatively shallow depths and all samples appear to be well crystallized. Another problem associated with submarine basalts is low temperature alteration in seawater that may cause K addition or Ar loss, resulting in measured ages significantly less than crystallization ages. In this respect,  $^{40}\text{Ar}$ - $^{39}\text{Ar}$  incremental heating experiments are considered to be more successful in dating altered submarine rocks (e.g., Seidemann, 1978; Duncan and Hargraves, 1990). The lower temperature heating steps of the incremental heating method produces diffusion of Ar from grain boundaries and other low-retention sites in the rock (clays, zeolites). Higher temperature steps release Ar from the more unaltered crystal interiors, thus giving Ar isotopic compositions that more likely reflect the crystallization age of the sample.

With these criteria in mind, the fresh lavas from the Wolf-Darwin lineament and the southern escarpment were analyzed by K-Ar. All other samples were analyzed by both K-Ar and  $^{40}\text{Ar}$ - $^{39}\text{Ar}$  methods or by  $^{40}\text{Ar}$ - $^{39}\text{Ar}$  only. Some of the low  $\text{K}_2\text{O}$  samples from the northeastern seamounts were analyzed by  $^{40}\text{Ar}$ - $^{39}\text{Ar}$  total fusion heating because the expected radiogenic Ar content was too low to divide the gas into many increments. PL10-5 was analyzed by K-Ar and both incremental and total fusion  $^{40}\text{Ar}$ - $^{39}\text{Ar}$  methods.

All samples were crushed in a ceramic jaw crusher and sieved to a uniform 0.5-1 mm grain size. The samples were then ultrasonically cleaned to remove any salts. For K-Ar analyses, samples were split into two aliquots, one was powdered and analyzed for

Table II.1: Sample Location and Analytic Method

Sample	Location	Analysis
PL1-12	02° 01.47'S - 85° 40.34'W	K-Ar, $^{40}\text{Ar}$ - $^{39}\text{Ar}$ (IH)
PL1-46	02° 01.47'S - 85° 40.34'W	K-Ar, $^{40}\text{Ar}$ - $^{39}\text{Ar}$ (IH)
PL2-02	00° 22.40'S - 85° 09.70'W	K-Ar, $^{40}\text{Ar}$ - $^{39}\text{Ar}$ (IH)
PL4-19	00° 55.92'S - 87° 07.46'W	$^{40}\text{Ar}$ - $^{39}\text{Ar}$ (IH)
PL5-01	01° 17.40'S - 88° 21.20'W	$^{40}\text{Ar}$ - $^{39}\text{Ar}$ (IH)
PL8-01	01° 17.40'S - 88° 21.20'W	$^{40}\text{Ar}$ - $^{39}\text{Ar}$ (IH)
PL9-50	00° 28.13'S - 88° 32.11'W	$^{40}\text{Ar}$ - $^{39}\text{Ar}$ (IH)
PL10-05	00° 34.04'S - 88° 35.44'W	K-Ar, $^{40}\text{Ar}$ - $^{39}\text{Ar}$ (IH,TF)
PL11-7	00° 11.70'S - 88° 40.10'W	$^{40}\text{Ar}$ - $^{39}\text{Ar}$ (TF)
PL11-12	00° 11.70'S - 88° 40.10'W	$^{40}\text{Ar}$ - $^{39}\text{Ar}$ (IH)
PL12-1	00° 14.45'S - 88° 38.20'W	K-Ar, $^{40}\text{Ar}$ - $^{39}\text{Ar}$ (TF)
PL14-1	00° 06.00'N - 89° 05.80'W	K-Ar
PL16-03	00° 06.44'S - 89° 49.26'W	K-Ar, $^{40}\text{Ar}$ - $^{39}\text{Ar}$ (IH)
PL17-01	01° 11.38'S - 89° 06.58'W	$^{40}\text{Ar}$ - $^{39}\text{Ar}$ (IH)
PL17-04	01° 11.38'S - 89° 06.58'W	$^{40}\text{Ar}$ - $^{39}\text{Ar}$ (IH)
PL20-02	01° 37.73'S - 90° 10.70'W	$^{40}\text{Ar}$ - $^{39}\text{Ar}$ (IH)
PL22-01	01° 18.23'S - 90° 44.92'W	K-Ar
PL23-01	01° 20.03'S - 90° 59.84'W	K-Ar
PL24-01	01° 18.60'S - 90° 55.60'W	K-Ar
PL26-25	00° 50.50'N - 91° 17.30'W	K-Ar
PL27-17	00° 53.80'N - 91° 19.80'W	K-Ar
PL28-10	01° 00.19'N - 91° 33.34'W	K-Ar
PL29-02	01° 00.19'N - 91° 33.34'W	K-Ar
PL29-48	01° 00.19'N - 91° 33.34'W	K-Ar
PL30-01	01° 33.63'N - 91° 55.66'W	K-Ar

K<sub>2</sub>O by atomic absorption methods by Christine McBirney at the University of Oregon . About 5g of material was fused for the argon isotopic dilution measurement by mass spectrometric methods (Dalrymple and Lanphere, 1969). For each <sup>40</sup>Ar-<sup>39</sup>Ar analysis, 0.5-1.0 g of material was sealed in an evacuated quartz glass vial and irradiated for 6-8 hours at the OSU TRIGA nuclear reactor facility. Argon extraction for both methods was done in a conventional glass extraction system after the system was baked out at 180°C for at least 12 hours. Heating of the samples was done by radio frequency induction using outgassed Mo sample crucibles. K-Ar and total fusion (TF) samples were completely fused in one step. <sup>40</sup>Ar-<sup>39</sup>Ar incremental heating (IH) samples were heated in progressively higher temperature steps, then fused. Ideally, each IH sample should have as many heating steps as possible without jeopardizing the precision of each step. Because of the low K<sub>2</sub>O and relatively young age of the samples, only four or five heating steps were done and were spaced to release approximately equal amounts of <sup>39</sup>Ar. For both methods, argon compositions were then measured using an AEI MS-10S mass spectrometer. Neutron flux during irradiation was monitored by Mmhb-1 hornblende (520.4 Ma, Samson and Alexander, 1987) and FCT-3 biotite (27.7 Ma, Kunk et al., 1985).

K-Ar analyses were calculated using the methods described in Dalrymple and Lanphere (1969) after correction for mass fractionation (Table II.2). Individual ages for each step of the TF and for each IH experiment were calculated after corrections for background, mass fractionation, and isotopic interferences were made (Table II.3 and II.4). In reducing each sample analyzed by <sup>40</sup>Ar-<sup>39</sup>Ar IH, age spectrum diagrams of age vs. % <sup>39</sup>Ar were generated (Appendix 1). Plateau ages are calculated from consecutive steps that are concordant within 1σ error using the procedure described in Dalrymple et al. (1988), in which step ages are weighted by the inverse of the variance (Table II.5).



The age of each step was calculated under the assumption that the original argon content was atmospheric. However, it is possible that the samples did not completely equilibrate with an atmospheric composition. One powerful aspect of the  $^{40}\text{Ar}$ - $^{39}\text{Ar}$  method is that an isochron can be calculated, in which a linear correlation of the step isotopic compositions ( $^{36}\text{Ar}/^{40}\text{Ar}$  vs.  $^{39}\text{Ar}/^{40}\text{Ar}$ ) can provide an age (calculated from the slope) and an initial isotopic composition (from the  $^{36}\text{Ar}/^{40}\text{Ar}$  intercept; see Appendix 1).

## Results

### *The Central Platform/Carnegie Ridge*

Dredges PL1 to PL8 and PL17 to PL24 are from the central platform (Fig II.1). Dated samples from these dredge sites show a general increase in age towards the east (Fig. II.2). Samples PL1-12 and PL1-46 have plateau ages of 8.7 and 9.1 Ma, respectively. Correlation diagrams give isochron ages that are statistically indistinguishable from the plateau ages and  $^{40}\text{Ar}/^{36}\text{Ar}$  intercepts that are near atmospheric (Table II.5). PL2-2 has a plateau age of 11.1 Ma. A correlation diagram gives an isochron age of 9.1 Ma and a slightly elevated  $^{40}\text{Ar}/^{36}\text{Ar}$  intercept (302.4). K-Ar ages from these two samples (5.1 and 5.8 Ma) are significantly lower than the IH ages. Judging from the altered condition of the samples (clay mineral, vesicle filling), it is likely that the K-Ar ages reflect the effects of low-temperature alteration. Samples from the other dredges along the western Carnegie Ridge and central platform (PL4, PL5, PL8, and PL17) were analyzed by  $^{40}\text{Ar}$ - $^{39}\text{Ar}$  IH only. Isochron ages are similar to the plateau ages for PL8 and PL17 samples, but are slightly older for PL4 and PL5 samples. All  $^{40}\text{Ar}/^{36}\text{Ar}$  intercepts are near atmospheric, with the exception of PL5-1, which is slightly lower (Table II.5).

Table II.2: K/Ar Data for Galápagos Platform Basalts

Sample	%K	%Radiogenic $^{40}\text{Ar}$	Age $\pm 1\sigma$ (Ma)
PL1-12	0.216	8.58	$5.78 \pm 0.43$
PL1-46	0.457	3.71	$5.07 \pm 0.22$
PL2-2	0.191	16.83	$0.89 \pm 0.07$
PL10-5	0.174	4.67	$1.10 \pm 0.11$
PL12-1	0.150	2.20	$0.63 \pm 0.11$
PL14-1	0.030	0.73	$8.95 \pm 1.65$
PL16-3	0.300	6.00	$2.90 \pm 0.19$
PL22-1	0.450	6.32	$1.69 \pm 0.06$
PL23-1	0.510	1.50	$0.18 \pm 0.04$
PL24-1	0.500	1.62	$0.14 \pm 0.02$
PL26-25	0.200	0.19	$0.03 \pm 0.13$
PL27-17	0.200	0.24	$0.13 \pm 0.16$
PL28-10	0.200	0.83	$0.34 \pm 0.17$
PL29-2	0.200	0.16	$0.03 \pm 0.05$
PL29-48	0.232	2.25	$1.60 \pm 0.07$
PL30-1	0.410	0.82	$0.25 \pm 0.05$

Ages calculated using the following decay and abundance constants:  $\lambda_{\epsilon} = 0.581 \times 10^{-10} \text{ yr}^{-1}$ ;  $\lambda_{\beta} = 4.962 \times 10^{-10} \text{ yr}^{-1}$ ;  $^{40}\text{K}/\text{K} = 1.167 \times 10^{-4} \text{ mol/mol}$ .

Table II.3:  $^{40}\text{Ar}$ - $^{39}\text{Ar}$  Total Fusion Ages for Galápagos Platform Basalts

Sample	$^{40}\text{Ar}/^{36}\text{Ar}$	$^{40}\text{Ar}/^{39}\text{Ar}$	$^{*37}\text{Ar}/^{40}\text{Ar}$	% Radiogenic $^{40}\text{Ar}$	% K	Age $\pm 1\sigma$ (Ma)
PL10-5	309.5	20.3	2.777	4.53	0.17	$3.3 \pm 1.2$
PL11-7	380.2	53.7	.765	22.27	0.10	$41.7 \pm 0.9$
PL12-1	319.8	32.0	1.178	7.61	0.15	$8.6 \pm 1.9$

\* corrected for  $^{37}\text{Ar}$  decay since irradiation

Table II.4: Isotopic Data for  $^{40}\text{Ar}$ - $^{39}\text{Ar}$  Analyses

Increment	$^{40}\text{Ar}/^{36}\text{Ar}$	$^{40}\text{Ar}/^{39}\text{Ar}$	$^{*37}\text{Ar}/^{40}\text{Ar}$	%Radiogenic $^{40}\text{Ar}$	% $^{39}\text{Ar}$ of Total	Age $\pm 1\sigma$ (Ma)
<u>PL1-2</u>						
1	303.7	43.6	.113	6.58	50.9	$8.5 \pm 0.5$
2	313.9	12.5	1.874	23.30	30.8	$8.7 \pm 0.8$
3	291.2	91.6	.273	3.85	10.6	$10.6 \pm 2.4$
4	276.4	232.1	.640	1.49	7.7	$11.4 \pm 3.5$
<u>PL1-46</u>						
1	293.0	132.3	.0094	2.36	50.2	$9.2 \pm 0.7$
2	297.5	55.6	.222	5.48	33.5	$9.1 \pm 0.5$
3	290.0	100.5	.231	3.10	8.0	$9.3 \pm 2.1$
4	280.8	135.7	.529		8.3	$9.4 \pm 2.1$
<u>PL2-2</u>						
1	302.0	268.1	.005	5.44	19.5	$16.0 \pm 3.7$
2	323.8	73.0	.113	12.61	37.8	$10.1 \pm 2.6$
3	314.8	88.8	.311	11.60	28.9	$11.5 \pm 1.8$
4	284.8	156.3	.834	6.10	13.8	$11.4 \pm 4.0$
<u>PL4-19</u>						
1	288.6	206.0	.034	1.03	39.2	$7.2 \pm 2.5$
2	278.0	71.3	.893	3.34	28.7	$8.5 \pm 1.6$
3	249.1	37.7	2.606	4.63	19.6	$6.4 \pm 3.6$
4	241.8	135.5	2.584	0.99	7.8	$6.0 \pm 6.7$
<u>PL5-1</u>						
1	299.9	51.6	.155	5.66	33.4	$10.1 \pm 4.9$
2	255.0	7.1	6.472	35.29	37.2	$8.8 \pm 2.6$
3	265.9	35.4	1.281	3.86	13.1	$5.0 \pm 4.8$
4	283.6	84.0	.463	2.52	6.4	$7.5 \pm 2.8$
5	242.7	76.5	2.869	2.63	9.9	$8.0 \pm 3.9$
<u>PL8-1</u>						
1	300.3	41.4	.118	4.76	21.0	$6.8 \pm 1.2$
2	298.8	24.8	.602	8.66	37.8	$7.4 \pm 0.8$
3	290.2	30.9	.344	7.13	14.6	$7.6 \pm 1.4$
4	282.2	37.9	.923	5.64	26.6	$7.5 \pm 1.4$
<u>PL9-50</u>						
1	309.6	30.3	.043	7.62	33.0	$7.2 \pm 1.5$
2	288.1	27.2	.590	6.26	37.3	$5.3 \pm 0.7$
3	291.2	19.8	.903	9.74	10.9	$6.1 \pm 2.4$
4	289.3	77.0	.177	3.50	5.0	$8.5 \pm 5.5$
5	272.7	66.5	1.187	5.40	13.8	$11.4 \pm 4.1$

\* corrected for  $^{37}\text{Ar}$  decay since irradiation

Table II.4 (cont'd): Isotopic Data for  $^{40}\text{Ar}$ - $^{39}\text{Ar}$  Analyses

Increment	$^{40}\text{Ar}/^{36}\text{Ar}$	$^{40}\text{Ar}/^{39}\text{Ar}$	$^{*37}\text{Ar}/^{40}\text{Ar}$	%Radiogenic $^{40}\text{Ar}$	% $^{39}\text{Ar}$ of Total	Age $\pm 1\sigma$ (Ma)
<u>PL10-5</u>						
1	301.4	3196	.002	1.98	17.2	$68.8 \pm 10$
2	297.2	124.4	.284	4.52	47.7	$6.0 \pm 2.0$
3	290.1	281.9	.125	1.27	17.5	$3.9 \pm 5.4$
4	273.5	206.3	.858	2.08	17.6	$5.3 \pm 4.0$
<u>PL11-12</u>						
1	298.9	68.2	.051	1.60	9.2	$3.2 \pm 4.2$
2	283.6	97.1	.966	11.30	54.1	$3.4 \pm 0.5$
3	249.8	27.1	.321	2.00	18.5	$1.7 \pm 2.1$
4	278.8	81.7	.063	1.90	6.9	$4.7 \pm 3.0$
5	269.2	79.7	1.057	1.99	11.3	$5.2 \pm 2.5$
<u>PL16-3</u>						
1	<i>No <math>^{39}\text{Ar}</math> released</i>					
2	307.1	66.2	.083	7.91	36.1	$5.8 \pm 2.1$
3	329.9	43.1	.301	20.59	41.1	$9.4 \pm 1.1$
4	307.6	67.4	.712	12.88	22.8	$9.8 \pm 2.8$
<u>PL17-1</u>						
1	307.1	48.0	.030	6.98	4.8	$10.9 \pm 5.3$
2	327.5	11.4	.316	14.95	29.1	$5.5 \pm 0.8$
3	368.8	5.21	.973	29.81	40.5	$5.1 \pm 0.5$
4	317.6	13.8	.467	13.41	12.2	$6.1 \pm 1.4$
5	274.8	26.8	1.270	5.87	13.4	$5.2 \pm 1.5$
<u>PL17-4</u>						
1	308.1	38.1	.163	8.41	7.4	$10.5 \pm 7.5$
2	329.5	4.94	2.890	35.85	36.5	$5.8 \pm 0.9$
3	295.9	21.1	.521	7.15	30.1	$4.9 \pm 1.8$
4	290.5	42.3	.466	5.18	14.1	$7.2 \pm 4.6$
5	244.8	63.2	2.650	4.33	11.9	$10.1 \pm 6.5$
<u>PL20-2</u>						
1	<i>No <math>^{39}\text{Ar}</math> released</i>					
2	307.4	65.5	.019	7.91	5.7	$5.7 \pm 2.0$
3	330.0	17.1	.091	14.74	21.4	$2.8 \pm 0.5$
4	367.6	13.8	.220	19.97	22.3	$3.0 \pm 0.5$
5	300.3	38.4	.073	6.11	14.4	$2.6 \pm 1.4$
6	294.5	43.8	.196	5.21	36.2	$2.5 \pm 0.8$

\* corrected for  $^{37}\text{Ar}$  decay since irradiation

Table II.4: Plateau and Isochron Age Calculations for Galápagos Platform Basalts

Sample	<u>Plateau Calculation</u>			<u>Isochron Calculation</u>		
	Age (m.y) $\pm 1\sigma$	Steps Used	% of Total $^{39}\text{Ar}$	Age (m.y) $\pm 1\sigma$	Steps Used	Intercept $\pm 1\sigma$
PL1-12	$8.7 \pm 0.4$	1,2,3,4	100	$8.1 \pm 0.5$	1,2,3,4	$297.0 \pm 1.9$
PL1-46	$9.1 \pm 0.4$	1,2,3,4	100	$9.0 \pm 0.1$	1,2,3,4	$295.7 \pm 1.2$
PL2-2	$11.1 \pm 1.4$	2,3,4	80.5	$10.2 \pm 1.6$	2,3,4	$298.6 \pm 13.3$
PL4-19	$7.8 \pm 1.2$	1,2,3,4	100	$6.4 \pm 1.1$	2,3,4	$298.3 \pm 9.0$
PL5-1	$8.0 \pm 1.5$	1,2,3,4,5	100	$9.8 \pm 2.8$	1,2,4,5	$286.3 \pm 4.2$
PL8-1	$7.3 \pm 0.5$	1,2,3,4	100	$7.0 \pm 0.3$	1,2,3,4	$296.2 \pm 7.3$
PL9-50	$5.7 \pm 0.6$	1,2,3,4	86.2	$4.3 \pm 2.1$	2,3,4	$301.0 \pm 9.8$
PL10-5	$5.6 \pm 1.4$	2,3,4	82.8	$6.0 \pm 0.4$	2,3,4	$293.9 \pm 8.8$
PL11-2	$3.2 \pm 0.5$	1,2,3,4,5	100	$3.2 \pm 0.3$	1,2,3,4,5	$296.6 \pm 2.9$
PL16-3	$9.5 \pm 1.0$	3,4	63.9	$11.5 \pm 2.8$	2,3,4	$278.1 \pm 20.5$
PL17-1	$5.3 \pm 0.4$	2,3,4,5	95.2	$4.9 \pm 0.2$	1,2,3,4,5	$300.1 \pm 6.4$
PL17-4	$5.8 \pm 0.8$	1,2,3,4,5	100	$5.5 \pm 0.6$	1,2,3,4,5	$298.0 \pm 7.0$
PL20-2	$2.8 \pm 0.3$	3,4,5,6	94.3	$3.1 \pm 0.2$	2,3,4,5,6	$291.6 \pm 7.6$

### *Northeast Seamounts*

Many of the samples from the northeastern seamounts low have  $K_2O$ . Despite these unfavorable compositions, IH experiments were performed on samples from PL9, PL10, PL11, and PL16.  $^{40}Ar$ - $^{39}Ar$  (TF) and K-Ar analyses were performed on samples from PL10, PL12, and PL14.

Sunray Seamount (PL9 and PL10) is the southeasternmost of this group. For sample PL 10-5, the K-Ar age of 1.1 Ma and the TF age of 3.3 Ma are considerably younger than the IH plateau age of 5.6 Ma, indicating some Ar loss. This plateau age is indistinguishable from the 5.7 Ma plateau age for PL9-50. Isochron ages are consistent with the plateau ages and  $^{40}Ar/^{36}Ar$  intercepts are near-atmospheric (Table II.5). Fitzroy Seamount (PL11 and PL12) lies northwest of Sunray. Sample PL11-2 have both a plateau and isochron age of 3.2 Ma. The calculated TF age for PL11-2 is 41.7 Ma. PL12-1 was analyzed by TF and K-Ar, resulting in ages of 8.6 Ma and 0.6 Ma, respectively. PL13 and PL14 were taken from an unnamed seamount to the northwest of Fitzroy. The K-Ar age of PL14-1 is 9.0 Ma. PL16-3 was taken from a seamount ~120 km west of Fitzroy; K-Ar analysis yielded an age of 2.9 Ma, while IH analysis revealed a plateau age of 9.5 Ma and an isochron of 11.5 Ma. The IH age is suspect, however, because it was calculated from only two of three heating steps in which  $^{39}Ar$  was released (see Appendix I).

### *Wolf-Darwin Lineament*

Samples from five dredges along the Wolf-Darwin lineament were analyzed by K-Ar. Ages along the lineament range from 0 to 1.6 Ma, similar to the K-Ar ages determined for Wolf and Darwin Islands (White et al., 1992). There is no coherent age progression displayed along the lineament (Fig. II.2). In fact, the youngest ages are at the extreme ends of the lineament.

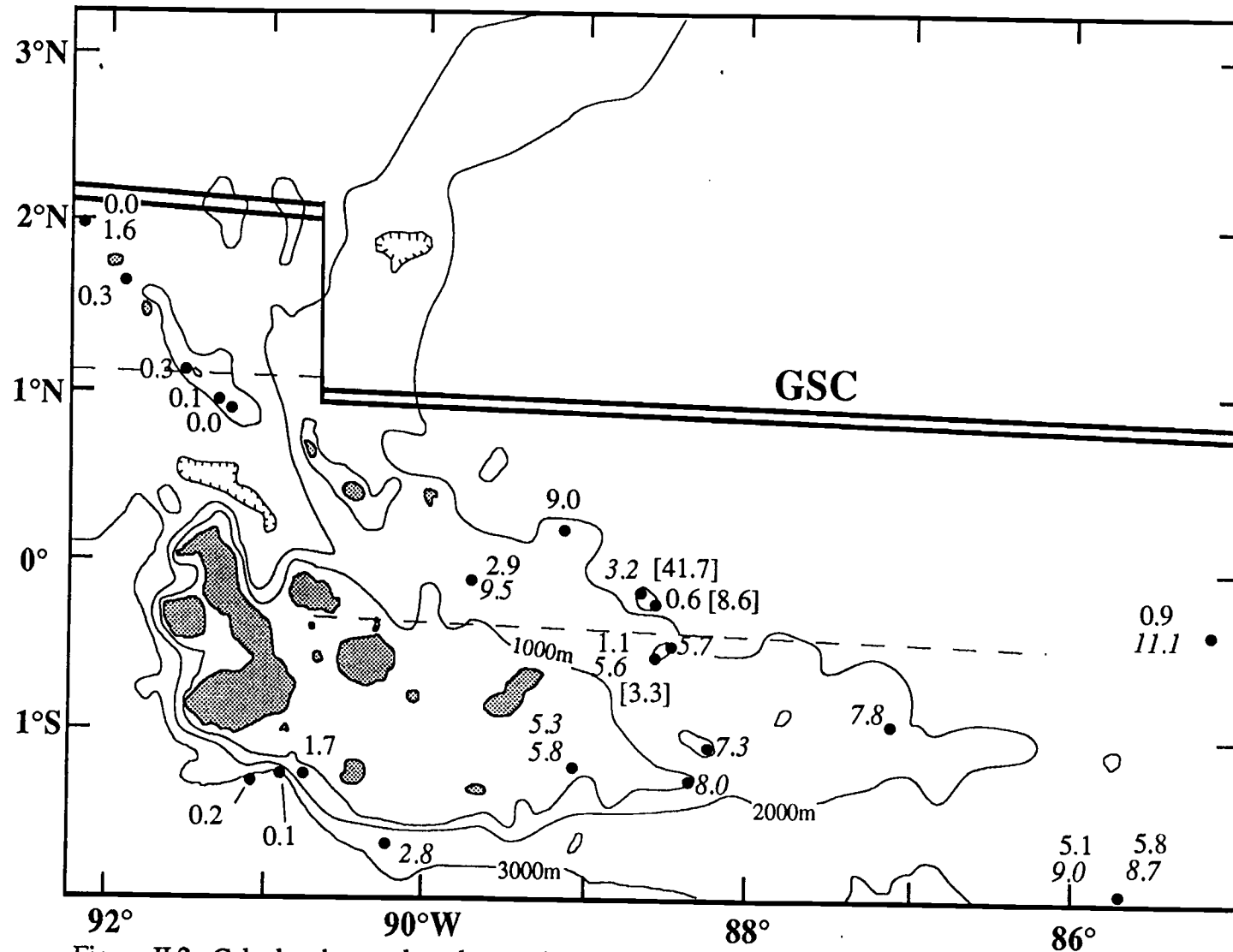


Figure II.2. Calculated ages plotted on regional map. Plain text ages are K-Ar, italics are  $^{40}\text{Ar}$ - $^{39}\text{Ar}$  incremental heating, and those enclosed in brackets are  $^{40}\text{Ar}$ - $^{39}\text{Ar}$  total fusion. The dashed line represents the 5 Ma magnetic isochron from Hey et al. (1977)

## Discussion

For those samples that were dated by more than one method, the best estimate of the crystallization age needs to be selected. One constraint that was used to evaluate the ages was comparison to the age of the underlying crust. Hey et al. (1977) used seafloor magnetic anomalies to reconstruct the age of the crust in the vicinity of the GSC. Because the resolution of the magnetic anomalies on the platform was very poor, much of the data is extrapolated from crust surrounding the platform. Assuming this analysis is more or less accurate, the crust to the east of the  $\sim 90.5^\circ$  fracture zone and to the north of Santa Cruz can be no more than 5 Ma (Fig. II.2). Thus, the calculated ages for PL14-1 (9.0; K-Ar), PL11-7 (41.7; TF), PL12-1 (8.6; TF), and PL16-3 (9.5; IH) can be rejected as it is impossible for seamounts of these ages to lie on crust that is  $< 5$  Ma. Their anomalously old ages indicate that these samples contained excess radiogenic argon. Because of the low  $K_2O$  of these rocks, and their apparently young age, the amount of K-supported radiogenic Ar is small, and even small amounts of non-outgassed, mantle-derived Ar have significant effects on the measured ages.

Where both K-Ar and IH were employed (northeast seamounts and Carnegie Ridge samples), the K-Ar ages were systematically younger than the IH ages (Fig. II.3). This is likely due to both loss of radiogenic argon and addition of potassium to the rock during seawater alteration. Thus, K-Ar and TF ages from PL1, PL2, and PL10 are rejected as they are too young compared to the IH ages. Because of the problem of alteration and the similarity in the plateau age to that of the other Sunray sample (PL9-50; 5.7 Ma), it is likely that the IH ages are the more accurate. Although the K-Ar age for PL16-3 (2.9 Ma) is not unreasonable, its IH spectrum is so disturbed that we reject it.



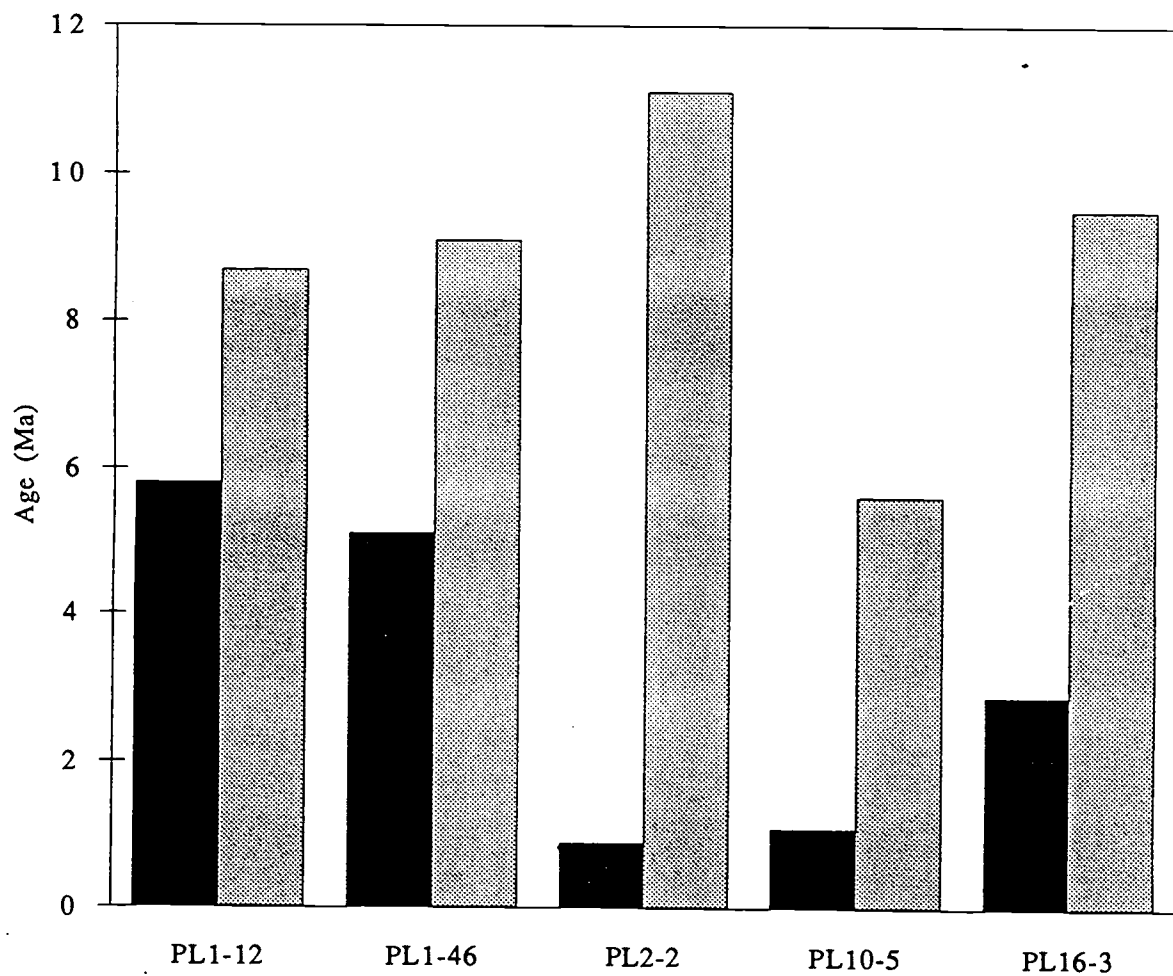


Figure II.3. Graph showing the disparity between calculated K-Ar and  $^{40}\text{Ar}$ - $^{39}\text{Ar}$  IH ages for the same sample.  $^{40}\text{Ar}$ - $^{39}\text{Ar}$  IH ages are systematically higher than the K-Ar ages, indicating that either Ar loss or K addition from low temperature alteration has occurred.

*Central Platform /Carnegie Ridge*

The submarine samples from the central platform and Carnegie Ridge are generally older towards the east (Fig. II.2), which is in accord with the model of the Nazca plate moving over a stationary hotspot and extends the trend seen in the island age data (White et al., 1992). The approximate velocity of the Nazca plate over the hotspot can be derived by plotting the age vs. the distance from the western edge of the platform for samples from the central platform (Fig. II.4). The slopes of an unweighted regression line fitted to the data points between ~5 and ~11 Ma gives a plate velocity of  $75 \pm 13$  mm/yr. An unweighted regression of the data points  $< 3$  Ma gives a plate velocity of  $37 \pm 5$  mm/yr. This is the same value given by Gripp and Gordon, 1990, who, using Pacific plate hotspot tracks, indicated that the Nazca plate has been moving at about 37 mm/yr over the past 3 Ma. Thus it would seem that the Nazca plate velocity over the hotspot has been progressively decreasing over the past 11 Ma. An unweighted regression of all the data gives a plate velocity value of  $59 \pm 5$  mm/yr (Fig. II.4). This analysis, however, assumes that the sampled lavas were erupted at the leading edge of the hotspot. If the present volcanic pattern is extrapolated to the past, then it is possible that the older lavas represent later stages of volcanism. Thus, the calculated plate velocities should be regarded as maximum values.

The calculated ages from the central platform and Carnegie Ridge samples can also be used to examine any compositional changes in volcanism over time. According to Hey (1977), at 10 Ma the hotspot was located on the Cocos plate, north of the GSC. Between that time and 5 Ma, the GSC straddled the hotspot. From 5 Ma, to the present the hotspot has accreted material to the Nazca plate only. Assuming this history is correct, then all of the dated samples from the western platform and the Carnegie Ridge that are older than 5 Ma must have been produced by a ridge-centered hotspot. Thus, we can expect an increased MORB compositional signature in these lavas relative to those

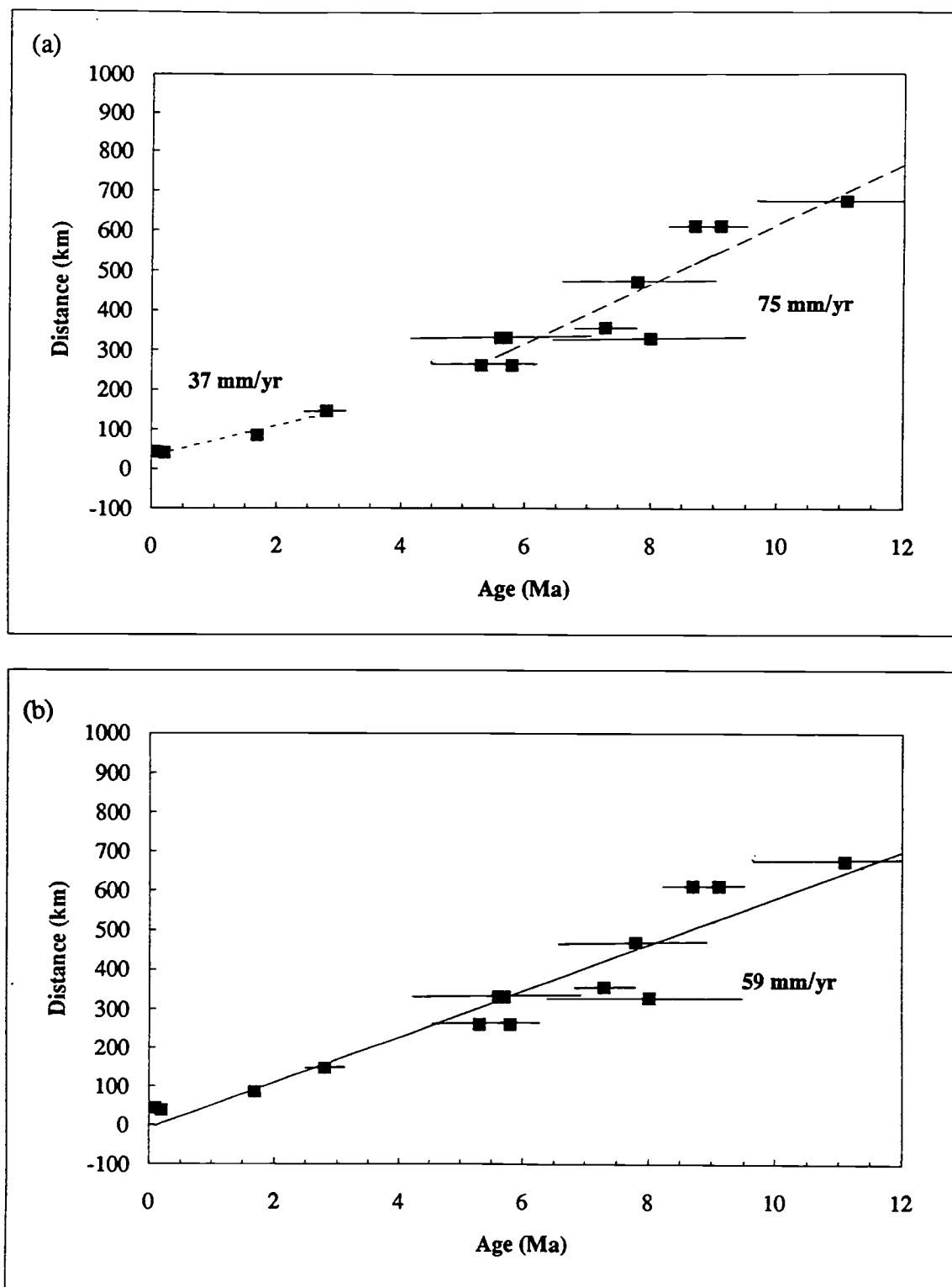


Figure II.4. Plot of age vs. distance from the western edge of the platform for central platform and Carnegie Ridge samples from PLUME2. Data used are IH plateau ages from PL1, PL2, PL4, PL5, PL8, PL17, and PL20, and K-Ar ages from PL22, PL23, and PL24. (a) Unweighted linear regressions calculated for samples older than 5 Ma and younger than 5 Ma. (b) Unweighted linear regression for all of the data points.

erupted by an off-axis Galápagos hotspot (<5 Ma). This possibility can be explored using whole rock data (A. McBirney, unpublished data) plotted on a  $\text{TiO}_2$  vs. MgO diagram (Fig. II.5).  $\text{TiO}_2$  is typically greater at a given MgO content in ocean island basalts than mid-ocean ridge basalts. In addition,  $\text{TiO}_2$  is relatively immobile during alteration and can be used with some confidence as a geochemical indicator. The data show that all of the samples that are less than 5 Ma old show a distinct elevation in  $\text{TiO}_2$  at a given MgO content compared to lavas older than 5 Ma. It should be noted that two PL17 samples were omitted as they bore evidence of either plagioclase or olivine accumulation in the analyses. Though the data are rather sparse, the pattern is striking and may indeed reflect the increasing influence of a mantle plume component in the more recent Galápagos volcanism.

#### *Wolf-Darwin Lineament*

In contrast to the central platform samples, rocks from the Wolf-Darwin lineament show no obvious age progression. This and the NW-SE orientation of the lineament suggest that volcanism along the lineament is perhaps controlled by the structure of the lithosphere, rather than by plate motion over mantle thermal anomalies. This hypothesis is supported by gravity data which indicate that the lineament coincides with a lithospheric fault (Feighner and Richards, 1992), though the movement along the fault is not specified. The lineament itself is one of many NW-trending features on variable spatial scales, such as fissures on Santiago and Isabela Islands, that are apparent on the platform (McBirney and Williams, 1969). Lavas along the lineament are isotopically variable (Harpp et al., 1990) and probably reflect lateral mantle heterogeneities beneath the lithosphere along the feature.

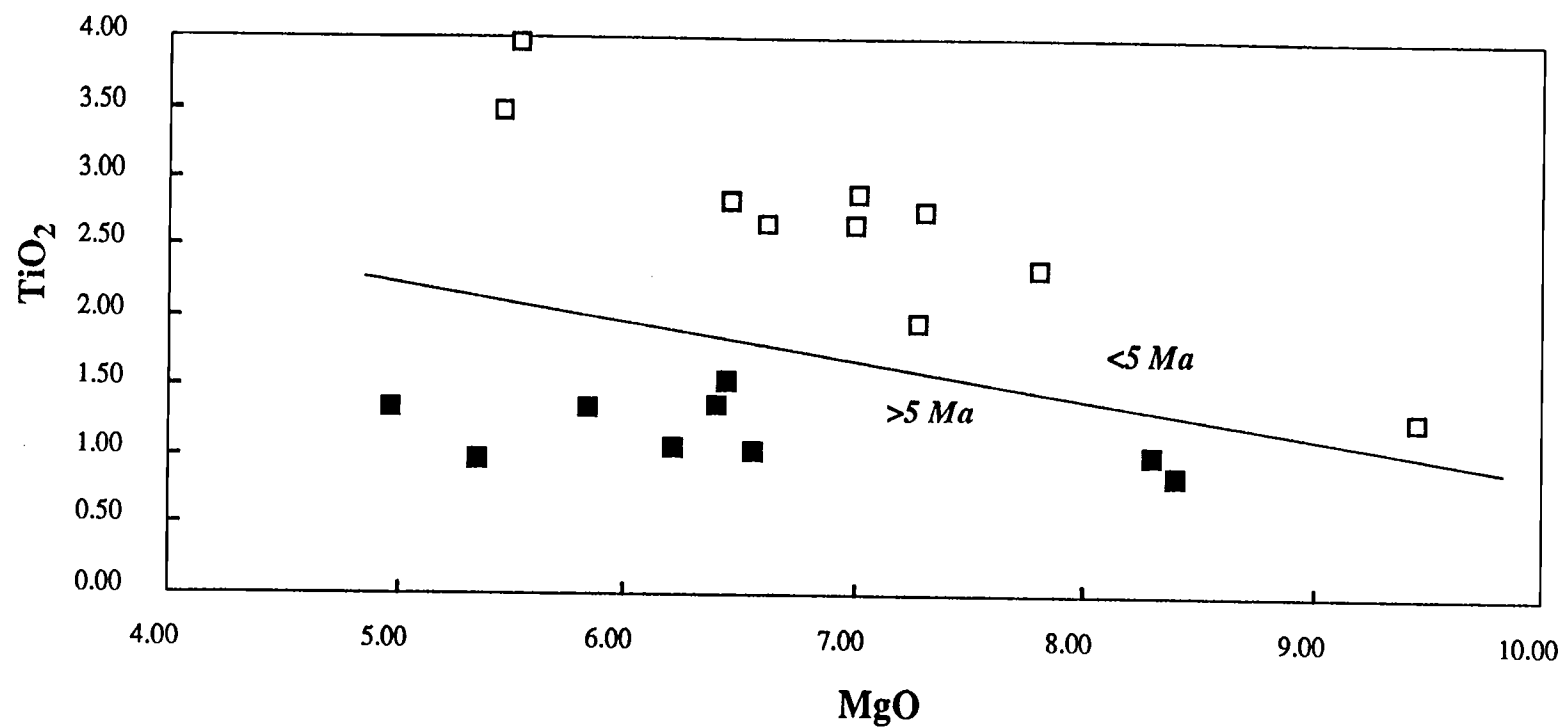


Figure II.5. Plot of MgO vs. TiO<sub>2</sub> for whole rock compositions of PLUME2 samples. The open squares have calculated ages less than 5 Ma and the closed squares are samples that are older than 5 Ma.

### *Northeastern Seamounts*

The northeastern seamounts, Sunray and Fitzroy, and the unnamed seamount (PL13 and PL14) are compositionally and petrologically similar to the island of Genovesa. Pillow-rim glasses from samples recovered from these volcanoes are low in  $\text{TiO}_2$  and  $\text{K}_2\text{O}$  and have depleted LREE signals (Harpp, unpub. data), similar to MORB. Some of the more primitive samples ( $\text{MgO} > 9\%$ ) are plagioclase-ultraphyric, containing 30-40% anorthite megacrysts (up to  $\text{An}_{92}$ ) that contain abundant melt inclusions. The bulk compositions of inclusions from PL13 samples are primitive ( $\text{MgO} \sim 10\%$ ), very low in  $\text{TiO}_2$  and  $\text{K}_2\text{O}$ , and rich in  $\text{Al}_2\text{O}_3$  and  $\text{CaO}$  (see Chapter III). Such primitive, high  $\text{Al}_2\text{O}_3$ - $\text{CaO}$ , plagioclase-ultraphyric lavas are similar to those found on the Lamont Seamounts (Allan et al., 1989), which lie off the ridge axis of the East Pacific Rise. This correlation suggests that the northeastern seamount lavas are derived from processes similar to those that created the Lamont seamount lavas, which are considered to be derived from partial melts of a depleted MORB mantle source that have bypassed an axial magma chamber (Allan et al., 1989).

The northern islands of Pinta and Marchena are situated on a NW-trending scarp that runs parallel to the Wolf-Darwin lineament (Fig. II.1). The unnamed seamount, Sunray, and Fitzroy are in a rough linear trend that also trends NW. As a thought experiment, it is assumed that the northern islands and seamounts that are aligned along lineaments were formed by lithospheric tears and not directly as impingement of a mantle plume beneath the volcanoes. Thus, the composition of the lavas would reflect the composition of the underlying mantle. Lavas from Pinta show a relative enrichment in radiogenic isotopes and incompatible elements compared to Marchena, Genovesa, and the northeastern seamounts. Pinta overlies crust that has apparently formed west of the Galápagos fracture zone. This crust formed on a ridge segment that has a plume component and, if this has been a characteristic over time, then the mantle under crust

that formed on this segment may retain this signal. Marchena lavas have incompatible element concentrations virtually identical to those of the nearby GSC segment (Vicenzi et al., 1990), though the  $^{87}\text{Sr}/^{86}\text{Sr}$  ratios for Marchena are slightly lower than those of the GSC directly to the north (Verma and Schilling, 1982). Genovesa and the northeastern seamounts also have MORB-like isotopic and trace element signals (White et al., 1992; K. Harpp, unpublished data). Thus, it may be possible that the intraplate volcanism to the north of the platform is directly related to the ambient stress patterns due to ridge processes. Reactivation of volcanism along lithospheric fractures may tap into a heterogeneous mantle that is a product of deep seated mixing of part of the Galápagos plume and MORB mantle.

The presence of two distinct linear trends, one oriented NW-SE and the other E-W, on the islands has been previously noted. The gross distribution of these trends is as follows: The NW-SE lineations are more pronounced on the western side of the  $90.5^\circ$  transform fault. The E-W trending faults are more pronounced on the islands and east of the  $90.5^\circ$  transform fault and on the Carnegie Ridge (van Andel et al., 1971). These two trends do overlap, for example, Santa Cruz is cut by E-W faults, but parasitic cones are oriented NW-SE (McBirney et al., 1969). Further east, near the Inca transform ( $\sim 85^\circ\text{W}$ ), fractures on the Carnegie Ridge are oriented in a NE-SW direction (Feighner and Richards, 1992). This symmetrical pattern indicates that the regional tectonic stresses that regulate the morphology of the ridge are responsible for the system of fractures and lineations on the platform.

Rounded cobbles recovered from the unnamed seamount (PL13) and Fitzroy seamount (PL11) indicate these features were subaerial at one point (Christie et al., 1992). Backtracking Fitzroy seamount to its original eruptive position can be accomplished using the calculated  $^{40}\text{Ar}/^{39}\text{Ar}$  IH age for PL11-2 and an estimated plate

velocity of 40 mm/yr in a ENE direction. This analysis indicates that eruption and crystallization of the lava occurred near the present position of Genovesa. This suggests that there is a fixed point of volcanism below Genovesa. Though there is no geochemical evidence for the mixing of a plume component in the Genovesa lavas, it is possible that thermal input from the hotspot either causes or augments partial melting and volcanism in this area. The apparent fixity of volcanism in this area indicates that volcanism is not purely a function of lithospheric tearing.

### Conclusions

Radiometric ages of submarine lavas from the central Galápagos Platform and western Carnegie Ridge are consistent with volcano formation over a stationary Galápagos hotspot. Age-distance relationships are consistent with the Nazca plate moving over the hotspot at a rate of ~75 mm/yr between 5 and 11 Ma, then slowing to ~37 mm/yr. Lower  $\text{TiO}_2$  concentrations in lavas older than 5 Ma may indicate the transition from a ridge centered hotspot to an off-axis hotspot. This age is in accord with that suggested by Hey (1977) for the northward migration of the GSC away from the hotspot. The apparent change in plate velocity and the ridge migration may indicate a major change in the regional plate tectonic environment at 5 Ma.

Lavas along the Wolf-Darwin lineament show no coherent age progression, which is consistent with volcanism being controlled by lithospheric weaknesses. The northeastern seamounts could have formed in the present positions of the northern islands of Pinta, Marchena, and Genovesa. Similarities in petrology and composition suggest the seamounts formed by processes similar to those that form these islands. The position of the northern islands indicates that they could not have formed by an eastward moving Nazca plate over a hotspot beneath Fernandina. The variable composition of the lavas and the placement of the northern islands on linear features suggests that they are derived



from partial melting of a laterally heterogeneous mantle triggered by lithospheric tearing. The heterogeneous character of the mantle may be due to deep seated mixing of a Galápagos plume component and MORB mantle.

## References

- Allan, J.F., Batiza, R., Perfit, M.R., Fornari, D.J., and Sack, R.O., 1989, Petrology of lavas from the Lamont seamount chain and adjacent East Pacific Rise, 10 N: *Journal of Petrology*, v. 30, p. 124-89.
- Christie, D.M., Duncan, R.A., McBirney, A.R., Richards, M.A., White, W.M., Harpp, K.S., and Fox, C.G., 1992, Drowned islands downstream from the Galápagos hotspot imply extended speciation times: *Nature*, v. 355, p. 246-248.
- Cox, A and Dalrymple, G.B., 1966, Paleomagnetism and potassium-argon ages of some volcanic rocks from the Galápagos Islands, *Nature*, v. 209, p. 776-777.
- Cullen, A., Vicenzi, E., and McBirney, A.R., 1989, Plagioclase-ultrapphyric basalts of the Galápagos archipelago: *Journal of Volcanology and Geothermal Research*, v. 37, p. 325-337.
- Dalrymple, G.B. and Lanphere, M.A., 1969, Potassium argon dating: principles, techniques, and application to geochronology, W.H. Freeman, New York, 258 pp.
- Duncan, R.A. and Hargraves, R.B., 1990,  $^{40}\text{Ar}$ - $^{39}\text{Ar}$  geochronology of basement ages from the Mascarene plateau, Chagos Bank, and the Maldives Ridge, *Proc. ODP Sci. Results*, v. 115, Ocean Drilling Program, p. 43-51.
- Feighner, M.A. and Richards, M.A., 1992, Lithospheric structure and compensation mechanisms of the Galápagos Archipelago, *Journal of Geophysical Research*, submitted.
- Geist, D.J., White, W.M., and Duncan, R.A., 1986, Geology and petrogenesis of lavas from San Cristobal Island, Galápagos Archipelago, *Geological Society of America Bulletin*, v. 97, p. 555-566.
- Geist, D.J., White, W.M., and McBirney, A.R., 1988, Plume-asthenosphere mixing beneath the Galápagos, *Nature*, v. 333, p. 657-660.
- Gripp, A.E. and Gordon, R.G., 1990, Current plate velocities relative to hotspots incorporating the NUVEL-1 global plate model, *Geophysical Research Letters*, v. 17, p. 1,109-1,112.
- Harpp, K, White, W.M., and Duncan, R.A., 1990, Geochemistry of the Wolf-Darwin lineament and ridge-plume interaction in the Galápagos, *Geological Society of Australia Absts.*, v. 27, p. 44.
- Hey, R., 1977, Tectonic evolution of the Cocos-Nazca spreading center, *Geological Society of America Bulletin*, v. 88, p. 1404-1420.
- Hey R., Johnson, G.L., and Lowrie, A., 1977, Recent plate motions in the Galápagos area, *Geological Society of America Bulletin*, v. 88, p. 1385-1403.
- Kunk, M.J., Sutter, J.F., and Naeser, C.W., 1985, High precision  $^{40}\text{Ar}$ - $^{39}\text{Ar}$  ages of sanidine, biotite, hornblende, and plagioclase from the Fish Canyon Tuff, San Juan volcanic field, south central Colorado, *Geological Society of America Abst.*, v 17(7), p. 636.

- McBirney, A.R. and Williams H., 1969, Geology and petrology of the Galápagos Islands, Geological Society of America Memoir 118, 197 pp.
- McBirney, A.R., Cullen, A.B., Geist, D., Vicenzi, E.P., Duncan, R.A., Hall, M.L., and Estrella, M., 1985, The Galápagos Volcano Alcedo: a unique ocean caldera, *Journal of Volcanology and Geothermal Research*, v. 26, p. 173-177.
- McDougall, I. and Harrison, T.M., 1988, *Geochronology and thermochronology by the  $^{40}\text{Ar}/^{39}\text{Ar}$  method*, Oxford Univ. Press, Oxford.
- Morgan, W.J., 1971, Convection plumes in the lower mantle, *Nature*, v. 230, p. 42-43.
- Morgan, W. J., 1972, Deep mantle convection plumes and plate motion, *American Association of Petroleum Geologists Bulletin*, v. 56, p. 203-213.
- Richards, M.A. and Griffiths, R.W., 1989, Thermal entrainment by deflected plumes, *Nature*, v. 342, p. 900-902.
- Samson, S.D. and Alexander, E.C. Jr, 1987, Calibration of the inter-laboratory  $^{40}\text{Ar}/^{39}\text{Ar}$  dating standard MMhb-1, *Chemical Geology*, v. 66, p. 27-34.
- Schilling, J-G., Kingsley, R.H., and Devine, J.D., 1982, Galápagos hotspot-spreading center system 1. spatial, petrological, and geochemical variations (83W-101W), *Journal of Geophysical Research*, 87, 5593-5610.
- Seidemann, D.E., 1978,  $^{40}\text{Ar}/^{39}\text{Ar}$  studies of deep sea igneous rocks, *Geochimica et Cosmochimica Acta*, v. 42, p. 1721-1734.
- van Andel, Tj H., Heath, G.R., Malfait, B.T., Heinrichs, D.F., and Ewing, J.I., 1971, Tectonics of the Panama Basin, eastern equatorial Pacific, *Geological Society of America Bulletin*, v. 82, p. 1489-1504.
- Verma, S.P. and Schilling, J-G., 1982, Galápagos hotspot-spreading center system, 2.  $^{87}\text{Sr}/^{86}\text{Sr}$  and large ion lithophile element variations, *Journal of Geophysical Research*, v. 92, p. 13,687-13,707.
- Vicenzi, E.P., McBirney, A.R., White, W.M., and Hamilton, M., 1990, The geology and geochemistry of Isla Marchena, Galápagos Archipelago: an ocean island adjacent to a mid-ocean ridge, *Journal of Volcanology and Geothermal Research*, v. 40, p. 291-315.
- White, W.M., McBirney, A.R., and Duncan, R.A., submitted, Petrology and geochemistry of the Galápagos Islands: Portrait of a pathological mantle plume, submitted to *Journal of Geophysical Research*
- White, W.M. and Hoffman, A.W., 1978, Geochemistry of the Galápagos Islands: implications for mantle dynamics and evolution, *Carnegie Institute of Washington Yearbook*, v. 77, p. 548-562.

### **III. Near-Primary Melt Inclusions in Anorthite Phenocrysts from the Galápagos Platform**

Chris W. Sinton; David M. Christie; Valerie L. Coombs; Roger L. Nielsen; and Martin R. Fisk

submitted to Earth and Planetary Science Letters

### Abstract

Melt inclusions in anorthite ( $An_{90-91}$ ) phenocrysts from a Galápagos seamount lava are among the most primitive, highest CaO and  $Al_2O_3$  naturally occurring MORB compositions yet discovered. They are near primary, requiring addition of less than 5% olivine plus plagioclase in order to be in equilibrium with mantle olivine ( $Fo_{92}$ ). They occur in association with, and appear to be parental to a suite of MORB-like pillow lavas which require up to 40% fractionation of olivine plus plagioclase from the inclusion composition.

Similar high CaO- $Al_2O_3$  MORB lavas are associated with high-An plagioclase in a variety of oceanic settings. Minor element variations within the melt inclusions indicate that the host anorthite was exposed to discrete magma batches with different minor element compositions during crystallization. We propose that such magmas are derived from shallow, relatively depleted mantle and that they constitute one end member of a "spectrum" of primary MORB magma compositions .

## Preface

This manuscript has been submitted for publication. The version that is presented here in the thesis is slightly longer than the submitted version in order to present some of the relevant material that had to be cut in order to comply with the manuscript length restrictions. Specifically, comparisons to the island lavas and a longer discussion on high CaO-Al<sub>2</sub>O<sub>3</sub> basalts are presented as well more of the data in Appendix 2.

Because this manuscript involved the efforts of numerous people, their individual contributions need to be stated. Dave Christie and others were responsible for organizing and obtaining funding for the PLUME2 expedition and sample collection. Christie helped rewrite a significant portion of the text. Val Coombs did much of the melting and microprobe work. Roger Nielsen supervised the melting experiments, probe work, and differentiation modeling and probed some of the 1260° and 1270° runs. He also helped write some of the text. Marty Fisk promoted the idea of remelting inclusions and helped with revisions. Chris Sinton wrote the text, ran the remelting experiments with the help of Lance Forsythe and Coombs, analyzed the pillow rim glasses and minerals, and analyzed the inclusions with the help of Coombs and Nielsen.

## Introduction

Abundant anorthite megacrysts containing melt inclusions are present in high CaO-Al<sub>2</sub>O<sub>3</sub>, MORB-like lavas from seamounts along the northeastern margin of the Galápagos Platform. They resemble other occurrences of anorthitic phenocrysts and associated lavas from mid-ocean ridge environments (Davis and Clague, 1986, Natland, 1980), from off-axis seamounts (Allan et al., 1989), and from Iceland (Jakobsson et al., 1978). Such anorthitic phenocrysts in oceanic settings are typically associated with forsteritic olivine and aluminous spinel in basalts that are high in Al<sub>2</sub>O<sub>3</sub> and CaO and depleted in TiO<sub>2</sub> relative to the majority of MORB.

The origin of such lavas has remained unclear (Allan et al., 1988), however, and high-anorthite plagioclase has not yet been produced experimentally from any naturally occurring MORB compositions (Allan et al., 1988; Marsh et al., 1990). Naturally occurring anorthites must, therefore, be formed either under conditions or from compositions that have not been studied experimentally. Here we report on primitive, anorthite-hosted melt inclusions from the Galápagos Platform which appear to be in equilibrium with anorthite plus olivine plus spinel. We interpret these inclusions as near-primary, high CaO-Al<sub>2</sub>O<sub>3</sub> MORB liquids derived from depleted, plagioclase-bearing mantle at shallow depth.

Inclusions of basaltic glass in a phenocryst represent discrete liquids or liquid-crystal mixtures isolated at specific instants during the growth of the host crystal. If they are in equilibrium with their host, the bulk compositions of such inclusions can provide powerful constraints on the magmatic history of their associated melts (Watson, 1976; Falloon and Green, 1986; Donaldson and Brown, 1977; Vicenzi, 1990). Accurate analysis of such melt inclusions has, however, proven difficult because of post-entrapment devitrification and reaction with the host (Watson, 1976; Donaldson and

Brown, 1977; Dungan and Rhodes, 1978; Falloon and Green, 1986; Sobolev and Shimizu, 1991) We have addressed this problem by heating individual plagioclase crystal fragments to temperatures spanning the liquidus temperature of the trapped melt, thereby homogenizing the inclusions.

*Anorthite-ultraphyric basalts from the Galápagos Platform*

Anorthitic plagioclase-phyric lavas were recovered from several seamounts along the northeastern margin of the platform during Leg 2 of the PLUME expedition of R/V *Thomas Washington* in January 1990 (Fig. III.1). These seamounts are older (3.4-5.7 Ma, Sinton and Duncan, unpub. data) than the more northerly islands of Pinta, Marchena, and Genovesa (0-0.89 Ma), and rounded cobbles indicate that some of the seamounts have been subaerially exposed (Christie et al., 1992). Some of the seamount lavas are considerably more primitive than the island lavas and the most primitive are from an unnamed seamount near 0° 06' N, 89° 03'W (Fig. III.1 - dredge PL13).

This dredge haul recovered both anorthite-ultraphyric (~30-40% phenocrysts and glomerocrysts) and sparsely phyric pillow basalts. Pillow-rim glasses from the ultraphyric samples have MgO >9.5% and are rich in both CaO (~13%) and Al<sub>2</sub>O<sub>3</sub> (~17%) (Table III.1). The ultraphyric lavas contain <5% microphenocrysts (50-400 µm) of olivine (Fo<sub>89-90</sub>) and megacrysts and glomerocrysts of plagioclase up to 1 cm that vary in shape from rounded to euhedral. The sparsely phyric lavas of PL13 are more evolved (MgO 8.2-9.0%) than the ultraphyric lavas (Table III.1) and contain rare glomerocrysts of high An plagioclase and olivine microphenocrysts.



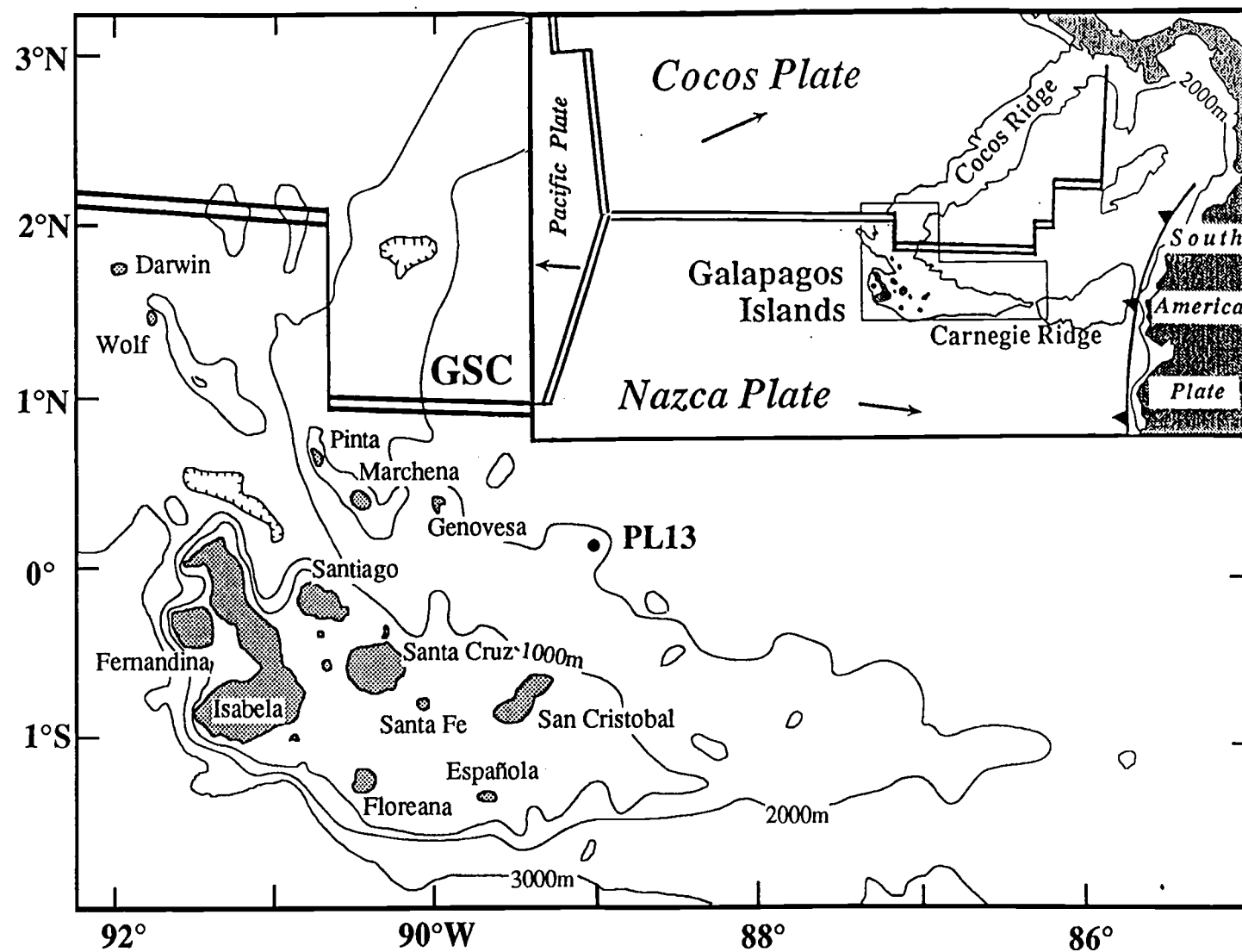


Figure III.1. Generalized map of the Galápagos platform. PLUME2 dredge site PL13 is marked with a closed circle. GSC is the Galápagos Spreading Center.

Table III.1: Analyses of representative pillow-rim glasses

	PL13-12	PL13-18	PL13-21	PL13-23	PL13-28	F-3-4
	p	s	p	s	s	
SiO <sub>2</sub>	47.94	49.93	47.90	49.98	49.57	48.81
TiO <sub>2</sub>	0.83	1.02	0.81	1.18	1.14	0.83
Al <sub>2</sub> O <sub>3</sub>	17.15	16.20	17.28	15.35	15.69	17.91
FeO	8.36	9.25	8.29	9.83	9.58	8.40
MnO	0.11	0.10	0.12	0.11	0.12	n.a.
MgO	9.99	8.89	10.10	8.23	8.63	9.53
CaO	12.91	12.74	12.85	12.91	12.94	12.90
Na <sub>2</sub> O	2.17	2.44	2.10	2.55	2.33	2.08
K <sub>2</sub> O	0.00	0.04	0.01	0.04	0.03	0.01
P <sub>2</sub> O <sub>5</sub>	0.04	0.08	0.06	0.04	0.07	0.09
Total	99.51	100.69	99.52	100.22	100.08	100.56

PL13 pillow rim compositions are averages of 5 microprobe analyses of a single glass chip; p = phyric sample s = sparsely-phyric sample. F-3-4 is from the Lamont Seamounts (Allan et al., 1989)

The Galápagos plagioclase-ultraphyric seamount lavas are texturally similar, but are significantly more primitive than plagioclase-ultraphyric lavas of the nearby islands of Genovesa, Pinta, and Marchena (Vicenzi, 1990; Vicenzi et al., 1990; Cullen et al., 1989). The phenocrysts of PL13 have much higher anorthite content (An<sub>90-94</sub>) than those from the nearby islands (typically An<sub>78-86</sub>) (Cullen et al., 1989) and the PL13 glasses are more primitive (MgO 8.2-10.1%) than groundmass compositions from the islands (MgO 6.4-7.2%)(Cullen et al., 1989).

The megacrysts and glomerocrysts from PL13 ultraphyric lavas are compositionally homogeneous (An<sub>90-91</sub>) except for narrow, less calcic rims (An<sub>78-81</sub>) that are compositionally similar to groundmass plagioclase. Within most of the PL13 plagioclase phenocrysts of both the ultraphyric and sparsely-phyric lavas, inclusions of

forsteritic olivine (Fo<sub>90</sub>), aluminous spinel (45-48% Al<sub>2</sub>O<sub>3</sub>), and melt are found, with the melt inclusions being the most abundant. Melt inclusions range from small (2-20 microns) and spherical to large (<500 microns) and irregular. They occur within concentric bands or as clusters in the core of the host phenocryst (Fig. III.2). All melt inclusions have crystallized to some extent and have thin sodic rims. The inclusions do not display resorption features such as those observed in plagioclase-hosted melt inclusions from some Atlantic Ocean lavas (Donaldson and Brown, 1977 and Dungan and Rhodes, 1978).

#### *Melt Inclusions in Galápagos Island Lavas*

Plagioclase-hosted melt inclusions are a common feature of highly-phyric basaltic lavas from several islands (Vicenzi, 1990; Vicenzi et al., 1990; Cullen et al., 1989). Vicenzi (1990) conducted similar remelting experiments to those described here using plagioclase from the northern Galápagos islands of Pinta, Marchena, and Genovesa. Melt inclusions from Pinta and Genovesa are more primitive (Mg# 65-70) than their respective host lavas (Mg# 50-58), but those from Marchena have Mg# similar (50-56) to that of the host lavas. REE patterns from the inclusions and the host lavas for all three islands are similar, suggesting that the inclusions and lavas are genetically related. We reach the same conclusion in our investigation of the PL13 lavas.

#### Results

Anorthite fragments (2-5 mm) were separated from sample PL13-12, one of the highly-phyric rocks recovered from PL13 (Table III.1), and heated for one hour in a vertical gas mixing furnace controlled to the QFM buffer. To bracket the liquidus temperature of the melt inclusions, separate runs were made at 1240°, 1250°, 1260°, 1270°, and 1280° C using 4-5 different crystal fragments for each run. The resulting

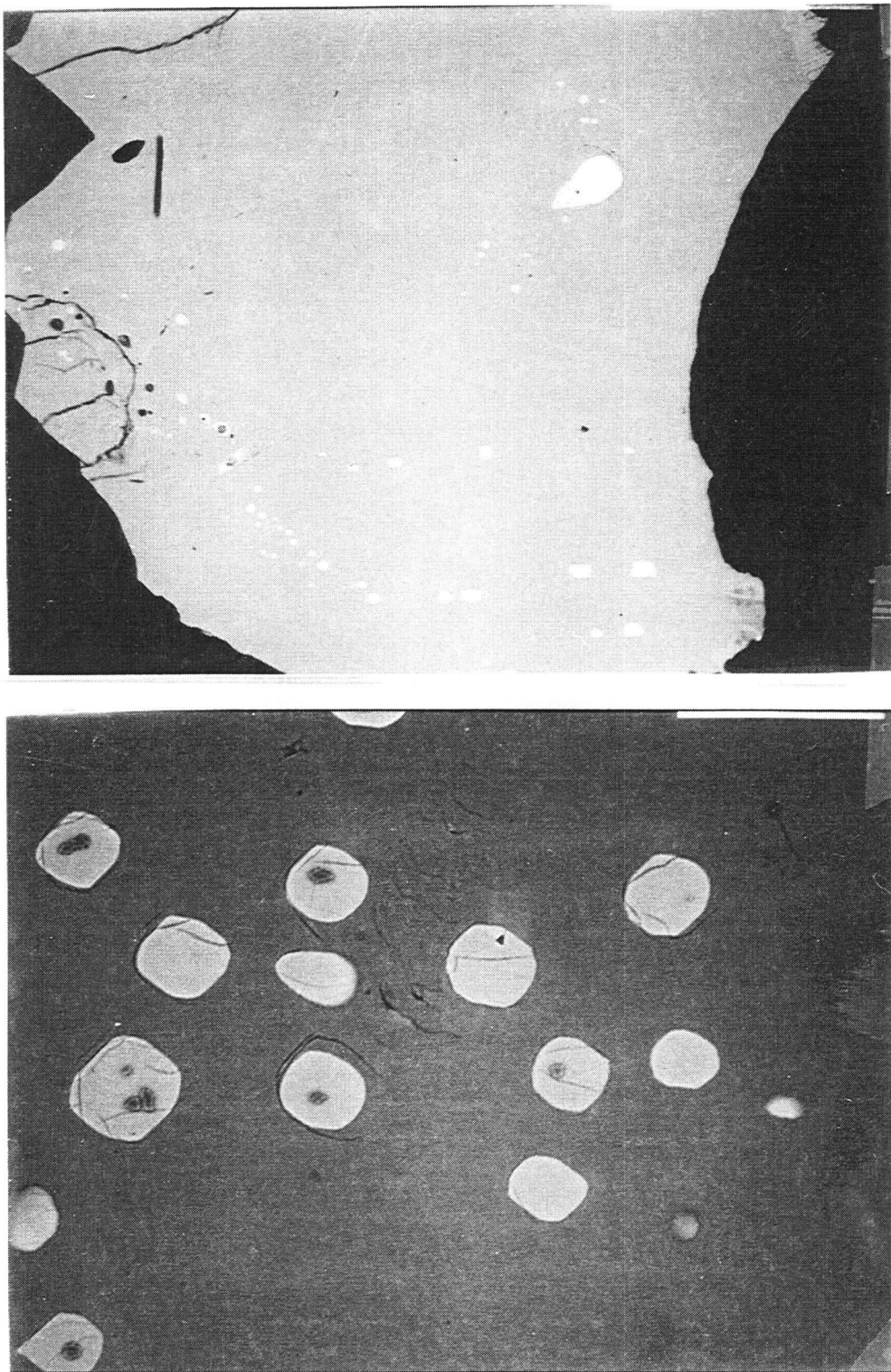


Figure III.2. Backscatter electron images of PL13 anorthite-hosted melt inclusions. (a) Inclusions from sample heated to 1280°C. The large, bright inclusion is a spinel with melt. (b) Fo<sub>91</sub> olivine (small dark crystals) in melt inclusions (round light inclusions) in anorthite fragment heated to 1260°C.

rehomogenized glass inclusions and coexisting minerals were analyzed by electron microprobe.

Within the reheated inclusions, small olivine crystals (Fo<sub>87-91</sub>) are common in the 1240°, 1250°, and 1260°C runs, rare in the 1270° runs, and absent from the 1280° runs. The sodic rims are not observed in the 1270°C or 1280°C runs. A single, relatively large, aluminous spinel was found in contact with a melt inclusion in a 1280° run (Fig. III.2). This spinel, which is too large to have crystallized from the inclusion, must have been trapped with the included glass. The glass in contact with the spinel is virtually identical in composition to numerous nearby inclusions that lack spinel, indicating that the coexisting glass, plagioclase, and spinel were in equilibrium.

Melt inclusion compositions show a progressive increase in MgO and Al<sub>2</sub>O<sub>3</sub> with increasing temperature up to 1270°C, consistent with remelting of olivine+plagioclase in the inclusions. Between 1270° and 1280°, MgO begins to decrease while Al<sub>2</sub>O<sub>3</sub> continues to increase (Fig. III.3). Similar inflections are apparent when other major element data are plotted against MgO.

### Interpretation

Between 1270°C and 1280°, the inflections in MgO variation diagrams and the disappearance of olivine indicate that the rehomogenized melts have left the olivine-plagioclase cotectic and are reacting with the host plagioclase. In other words, the 1270° glass compositions must closely resemble the original trapped liquid compositions.

All the 1270°C inclusions are uniform in major element content (except MgO), but TiO<sub>2</sub>, Na<sub>2</sub>O, and P<sub>2</sub>O<sub>5</sub> vary well in excess of analytical error. These elements appear to be homogeneous within any band or cluster of inclusions, but they may vary between

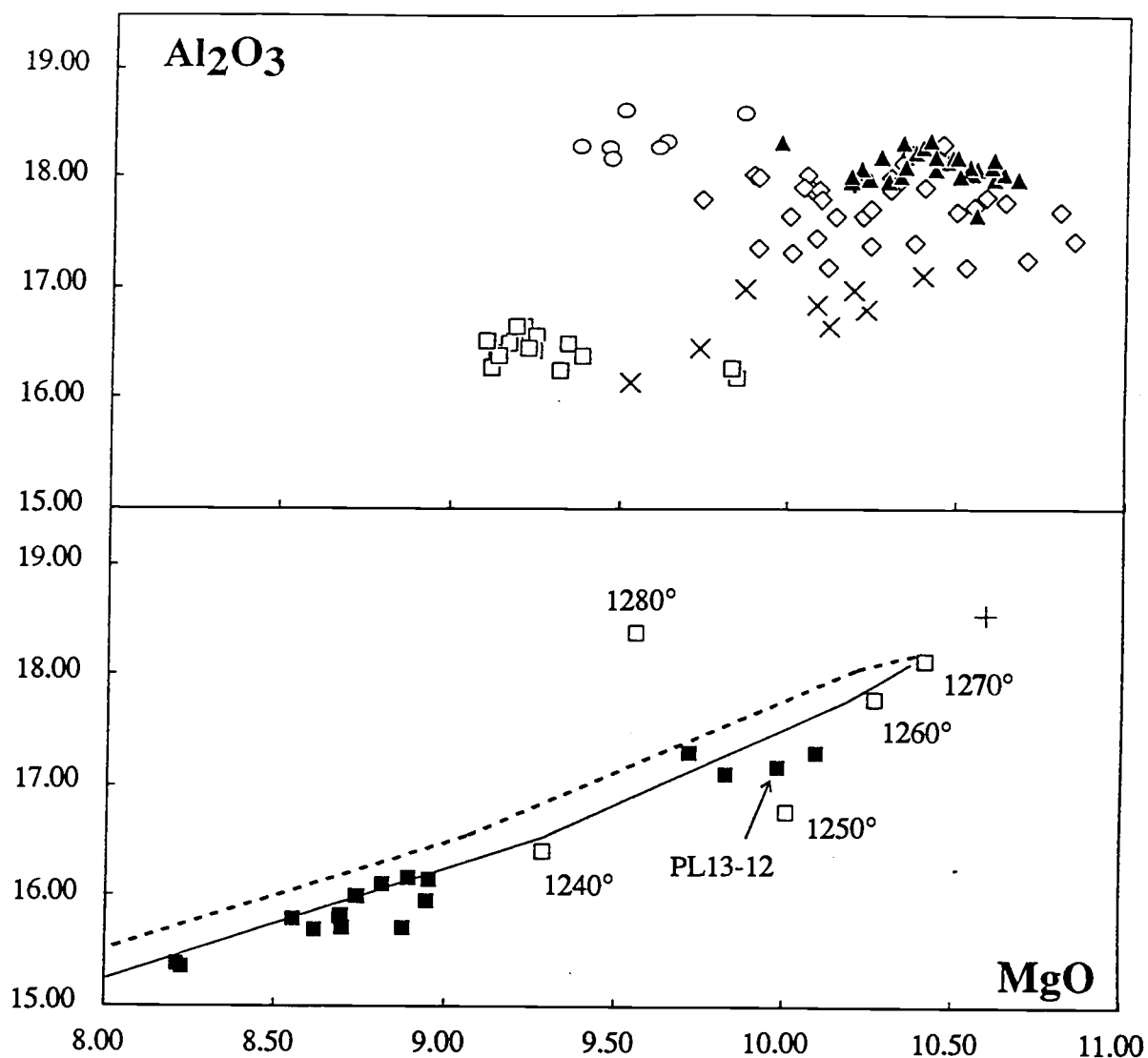


Figure III.3. (a)  $\text{Al}_2\text{O}_3$  vs.  $\text{MgO}$  of remelted inclusions from PL13-12 at 1240°C (open squares), 1250°C (x's), 1260°C (open diamonds), 1270°C (closed triangles), and 1280°C (open triangles). (b)  $\text{Al}_2\text{O}_3$  vs.  $\text{MgO}$  for liquid line of descent using a modified version of the Nielsen (1990) differentiation model. Averages of the high  $\text{TiO}_2$  (solid line) and low  $\text{TiO}_2$  (dashed line) 1270°C melt inclusions were used as starting compositions. The + is the composition of the calculated primary melt composition. The open squares are the averages of the remelted inclusions for each heating step. Closed squares are the PL13 pillow-rim glasses.

bands or clusters, even within individual phenocrysts. Two groups can be distinguished, one with high  $\text{TiO}_2$  (0.57-0.71%) and one with low  $\text{TiO}_2$  (0.23-0.46%) (Fig. III.4; Table III.2). The high  $\text{TiO}_2$  inclusions generally have higher  $\text{P}_2\text{O}_5$  and lower  $\text{Na}_2\text{O}$  than the low  $\text{TiO}_2$  group. We interpret these minor element variations as original characteristics of the melt inclusions and not as artifacts of either post-entrapment crystallization or the experimental process of re-homogenization. The effects of post-entrapment crystallization should have been obviated by the heating process and any incorporation of the host material in the inclusion would result in a dilution of both  $\text{TiO}_2$  and  $\text{Na}_2\text{O}$ , which is not the case. Similar variations have been reported for incompatible trace elements in olivine and plagioclase-hosted inclusions from the Mid-Atlantic Ridge (Shimizu, 1992).

In MgO variation diagrams, pillow-rim glasses from sample PL13-12 and other phyric and sparsely-phyric PL-13 lavas form linear arrays which extend away from the 1270°C inclusion compositions (Fig. III.4b) and which correspond well with calculated fractional crystallization liquid lines of descent for a 1270°C inclusion composition (Fig. III.4b). The pillow-rim glasses appear to be derived from the melt inclusions with the lowest  $\text{Na}_2\text{O}$  and highest  $\text{TiO}_2$  contents. Model calculations indicate that pillow rim glasses containing 10% and 8% MgO can be derived, respectively, by 15% and 40% fractional crystallization of olivine, plagioclase, and minor chromite (<2%) from the 1270° inclusion composition. Forty percent fractionation from 10.4 to 8% MgO represents about 15% crystallization for each weight percent drop in MgO, and a temperature drop of 80°C between the liquidus at 1270°C and a magma with 8% MgO at 1190°C.

A potential primary magma composition in equilibrium with Fo<sub>92</sub> mantle olivine can be calculated from the 1270°C melt inclusions by adding 5% olivine (Fo<sub>91</sub>) plus plagioclase (An<sub>91</sub>) in their cotectic proportions (1:2) to the included melt composition

Table III.2: Average compositions for inclusions and calculated primary melt

	1240°	1250°	1260°	1270°		1280°	primary melt
				low TiO <sub>2</sub>	high TiO <sub>2</sub>		
SiO <sub>2</sub>	49.21	48.54	48.74	48.89	48.13	47.76	48.41
TiO <sub>2</sub>	0.70	0.54	0.37	0.38	0.67	0.54	0.59
Al <sub>2</sub> O <sub>3</sub>	16.43	16.77	17.76	18.10	18.14	18.38	18.53
FeO	8.67	8.33	7.68	7.34	7.13	7.50	6.81
MnO	0.18	0.14	0.13	0.13	0.15	0.13	0.13
MgO	9.29	10.01	10.27	10.37	10.44	9.56	10.58
CaO	12.88	12.67	12.83	12.49	12.88	12.65	12.81
Na <sub>2</sub> O	2.17	1.95	2.12	2.25	2.12	2.40	2.08
K <sub>2</sub> O	0.04	0.12	0.03	0.03	0.02	0.03	0.03
P <sub>2</sub> O <sub>5</sub>	0.03	0.05	0.02	0.02	0.05	0.02	0.03
Total	99.60	99.12	99.94	100.02	99.73	98.97	100.00

The primary melt composition was calculated by adding 5% plagioclase (An<sub>91</sub>) and olivine (Fo<sub>91</sub>) in proportions of 2:1 respectively, to the average high TiO<sub>2</sub> melt composition.

(Table III.2; Coombs et al, 1991). In other words, the 1270°C melt compositions could have been derived from a mantle melt by only 5% fractional crystallization of olivine, plagioclase, and perhaps spinel.

### Discussion

The PL13 lavas and melt inclusions, like many other Galápagos lavas, have low minor element contents and other characteristics which are more typical of MORB than of typical ocean island basalts. Relative to other primitive MORB (Elthon, 1990), the melt inclusions of PL13 are rich in Al<sub>2</sub>O<sub>3</sub> and CaO and lower in FeO, TiO<sub>2</sub>, and K<sub>2</sub>O (Fig. III.5). Although some MORB glasses have higher CaO contents, the inclusions reported here are distinctly rich in both CaO and Al<sub>2</sub>O<sub>3</sub>. Similar Al<sub>2</sub>O<sub>3</sub>-rich (>17%) and CaO-rich (>12%) pillow rim glasses are found in mid-ocean ridge environments (Humphris et al., 1985; Natland and Melson, 1980; Price et al., 1986), fracture zones



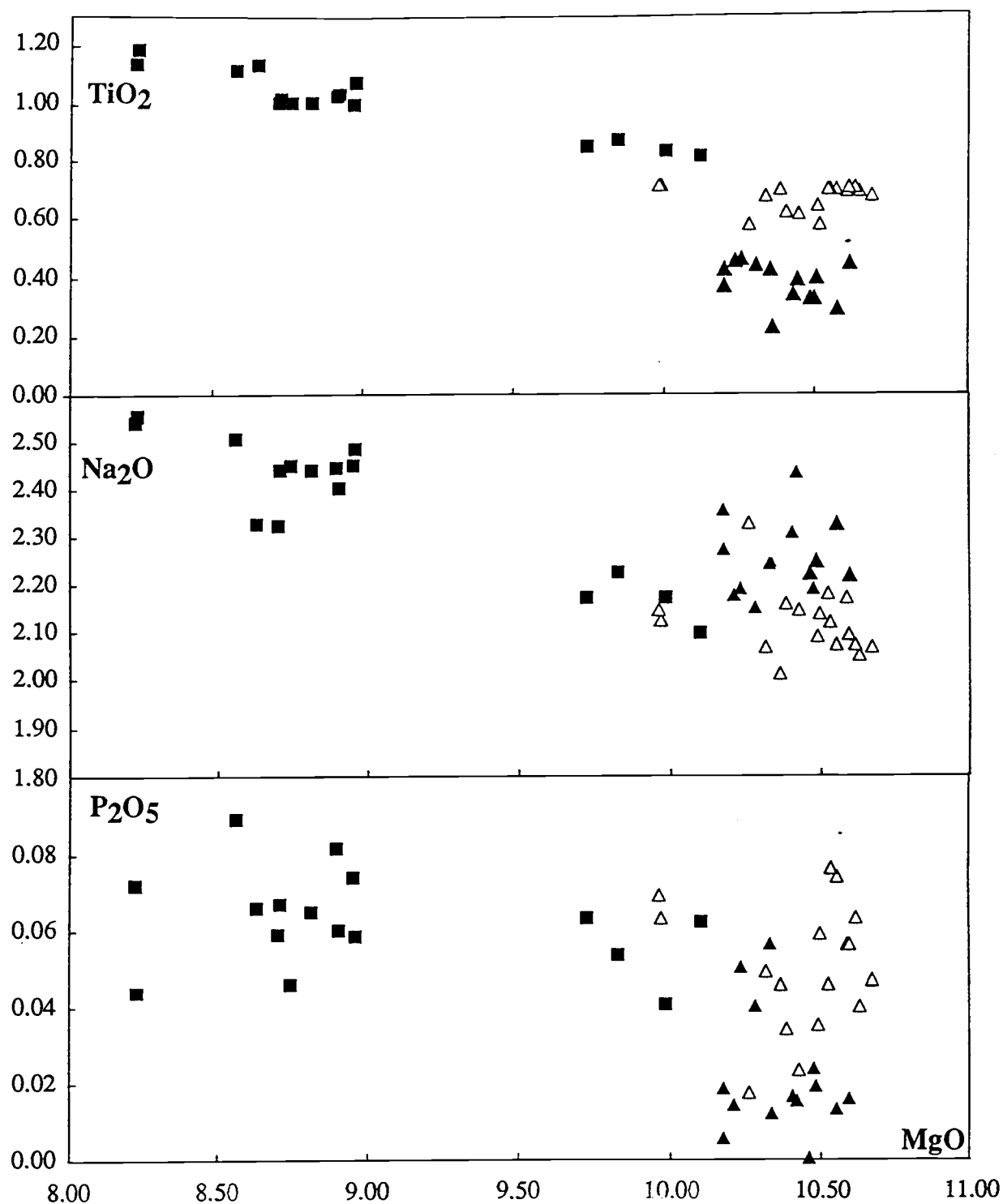


Figure III.4. MgO vs. TiO<sub>2</sub>, Na<sub>2</sub>O, and P<sub>2</sub>O<sub>5</sub> content of high TiO<sub>2</sub> (open triangles) and low TiO<sub>2</sub> (closed triangles) 1270°C melt inclusions. The PL13 pillow-rim glasses (closed squares) appear to be derived from the high TiO<sub>2</sub> melt inclusion composition.

(Natland and Melson, 1980), and off-axis seamounts (Allan et al., 1989). High CaO-Al<sub>2</sub>O<sub>3</sub> inclusions occur in plagioclase and olivine from the Mid-Atlantic Ridge, although they are not quite as primitive as the PL13 inclusions and have lower liquidus temperatures (<1240° C) (Sobolev et al., 1989). Thus, the Galápagos high CaO-Al<sub>2</sub>O<sub>3</sub> magmas are not a local phenomenon.

#### *High CaO-Al<sub>2</sub>O<sub>3</sub> Magmas from Mid-Ocean Ridges*

The compilation of primitive MORB glasses of Elthon (1990) can be sorted to find all glasses that have >12% CaO and >17% Al<sub>2</sub>O<sub>3</sub>. Such samples come from both the East Pacific Rise (EPR) and Mid-Atlantic Ridge (MAR). All have very low K<sub>2</sub>O (<0.05%), low but variable TiO<sub>2</sub> (0.51-0.98%) and Na<sub>2</sub>O (1.62-2.44). Two spinel-olivine phyric samples come from the EPR (DS3-3A and DS3-3B) and another (SD-7ED) is the most LREE depleted tholeiites of a suite of samples taken near the Siqueros fracture zone (Melson and Natland, 1980). Another lava recovered from ODP Hole 504B (35-1-15) contains high-An plagioclase (An<sub>86-90</sub>), aluminous spinel (Al<sub>2</sub>O<sub>3</sub>~42%) and forsteritic olivine (Fo<sub>88-90</sub>) and is the most primitive glass yet taken from the Galápagos Spreading Center (Natland et al., 1983). From the Atlantic, one sample taken from a ridge segment near Tristan da Cunha (107-7-20; Humphris et al., 1985) contains large, An<sub>86-89</sub> plagioclase and olivine microphenocrysts. Two high CaO-Al<sub>2</sub>O<sub>3</sub> lavas were recovered from DSDP Leg 3 (Frey et al., 1974). One (3-14-10-1) bears aluminous spinel (Al<sub>2</sub>O<sub>3</sub>~38%) an forsteritic olivine (Fo<sub>90</sub>) and no plagioclase, while the other contains up to 30% plagioclase as well as spinel and olivine. Both are LIL-element depleted, but differ in Na<sub>2</sub>O content with 2.28% and 1.62 %, respectively.

The PL13 samples are remarkably similar in mineralogy and composition to depleted lavas dredged from the Lamont Seamounts (Table III.1; Allan et al, 1989; Fornari et al., 1988). Compared to lavas from the nearby East Pacific Rise, these

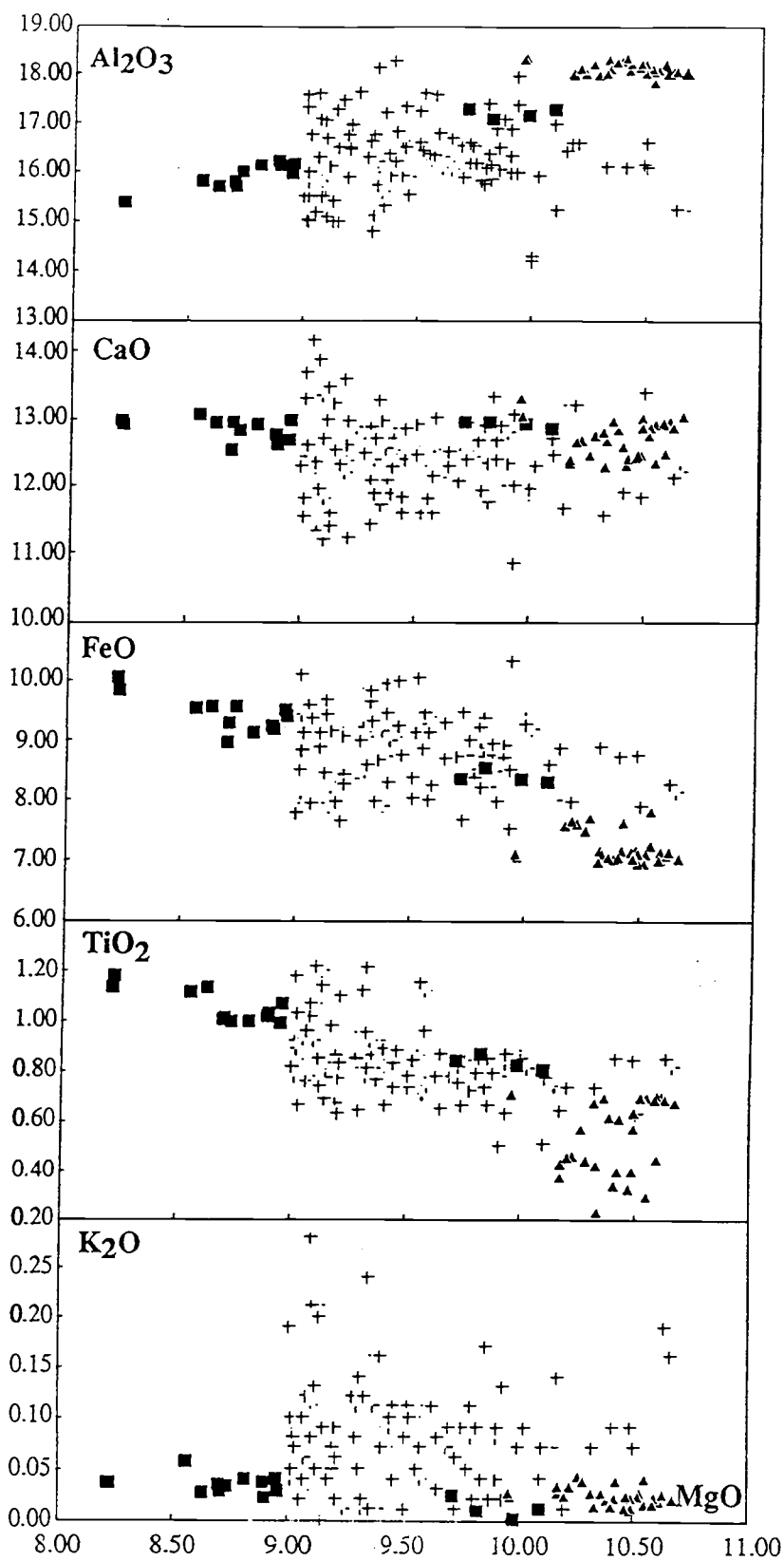


Figure III.5. Comparison of the PL13 1270°C inclusion (closed triangles) and pillow-rim glass compositions (closed squares) to primitive MORB glasses (from Elthon, 1990) (crosses).

seamount lavas are systematically more primitive and more LREE depleted (Allan et al., 1989) and may have formed at shallower depths (Batiza et al., 1990). Though the evidence is circumstantial, the similarities suggest that the Lamont Seamounts and the PL13 lavas were derived by similar processes.

#### *Possible mantle source*

The low  $\text{TiO}_2$  and the refractory mineral assemblage (high-temperature plagioclase) of PL13 lavas suggest that they may be a product of partial melting of a previously melted mantle source (Duncan and Green, 1980). However, the PL13 inclusions differ from most primitive tholeiites in that they are saturated not with olivine as is most common for MORB, but also plagioclase and spinel at low pressure. Kinzler and Grove (1992) have shown that a mantle containing olivine, clinopyroxene, spinel, and plagioclase can produce a liquid saturated with olivine, plagioclase, and spinel at pressures shallower than 10kb. Shallower than this depth, the location of the multiple-saturation surface is independent of pressure and ascending magmas will remain saturated with olivine, plagioclase, and spinel. Clinopyroxene will drop from the liquidus as pressure decreases (Bender et al., 1978; Kinzler and Grove, 1992). If the primary PL13 liquid were produced from a somewhat refractory mantle source, then the presence of plagioclase in the source requires that it segregated at relatively low pressure (<15kb) (e.g., Bender et al., 1978; Elthon and Scarfe, 1984).

#### *High $\text{CaO-Al}_2\text{O}_3$ Magmas as a MORB End Member*

The primitive (high MgO) character of the melt inclusions and glass rims of the ultraphyric pillows indicate that these liquids experienced a relatively short residence time in the crust and were not subjected to mixing or crystallization processes in axial magma chambers. Since the inclusions are also near-primary with  $\text{MgO} \sim 10.5\%$  MgO (Fig. III.5), they represent a distinct compositional subset of primitive MORB and are

parental to more evolved melts (i.e., the sparsely-phyric glasses) whose compositions lie within the observed global range of MORB compositions (Fig. III.5). We believe that the primary antecedents of these high CaO-Al<sub>2</sub>O<sub>3</sub> magmas represent one of several end member components which contribute to the compositional spectrum of MORB.

#### *Minor Element Variation in Melt Inclusions*

The relatively uniform major element composition of the included glasses and the compositional uniformity of the host anorthite crystals require growth conditions which are essentially buffered (in terms of pressure, temperature, and composition) for sufficient time to accommodate the formation of large phenocrysts. At the same time, minor and presumably trace element contents are variable on a much shorter time scale. Major element homogeneity and minor element heterogeneity are not consistent with crystallization in a large, well-mixed magma chamber, as the minor elements would require periodic influxes of new magma, but the major elements require that these influxes be uniform in composition and temperature.

One possibility is that plagioclase megacrysts grow by crystal-liquid reaction in a crystal mush zone such as that envisaged by Sinton and Detrick (1992). The possibility of uniform growth of euhedral crystals by such a reaction has recently been documented by Boudier (1991). If growth occurs in the upper mantle, both crystal and liquid compositions should be effectively buffered by the bulk mineralogy of the mantle. Minor and trace elements would be free to vary, controlled essentially by local heterogeneities. One probable source of such heterogeneity might be variable amounts of trapped melt from deeper levels in the melt column.

### Conclusions

- 1) The original compositions of devitrified melt inclusions in anorthite phenocrysts from the Galápagos Platform can be obtained if they are homogenized by heating a series of crystals to temperatures spanning the liquidus temperature. Included melts are primitive, high CaO-Al<sub>2</sub>O<sub>3</sub> melts which could have been derived from a potential primary melt by only 5% fractionation of plagioclase and olivine. More evolved, sparsely-phyric lavas from the same dredge site can be related to melt inclusions by approximately 40% additional fractional crystallization of plagioclase and olivine.
- 3) These liquid compositions resemble the great majority of naturally occurring MORB compositions in many respects although they tend to be high in both CaO and Al<sub>2</sub>O<sub>3</sub>.
- 4) Anorthitic plagioclase and high CaO-Al<sub>2</sub>O<sub>3</sub>, high MgO MORB glasses occur in a variety of axial and near-ridge locations. These melts may be a product of the last stage of fractional melting of a plagioclase-spinel peridotite at shallow levels. This type of mantle may have been entrained in the Galápagos mantle plume and melted to form the PL13 melts.
- 5) High CaO-Al<sub>2</sub>O<sub>3</sub> liquids from the uppermost mantle constitute an important end-member composition contributing to a broad range of MORB compositions.
- 6) The contrasting behavior of major and minor elements potentially provides powerful constraints on the magmatic history of these MORB liquids. At present we suggest that mineral-liquid equilibria within the melting region of the upper mantle may control the major element uniformity, while mantle heterogeneities, perhaps reflecting trapped liquids from deeper in the melt column, allow for minor, and likely trace, element variability on a shorter timescale.

## References

- Allan, J.F., Batiza, R., Perfit, M.R., Fornari, D.J., and Sack, R.O., 1989, Petrology of lavas from the Lamont seamount chain and adjacent East Pacific Rise, 10 N: *Journal of Petrology*, v. 30, p. 124-89.
- Basaltic Volcanism Study Project (BVSP), 1981: New York, Pergamon Press
- Batiza, R., Niu, Y., and Zayac, U.C., 1990, Chemistry of seamounts near the East Pacific Rise; Implications for the geometry of subaxial mantle flow: *Geology*, v. 18, p. 1122-1125.
- Bender, J.F., Hodges, F.N., and Bence, A.E., 1978, Petrogenesis of basalts from the Project FAMOUS area: Experimental study from 0 to 15 kb: *Earth and Planetary Science Letters*, v. 41, p. 277-302.
- Boudier, F., 1991, Olivine xenocrysts in picritic magmas: *Contributions to Mineralogy and Petrology*, v. 109, p. 114-123.
- Christie, D.M., Duncan, R.A., McBirney, A.R., Richards, M.A., White, W.M., Harpp, K.S., and Fox, C.G., 1992, Drowned islands downstream from the Galápagos hotspot imply extended speciation times: *Nature*, v. 355, p. 246-248.
- Coombs, V.L., Nielsen, R.L., Sinton, C.W., and Christie, D.M., 1991, The nature of the parent magma of high anorthite megacrysts from the Galápagos Platform: *EOS*, v. 72, p. 579.
- Cullen, A., Vicenzi, E., and McBirney, A.R., 1989, Plagioclase-ultraphyric basalts of the Galápagos archipelago: *Journal of Volcanology and Geothermal Research*, v. 37, p. 325-337.
- Davis, A.S., and Clague, D.A., 1987, Geochemistry, mineralogy, and petrogenesis of basalt from the Gorda Ridge: *Journal of Geophysical Research*, v. 92, p. 10467-10483.
- Donaldson, C.H., and Brown, R.W., 1977, Refractory megacrysts and magnesium-rich inclusions within spinel in oceanic tholeiites: Indicators of magma mixing and parental magma composition: *Earth and Planetary Science Letters*, v. 37, p. 81-89.
- Duncan, R.A., and Green, D.H., 1980, Role of multistage melting in the formation of oceanic crust: *Geology*, v. 8, p. 22-26.
- Duncan, R.A., and Green, D.H., 1987, The genesis of second-stage melts in the formation of oceanic crust: *Contributions to Mineralogy and Petrology*, v. 96, p. 326-342.
- Dungan, M.A., and Rhodes, J.M., 1978, Residual glasses and melt inclusions in basalts from DSDP Legs 45 and 46: Evidence for magma mixing: *Contributions to Mineralogy and Petrology*, v. 67, p. 417-431.
- Elthon, D., 1990, The petrogenesis of primary mid-ocean ridge basalts: *Reviews in Aquatic Sciences*, v. 2, p. 27-53.

- Elthon, D. and Scarfe, C.M., 1984, High pressure phase equilibria of high-magnesian basalt and the genesis of primary oceanic basalts: *American Mineralogist*, v. 69, p. 1-15.
- Falloon, T.J., and Green, D.H., 1986, Glass inclusions in magnesian olivine phenocrysts from Tonga: evidence for highly refractory parental magmas in the Tongan arc: *Earth and Planetary Science Letters*, v. 84, p. 95-103.
- Fornari, D.J., Perfit, M.R., Allan, J.F., Batiza, R., Haymon, R., Barone, A., Ryan, W.B.F., Smith, T., Simkin, T., and Luckman, M.A., 1988, Geochemical and structural studies of the Lamont seamounts as indicators of mantle processes: *Earth and Planetary Science Letters*, v. 86, p. 63-83.
- Frey, F.A., Bryan, W.B., and Thompson, G., 1974, Atlantic ocean seafloor: geochemistry and petrology of basalts from Legs 2 and 3 of the Deep Sea Drilling Program, *Journal of Geophysical Research*, v. 79, p. 5507- .
- Humphris, S.E., Thompson, G., Schilling, J-G., and Kingsley, R.H., 1985, Petrological and geochemical variations along the Mid-Atlantic Ridge between 46°S and 32°S: Influence of the Tristan da Cunha mantle plume: *Geochimica et Cosmochimica Acta*, v. 49, p. 1445-1464.
- Jakobssen, S.P., Jonsson, J., and Shido, F., 1978, Petrology of the Western Reykjanes Peninsula, Iceland: *Journal of Petrology*, v. 19, v. 669-705.
- Kinzler, R.J., and Grove, T.L., 1992, Primary magmas of mid-ocean ridge basalts I: Experiments and methods: *Journal of Geophysical Research*, v. 97, p. 6885-6906.
- Marsh, B.D., Fournelle, J., Myers, J.D., and Chou, I.M., 1990, On plagioclase thermometry in island arcs: Experiments and theory, *in* Spencer, R.J., and Chou, I.M. eds., *Fluid-Mineral Interactions: A Tribute to H.P. Eugster*: The Geochemical Society, Spec. Publ. 2.
- Natland, J.H., and Melson, W.G., 1980, Compositions of basaltic glasses from the East Pacific Rise and Siquieros Fracture Zone near 9°N, Initial Reports of the Deep Sea Drilling Project, v. 54, p. 705-723.
- Natland, J.H., Adamson, A.C., Laverne, C., Melson, W.G., and O'Hearn, T., 1983, A compositionally nearly steady-state magma chamber at the Costa Rica Rift: evidence from basalt glass and mineral data DSDP 501, 504, 505, Initial Reports of the Deep Sea Drilling Project, v. 69, v. 11, p. 811-825.
- Price, R.C., Kennedy, A.K., Riggs-Sneeringer, M., and Frey, F.A., 1986, Geochemistry of basalts from the Indian Ocean triple junction: implications for the generation and evolution of Indian Ocean ridge basalts: *Earth and Planetary Science Letters*, v. 78, p. 379-396.
- Roeder, P.L., and Emslie, R.F., 1970, Olivine-liquid equilibrium: *Contributions to Mineralogy and Petrology*, v.29, p. 275-289.
- Sinton, J.M. and Detrick, R.D., 1992, Mid-ocean ridge magma chambers: *Journal of Geophysical Research*, v. 97, p. 197-216.
- Shimizu, N., 1992, Geochemical significance of glass inclusions in MORB: V.M. Goldschmidt Conference, Programs and Abstracts, The Geochemical Society.



Sobolev, A.V., Danyushevskiy, L.V., Dmitriyev, L.V., and Sushchevskaya, N.M., 1989, High-alumina magnesian tholeiite as the primary basalt magma at midocean ridge: *Geochemical International*, v. 26, p. 128-133.

Vicenzi, E., 1990, Partly crystallized melt inclusions in plagioclase megacrysts: Textural and compositional constraints on the origin of feldspar-rich basalt, Ph.D. thesis, Rennselaer Polytechnic Institute.

Vicenzi, E.P., McBirney, A.R., White, W.M., and Hamilton, M., 1990, The geology and geochemistry of Isla Marchena, Galápagos Archipelago: an ocean island adjacent to a mid-ocean ridge, *Journal of Volcanology and Geothermal Research*, v. 40, p. 291-315.

Watson, E.B., 1976, Glass inclusions as samples of early magmatic liquid: Determinative method and application to south Atlantic basalt: *Journal of Volcanology and Geothermal Research*, v. 1, p. 73-84.

White, W.M., McBirney, A.R., and Duncan, R.A., 1992, Petrology and geochemistry of the Galápagos Islands: Portrait of a pathological mantle plume, submitted.

#### IV. Conclusion

Previous geological studies of the Galápagos Platform have relied solely on the data gathered from the Galápagos Islands. The goal of the 1990 PLUME2 expedition of the R/V Thomas Washington was to expand the existing database by dredging, mapping, and surveying the gravity of some of the submarine features of the Galápagos platform. In this thesis, some of the results from these efforts are presented.

The data presented here, in conjunction with the existing island data and some of the other PLUME2 results (Harpp et al., 1990; Feighner and Richards, 1992) suggest that there are two separate volcanic mechanisms that have produced the present Galápagos platform. The first is directly related to the Galápagos hotspot. The central portion of the platform and the Carnegie Ridge appear to be caused by volcanism from a rising mantle plume. Volcanism begins on the western edge of the platform and can continue erupting for at least 2 Ma (e.g., San Cristobal island). At present, the geochemical patterns that are displayed by the islands are best explained by existing models in which the mantle plume incorporates upper asthenospheric material by thermal entrainment (Geist et al., 1988; White et al., 1992). Rocks from seamounts and drowned islands on the eastern platform and Carnegie Ridge display ages progressively older toward the east, thus agreeing with the island data and supporting the hotspot hypothesis for the formation of these features. The ages are used to estimate the velocity of the Nazca plate over the hotspot which has apparently decreased from approximately 75 mm/yr between 11 and 5 Ma to 37 mm/yr for the past 3 Ma (these data and Gripp and Gordon, 1990). The relative depletion in  $\text{TiO}_2$  in lavas older than 5 Ma compared to those that are younger than 5 Ma may record the coincidence of the hotspot with the GSC, at which point lavas with an increasing MORB component would have been expected to erupt. The apparent change in the plate

velocity and the northward migration of the GSC at 5 Ma indicate a significant reshuffling of the regional plate tectonic environment.

The second volcanic mechanism is responsible for the production of the volcanoes that lie to the north of the central platform. These include islands and seamounts along the Wolf-Darwin lineament, the northern islands of Pinta, Marchena, and Genovesa, and the northeastern seamounts. It is suggested here that volcanism in this area is predominantly a product of mantle upwelling associated with lithospheric fractures and thermal input from the Galápagos plume. These fractures are a result of regional tectonic stresses that form the pronounced NW-SE and E-W trending lineations that appear to be caused by ridge tectonic processes. The lavas from these volcanoes are generally MORB-like and lack the compositional variability characteristic of volcanoes on the central platform. Lavas and melt inclusions in high-An plagioclase from one of the northeastern seamounts (dredge PL13) are similar to other primitive, high  $\text{CaO-Al}_2\text{O}_3$  magmas found at ridge axes and off-axis seamounts, indicating that at least this seamount was formed by processes more typical of mid-ocean ridge settings.

Volcanism along the Wolf-Darwin lineament is isotopically heterogeneous (Harpp et al., 1990). Likewise, lavas from Pinta, Marchena, and Genovesa are distinct both isotopically and in terms of REE patterns (White et al., 1992). These heterogeneities may be a reflection of a heterogeneous mantle below the northern volcanoes. The mantle heterogeneities may be inherent in the upper mantle due to deep seated mixing of plume mantle with the upwelling mantle at the GSC.

There are many ideas that have been presented in this thesis, but, due to the constraints of time that can be allotted to a Masters thesis, these ideas are not as well

developed as they could be. However, it is useful, at least, to recognize some of the remaining questions:

- (1) The decreasing plate velocity will allow a greater accumulation of material from the hotspot, assuming that the flux of material remains constant over time. Can this be examined by estimating the volume proportions over time?
- (2) The history of ridge migration and its relevance to Galápagos volcanism can be more thoroughly examined. This includes temporal "snapshots", where the positions of volcanoes on the platform and the GSC are modeled for each time interval (1 Ma). This could be done assuming either a gradual migration of the GSC northward or a sudden ridge jump.
- (3) A more concise model for the genesis of the northern islands needs to be developed. This would include estimation of melting parameters, such as the depth and degree of melting. What are the conditions needed to produce these melts?
- (4) Plagioclase-ultraphyric basalts are found on all of the northern islands and most of the seamounts. Though the morphology of the megacrysts are similar (size, melt inclusions, homogeneous core), the An content varies between ~80% to 92%. There must be some physical process that is common to the evolution of these lavas, there are variables that determine An content (volatiles, pressure, temperature, magma composition) that must be different. Knowing the volatile content of the inclusions and the pillow-rim glasses would be invaluable.
- (5) Are there similar trends in the inclusions from other plagioclase-ultraphyric lavas from the platform?

## BIBLIOGRAPHY

- Allan, J.F., Batiza, R., Perfit, M.R., Fornari, D.J., and Sack, R.O., 1989, Petrology of lavas from the Lamont seamount chain and adjacent East Pacific Rise, 10 N: *Journal of Petrology*, v. 30, p. 124-89.
- Batiza, R., Niu, Y., and Zayac, U.C., 1990, Chemistry of seamounts near the East Pacific Rise; Implications for the geometry of subaxial mantle flow: *Geology*, v. 18, p. 1122-1125.
- Boudier, F., 1991, Olivine xenocrysts in picritic magmas: *Contributions to Mineralogy and Petrology*, v. 109, p. 114-123.
- Castillo, P.R., Batiza, R., Sinton, C.W., and Duncan, R.A., in prep., Anomalously young volcanoes on an old hotspot trace, 2. Petrology and isotope geochemistry of the Cocos Ridge and related seamounts.
- Christie, D.M., Duncan, R.A., McBirney, A.R., Richards, M.A., White, W.M., Harpp, K.S., and Fox, C.G., 1992, Drowned islands downstream from the Galápagos hotspot imply extended speciation times: *Nature*, v. 355, p. 246-248.
- Coombs, V.L., Nielsen, R.L., Sinton, C.W., and Christie, D.M., 1991, The nature of the parent magma of high anorthite megacrysts from the Galápagos Platform: *EOS*, v. 72, p. 579.
- Cox, A and Dalrymple, G.B., 1966, Paleomagnetism and potassium-argon ages of some volcanic rocks from the Galápagos Islands, *Nature*, v. 209, p. 776-777.
- Bender, J.F., Hodges, F.N., and Bence, A.E., 1978, Petrogenesis of basalts from the Project FAMOUS area: Experimental study from 0 to 15 kb: *Earth and Planetary Science Letters*, v. 41, p. 277-302.
- Cullen, A., Vicenzi, E., and McBirney, A.R., 1989, Plagioclase-ultraphyric basalts of the Galápagos archipelago: *Journal of Volcanology and Geothermal Research*, v. 37, p. 325-337.
- Dalrymple, G.B. and Lanphere, M.A., 1969, *Potassium argon dating: principles, techniques, and application to geochronology*, W.H. Freeman, New York, 258 pp.
- Davis, A.S., and Clague, D.A., 1987, Geochemistry, mineralogy, and petrogenesis of basalt from the Gorda Ridge: *Journal of Geophysical Research*, v. 92, p. 10467-10483.
- Donaldson, C.H., and Brown, R.W., 1977, Refractory megacrysts and magnesium-rich inclusions within spinel in oceanic tholeiites: Indicators of magma mixing and parental magma composition: *Earth and Planetary Science Letters*, v. 37, p. 81-89.
- Donnelly, T.W., Beets, D., Carr, M.J., Jackson, T., Klaver, G., Lewis, J., Maury, R., Schellenkens, H., Wadge, G., and Westercamp, D., 1990 History and tectonic setting of Caribbean magmatism, in *The Caribbean Region*, Dengo, G. and Case, J.E. (eds.), Geological Society of America, Boulder, CO, vol. H. p. 339-374.
- Duncan, R.A., and Green, D.H., 1980, Role of multistage melting in the formation of oceanic crust: *Geology*, v. 8, p. 22-26.

Duncan, R.A., and Green, D.H., 1987, The genesis of second-stage melts in the formation of oceanic crust: *Contributions to Mineralogy and Petrology*, v. 96, p. 326-342.

Duncan, R.A. and Hargraves, R.B., 1984, Plate tectonic evolution of the Caribbean region in the mantle reference frame, in *The Caribbean-South American plate boundary and regional tectonics*, Bonini, W.E., Hargraves, R.B., and Shagam, R. (eds.), Geological Society of America Memoir 162, Boulder, CO.

Duncan, R.A. and Hargraves, R.B., 1990,  $^{40}\text{Ar}$ - $^{39}\text{Ar}$  geochronology of basement ages from the Mascarene plateau, Chagos Bank, and the Maldives Ridge, *Proc. ODP Sci. Results*, v. 115, Ocean Drilling Program, p. 43-51.

Duncan, M.A., and Rhodes, J.M., 1978, Residual glasses and melt inclusions in basalts from DSDP Legs 45 and 46: Evidence for magma mixing: *Contributions to Mineralogy and Petrology*, v. 67, p. 417-431.

Elthon, D., 1990, The petrogenesis of primary mid-ocean ridge basalts: Reviews in *Aquatic Sciences*, v. 2, p. 27-53.

Elthon, D. and Scarfe, C.M., 1984, High pressure phase equilibria of high-magnesian basalt and the genesis of primary oceanic basalts: *American Mineralogist*, v. 69, p. 1-15.

Falloon, T.J., and Green, D.H., 1986, Glass inclusions in magnesian olivine phenocrysts from Tonga: evidence for highly refractory parental magmas in the Tongan arc: *Earth and Planetary Science Letters*, v. 84, p. 95-103.

Feighner, M.A. and Richards, M.A., 1992, Lithospheric structure and compensation mechanisms of the Galápagos Archipelago, *Journal of Geophysical Research*, submitted.

Fornari, D.J., Perfit, M.R., Allan, J.F., Batiza, R., Haymon, R., Barone, A., Ryan, W.B.F., Smith, T., Simkin, T., and Luckman, M.A., 1988, Geochemical and structural studies of the Lamont seamounts as indicators of mantle processes: *Earth and Planetary Science Letters*, v. 86, p. 63-83.

Frey, F.A., Bryan, W.B., and Thompson, G., 1974, Atlantic ocean seafloor: geochemistry and petrology of basalts from Legs 2 and 3 of the Deep Sea Drilling Program, *Journal of Geophysical Research*, v. 79, p. 5507- .

Geist, D.J., White, W.M., and Duncan, R.A., 1986, Geology and petrogenesis of lavas from San Cristobal Island, Galápagos Archipelago, *Geological Society of America Bulletin*, v. 97, p. 555-566.

Geist, D.J., White, W.M., and McBirney, A.R., 1988, Plume-asthenosphere mixing beneath the Galápagos, *Nature*, v. 333, p. 657-660.

Griffiths, R.W., 1986, The differing effects of composition and thermal buoyancies on the evolution of mantle diapirs, *Physics of Earth and Planetary Interiors*, v. 43, p. 261-273.

Gripp, A.E. and Gordon, R.G., 1990, Current plate velocities relative to hotspots incorporating the NUVEL-1 global plate model, *Geophysical Research Letters*, v. 17, p. 1,109-1,112.

Harpp, K., White, W.M., and Duncan, R.A., 1990, Geochemistry of the Wolf-Darwin lineament and ridge-plume interaction in the Galápagos, Geological Society of Australia Absts., v. 27, p. 44.

Hey, R., 1977, Tectonic evolution of the Cocos-Nazca spreading center, Geological Society of America Bulletin, v. 88, p. 1404-1420.

Hey R., Johnson, G.L., and Lowrie, A., 1977, Recent plate motions in the Galápagos area, Geological Society of America Bulletin, v. 88, p. 1385-1403.

Humphris, S.E., Thompson, G., Schilling, J-G., and Kingsley, R.H., 1985, Petrological and geochemical variations along the Mid-Atlantic Ridge between 46°S and 32°S: Influence of the Tristan da Cunha mantle plume: *Geochimica et Cosmochimica Acta*, v. 49, p. 1445-1464.

Jakobssen, S.P., Jonsson, J., and Shido, F., 1978, Petrology of the Western Reykjanes Peninsula, Iceland: *Journal of Petrology*, v. 19, p. 669-705.

Johnson, G.L. and Lowrie, A., 1972, Cocos and Carnegie ridges result of Galápagos "hotspot", *Earth and Planetary Science Letters*, v. 14, p. 279-280.

Kinzler, R.J., and Grove, T.L., 1992, Primary magmas of mid-ocean ridge basalts I: Experiments and methods: *Journal of Geophysical Research*, v. 97, p. 6885-6906.

Kunk, M.J., Sutter, J.F., and Naeser, C.W., 1985, High precision  $^{40}\text{Ar}$ - $^{39}\text{Ar}$  ages of sanidine, biotite, hornblende, and plagioclase from the Fish Canyon Tuff, San Juan volcanic field, south central Colorado, Geological Society of America Absts., v. 17(7), p. 636.

Marsh, B.D., Fournelle, J., Myers, J.D., and Chou, I.M., 1990, On plagioclase thermometry in island arcs: Experiments and theory, *in* Spencer, R.J., and Chou, I.M. eds., *Fluid-Mineral Interactions: A Tribute to H.P. Eugster*: The Geochemical Society, Spec. Publ. 2.

McBirney, A.R. and Williams H., 1969, Geology and petrology of the Galápagos Islands, Geological Society of America Memoir 118, 197 pp.

McBirney, A.R., Cullen, A.B., Geist, D., Vicenzi, E.P., Duncan, R.A., Hall, M.L., and Estrella, M., 1985, The Galápagos Volcano Alcedo: a unique ocean caldera, *Journal of Volcanology and Geothermal Research*, v. 26, p. 173-177.

Morgan, W.J., 1971, Convection plumes in the lower mantle, *Nature*, v. 230, p. 42-43.

Morgan, W. J., 1972, Deep mantle convection plumes and plate motion, *American Association of Petroleum Geologists Bulletin*, v. 56, p. 203-213.

Natland, J.H., and Melson, W.G., 1980, Compositions of basaltic glasses from the East Pacific Rise and Siquieros Fracture Zone near 9°N, *Initial Reports of the Deep Sea Drilling Project*, v. 54, U.S. Government Printing Office (Washington), p. 705-723.

Natland, J.H., Adamson, A.C., Laverne, C., Melson, W.G., and O'Hearn, T., 1983, A compositionally nearly steady-state magma chamber at the Costa Rica Rift: evidence from basalt glass and mineral data DSDP 501, 504, 505, Initial Reports of the Deep Sea Drilling Project, v. 69, U.S. Government Printing Office (Washington), v. 11, p. 811-825.

Price, R.C., Kennedy, A.K., Riggs-Sneeringer, M., and Frey, F.A., 1986, Geochemistry of basalts from the Indian Ocean triple junction: implications for the generation and evolution of Indian Ocean ridge basalts: *Earth and Planetary Science Letters*, v. 78, p. 379-396.

Richards, M., Duncan, R.A., and Courtillot, V., 1989, Flood basalts and hot-spot tracks: plume heads and tails, *Science*, 246:103-107.

Richards, M.A. and Griffiths, R.W., 1989, Thermal entrainment by deflected plumes, *Nature*, v. 342, p. 900-902.

Samson, S.D. and Alexander, E.C. Jr, 1987, Calibration of the inter-laboratory  $^{40}\text{Ar}/^{39}\text{Ar}$  dating standard MMhb-1, *Chemical Geology*, v. 66, p. 27-34.

Schilling, 1973, Icelandic mantle plume: geochemical evidence along the Reykjanes ridge, *Nature*, 242: 565-571.

Schilling, J-G., Kingsley, R.H., and Devine, J.D., 1982, Galápagos hotspot-spreading center system 1. spatial, petrological, and geochemical variations (83W-101W), *Journal of Geophysical Research*, 87, 5593-5610.

Seidemann, D.E., 1978,  $^{40}\text{Ar}/^{39}\text{Ar}$  studies of deep sea igneous rocks, *Geochimica et Cosmochimica Acta*, v. 42, p. 1721-1734.

Sinton, C.W. and Duncan, R.A., 1992, Temporal evolution of the Caribbean Cretaceous Basalt Province: Results from  $^{40}\text{Ar}$ - $^{39}\text{Ar}$  dating, *EOS Trans. Am. Geophys. Union*, v. 73, p. 352.

Sinton, J.M. and Detrick, R.D., 1992, Mid-ocean ridge magma chambers: *Journal of Geophysical Research*, v. 97, p. 197-216.

Shimizu, N., 1992, Geochemical significance of glass inclusions in MORB: V.M. Goldschmidt Conference, Programs and Abstracts, The Geochemical Society.

Sobolev, A.V., Danyushevskiy, L.V., Dmitriyev, L.V., and Sushchevskaya, N.M., 1989, High-alumina magnesian tholeiite as the primary basalt magma at midocean ridge: *Geochemical International*, v. 26, p. 128-133.

van Andel, Tj H., Heath, G.R., Malfait, B.T., Heinrichs, D.F., and Ewing, J.I., 1971, Tectonics of the Panama Basin, eastern equatorial Pacific, *Geological Society of America Bulletin*, v. 82, p. 1489-1504.

Verma, S.P. and Schilling, J-G., 1982, Galápagos hotspot-spreading center system, 2.  $^{87}\text{Sr}/^{86}\text{Sr}$  and large ion lithophile element variations, *Journal of Geophysical Research*, v. 92, p. 13,687-13,707.



Vicenzi, E., 1990, Partly crystallized melt inclusions in plagioclase megacrysts: Textural and compositional constraints on the origin of feldspar-rich basalt, Ph.D. thesis, Rensselaer Polytechnic Institute.

Vicenzi, E.P., McBirney, A.R., White, W.M., and Hamilton, M., 1990, The geology and geochemistry of Isla Marchena, Galápagos Archipelago: an ocean island adjacent to a mid-ocean ridge, *Journal of Volcanology and Geothermal Research*, v. 40, p. 291-315.

Watson, E.B., 1976, Glass inclusions as samples of early magmatic liquid: Determinative method and application to south Atlantic basalt: *Journal of Volcanology and Geothermal Research*, v. 1, p. 73-84.

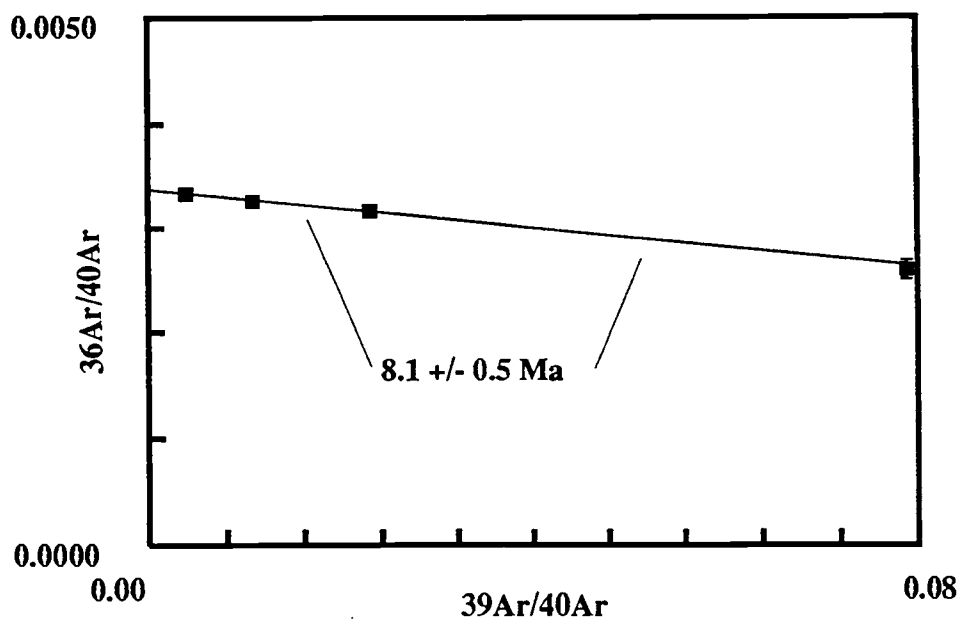
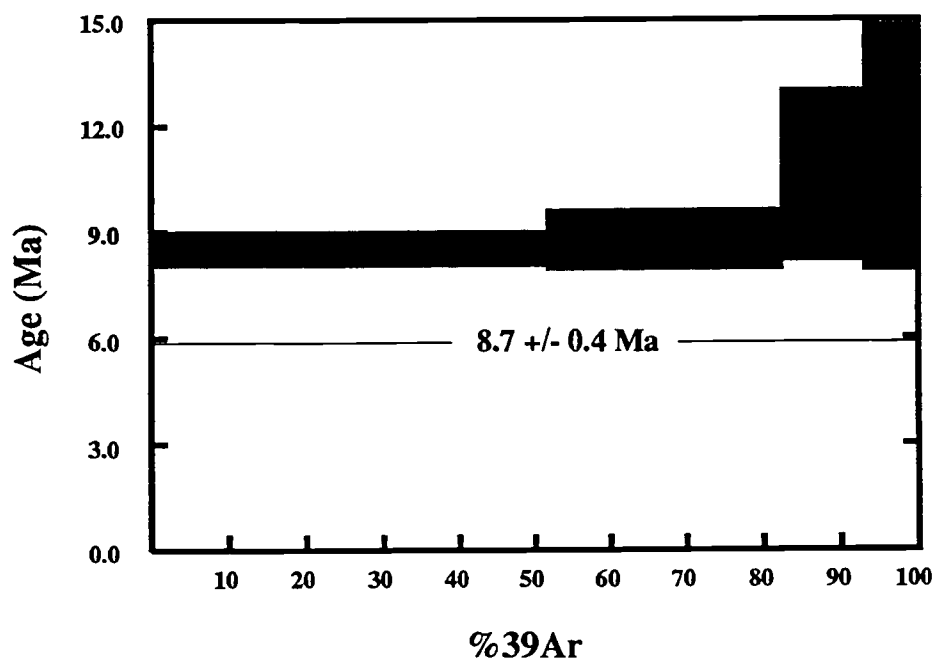
White, W.M. and Hoffman, A.W., 1978, Geochemistry of the Galápagos Islands: implications for mantle dynamics and evolution, *Carnegie Institute of Washington Yearbook*, v. 77, p. 548-562.

White, W.M., McBirney, A.R., and Duncan, R.A., 1992, Petrology and geochemistry of the Galápagos Islands: Portrait of a pathological mantle plume, submitted.

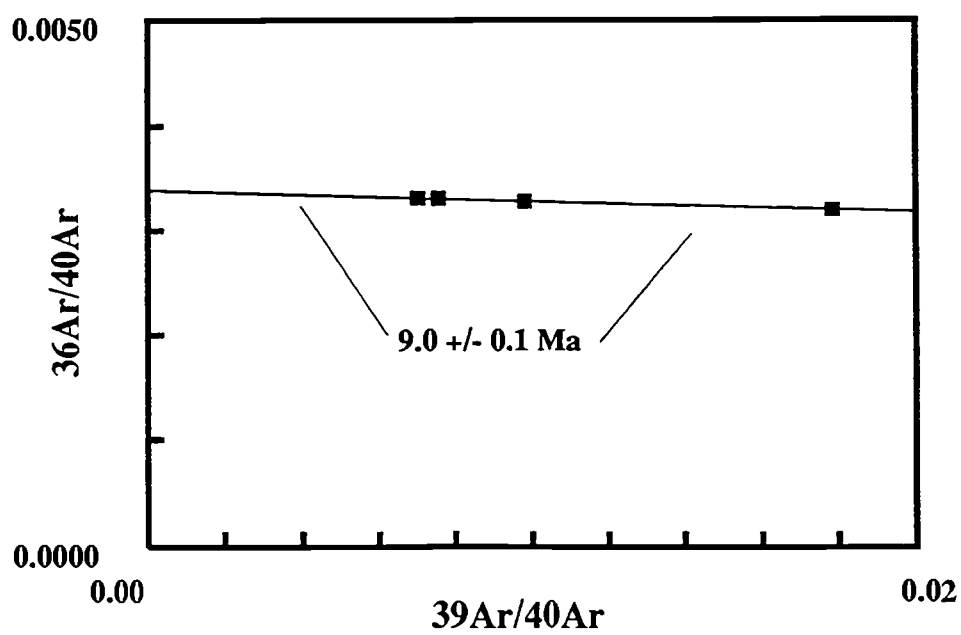
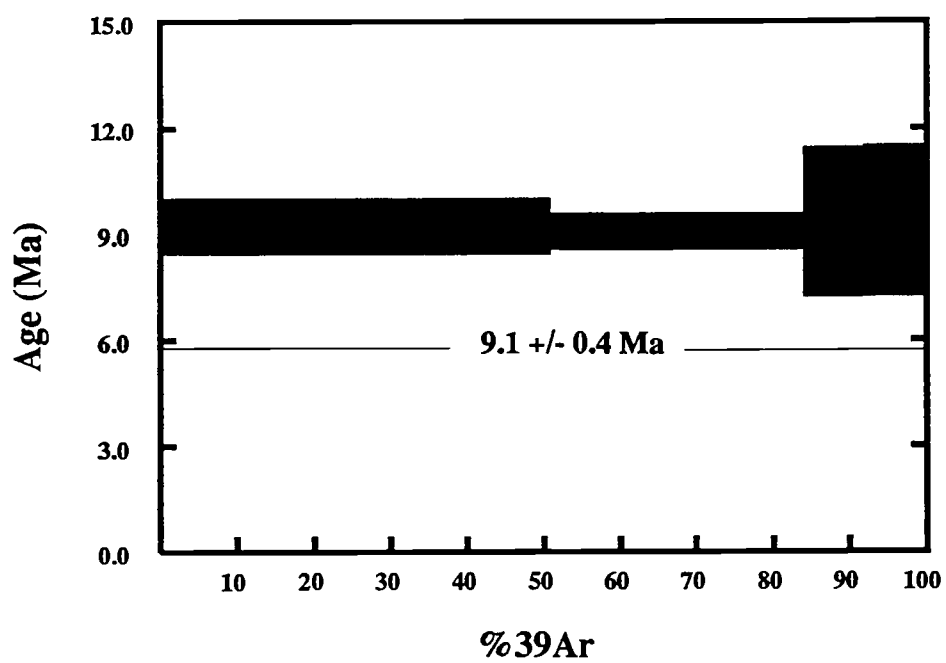
## **APPENDICES**

**APPENDIX 1: Age Spectrum and Correlation Diagrams**

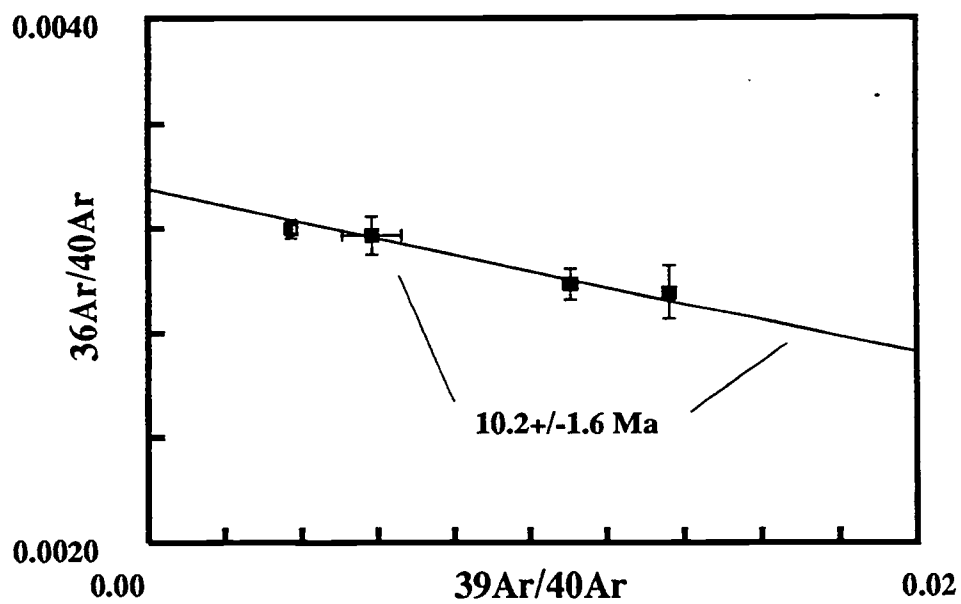
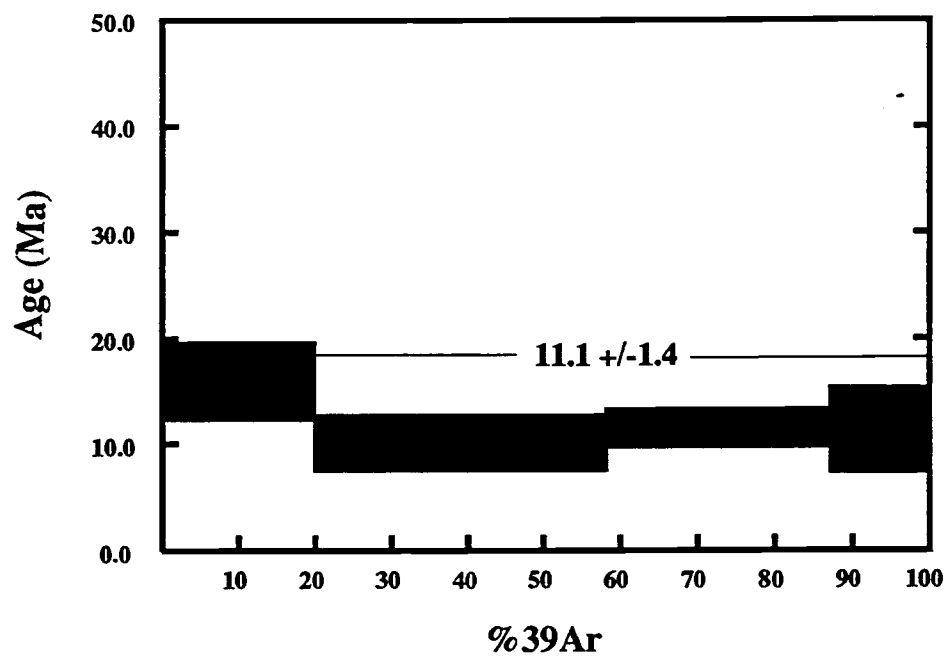
## Galapagos basalt PL1-12



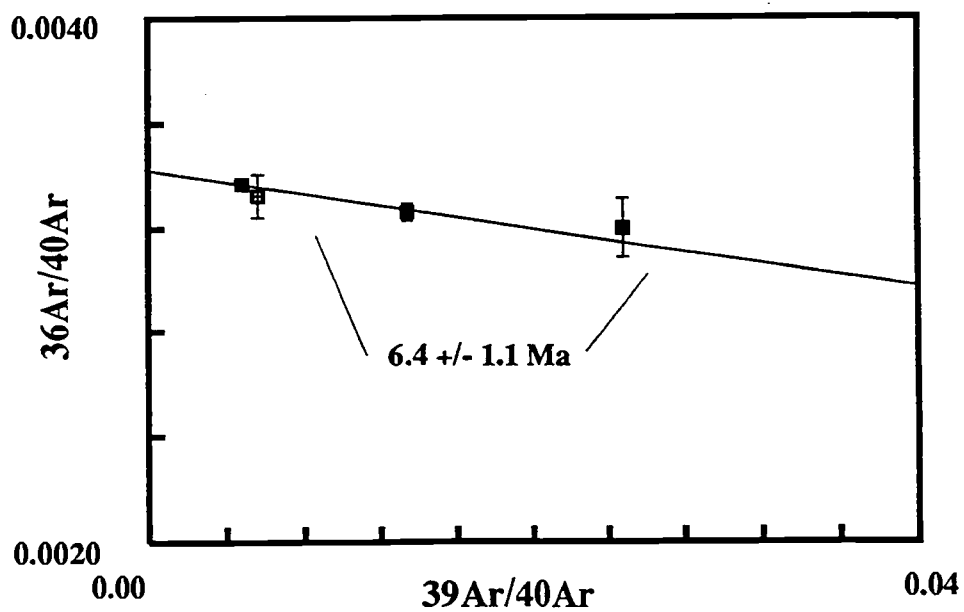
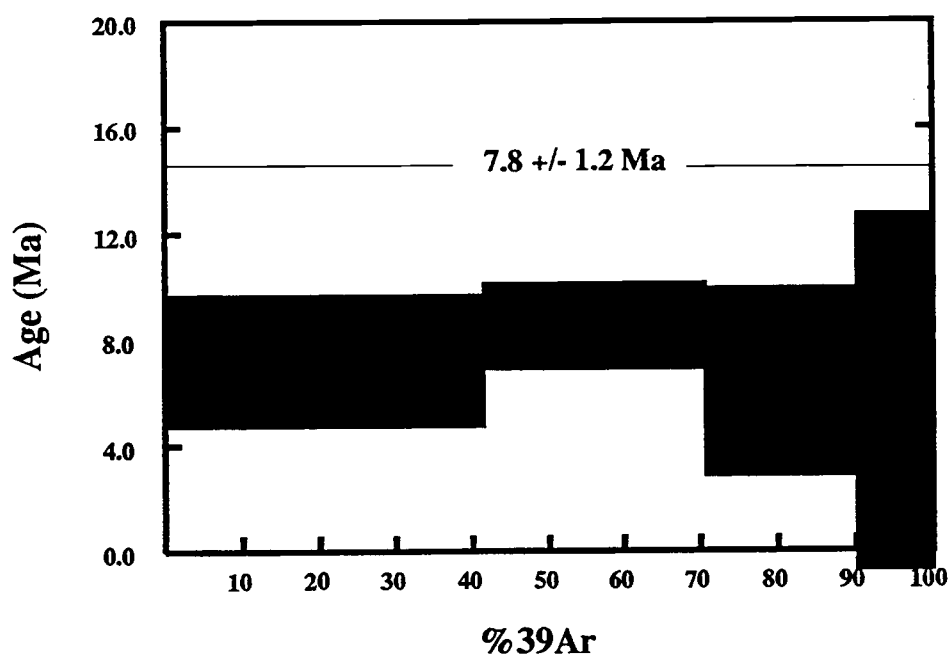
## Galapagos basalt PL1-46



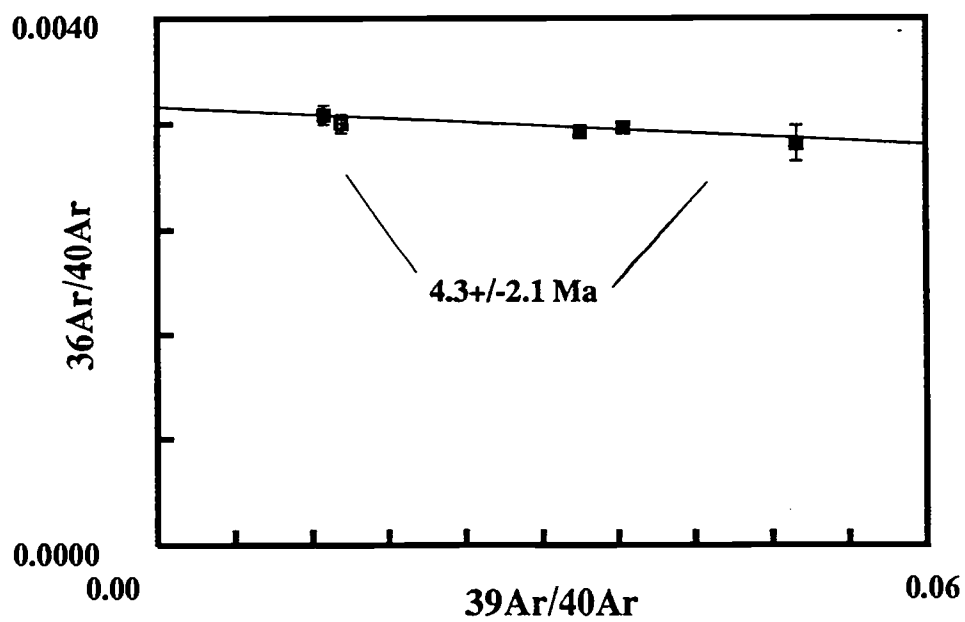
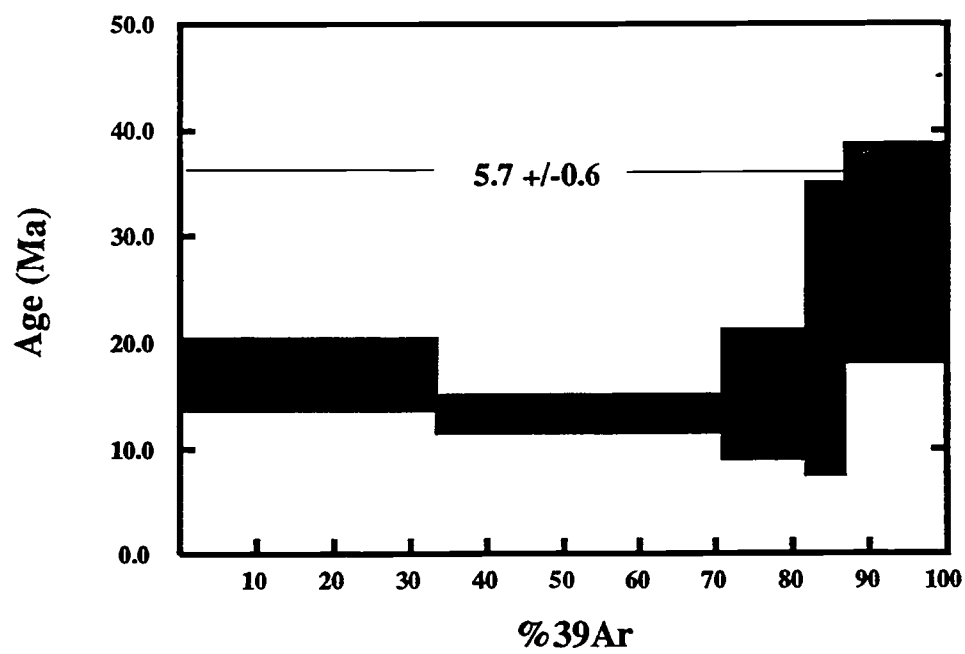
## Galapagos basalt PL2-2



## Galapagos basalt PL4-19

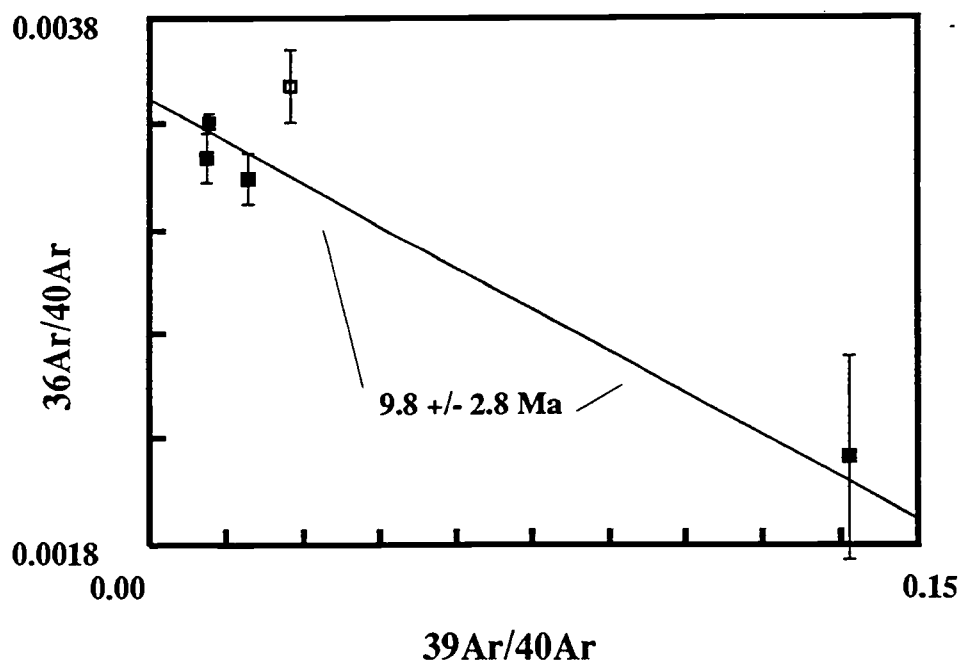
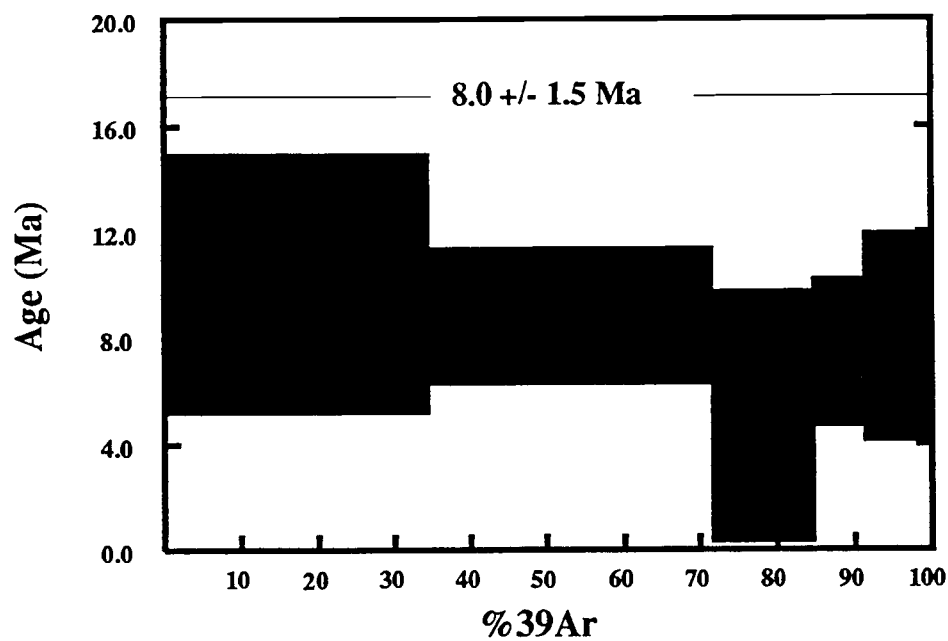


## Galapagos basalt PL2-9-50

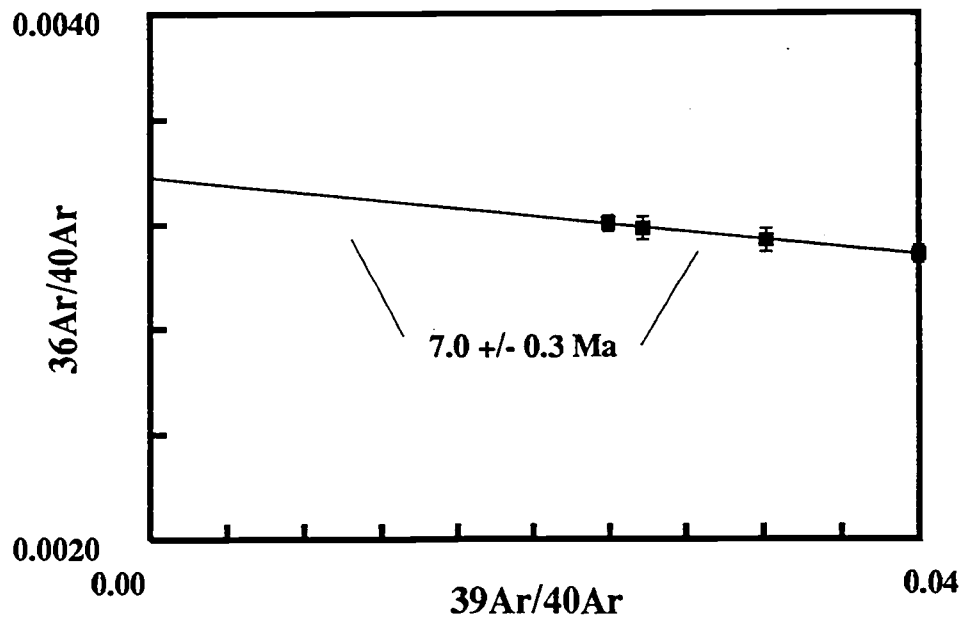
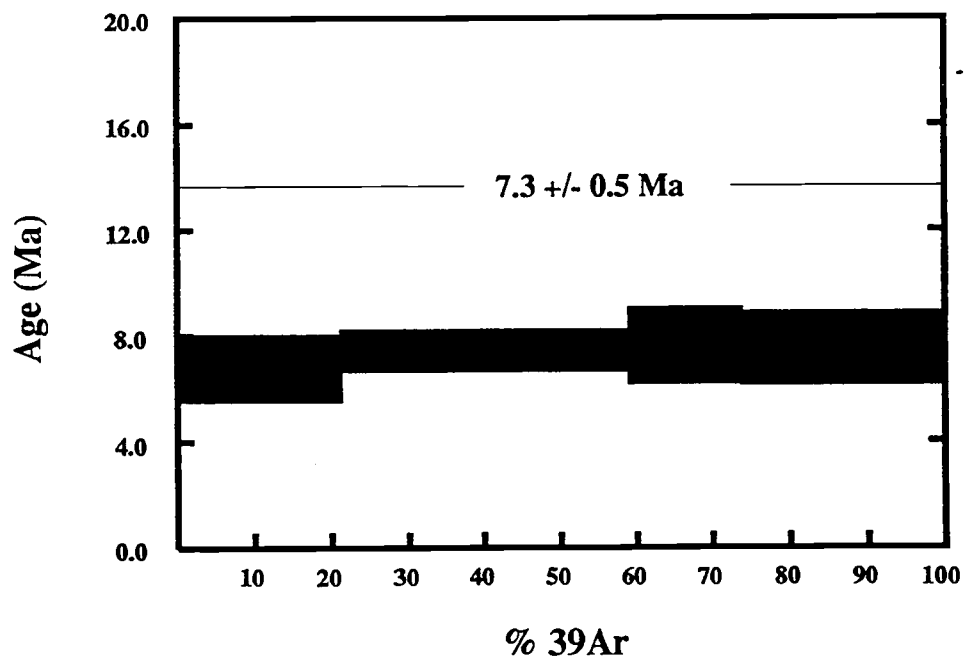




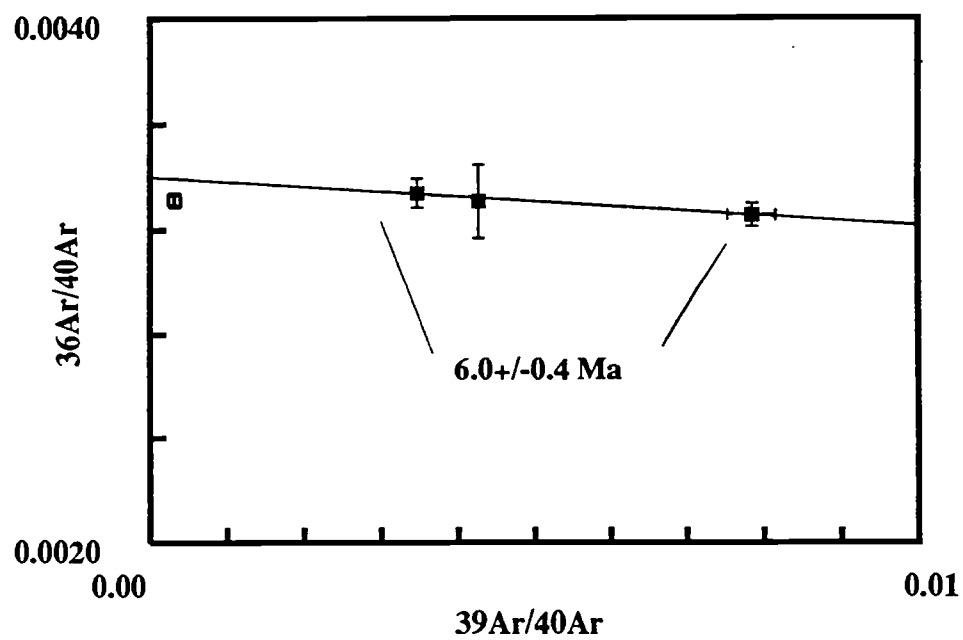
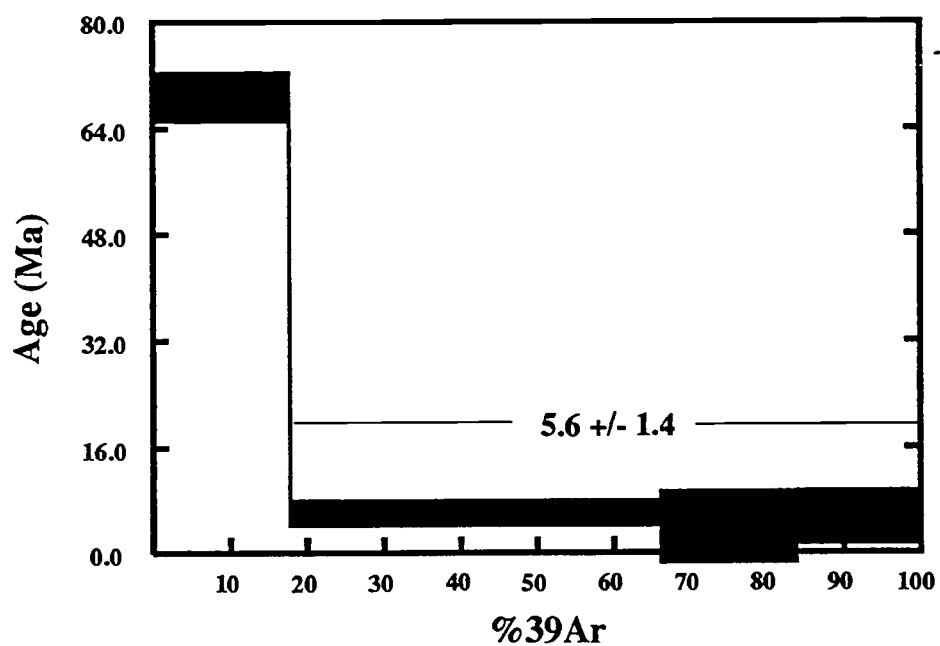
## Galapagos basalt PL5-1



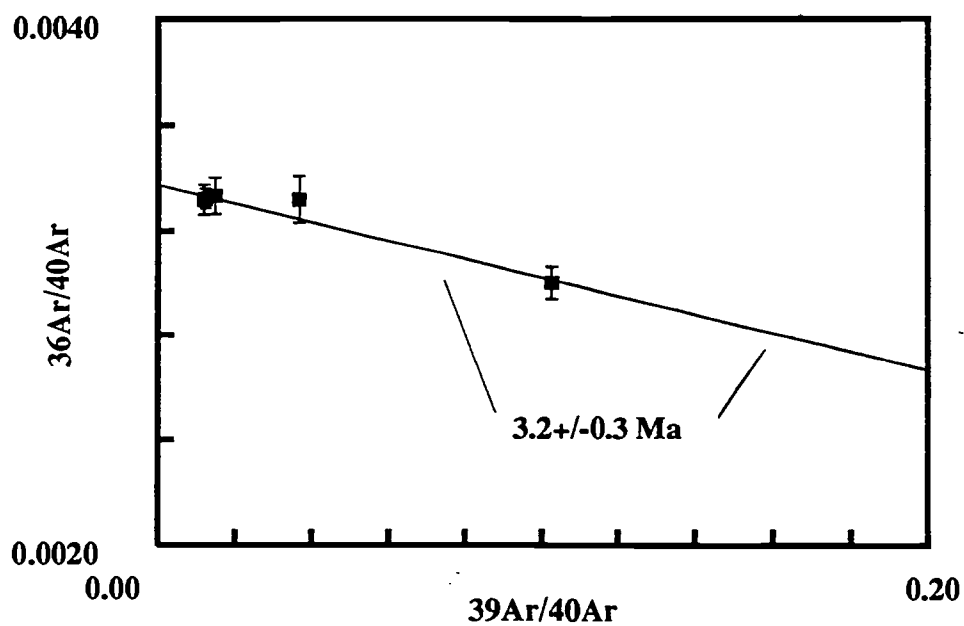
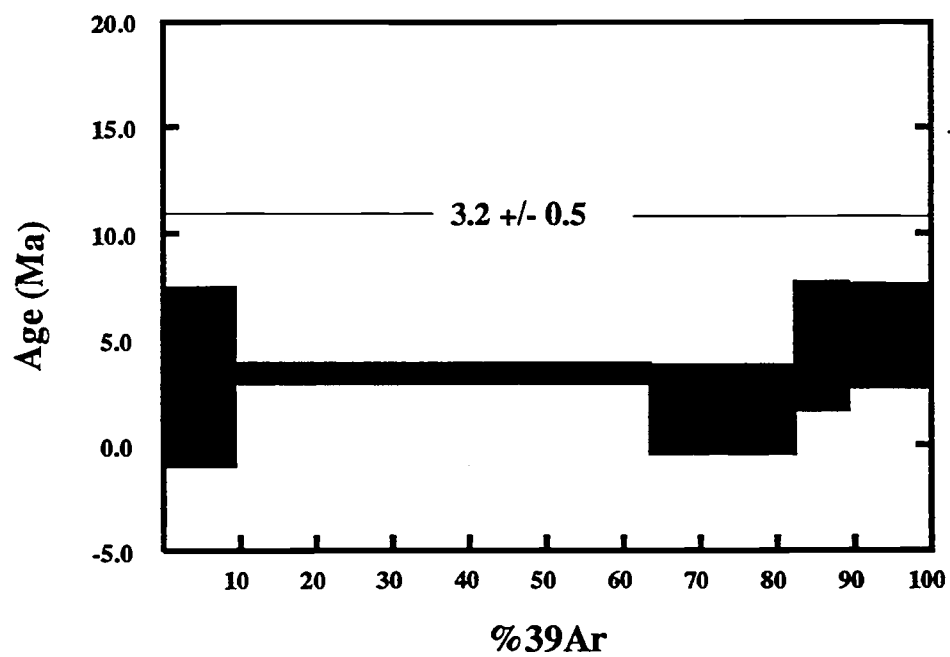
## Galapagos basalt PL8-1



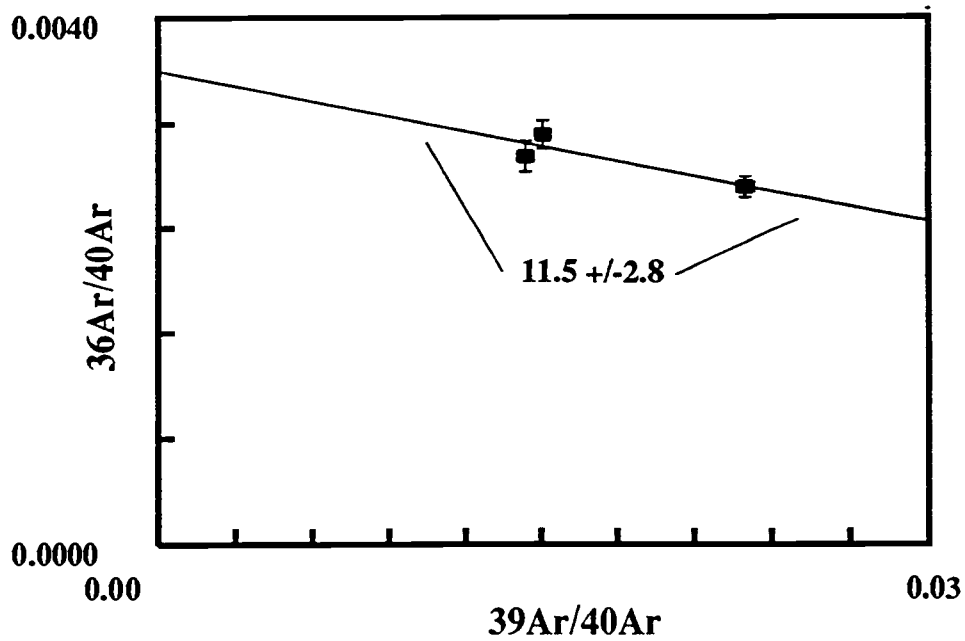
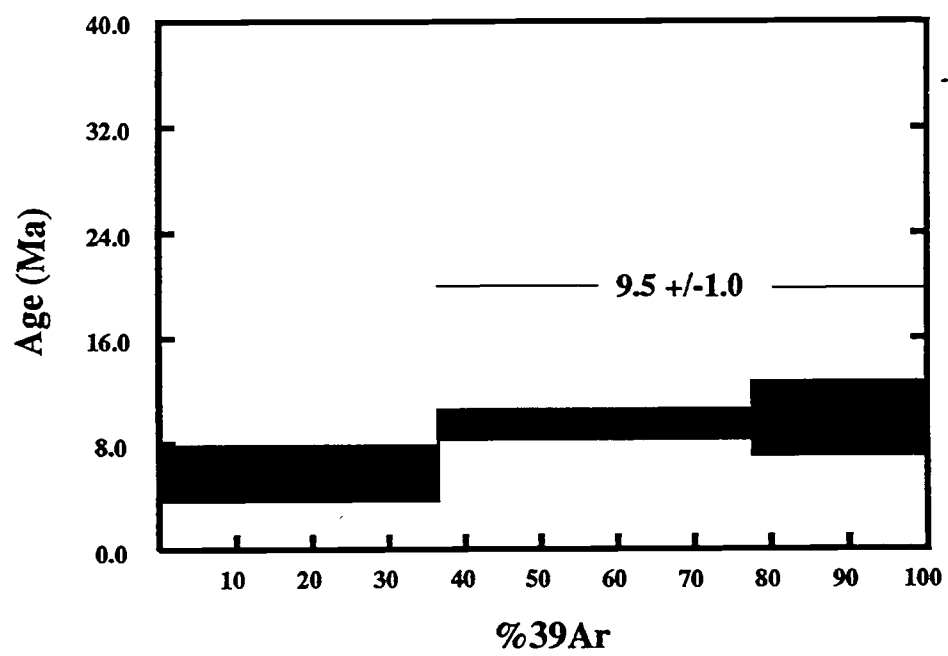
## Galapagos basalt PL10-5



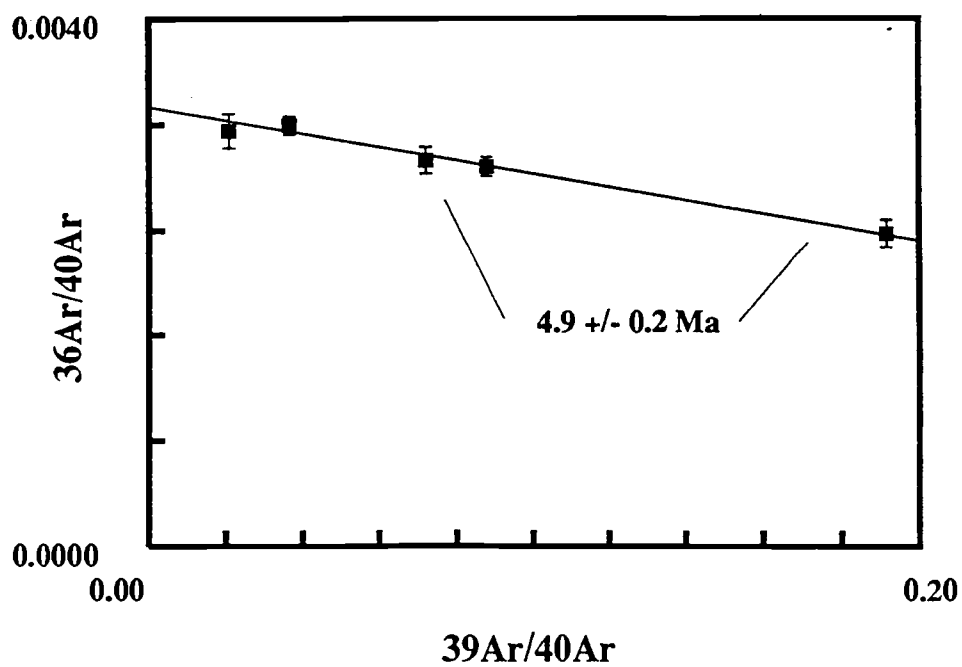
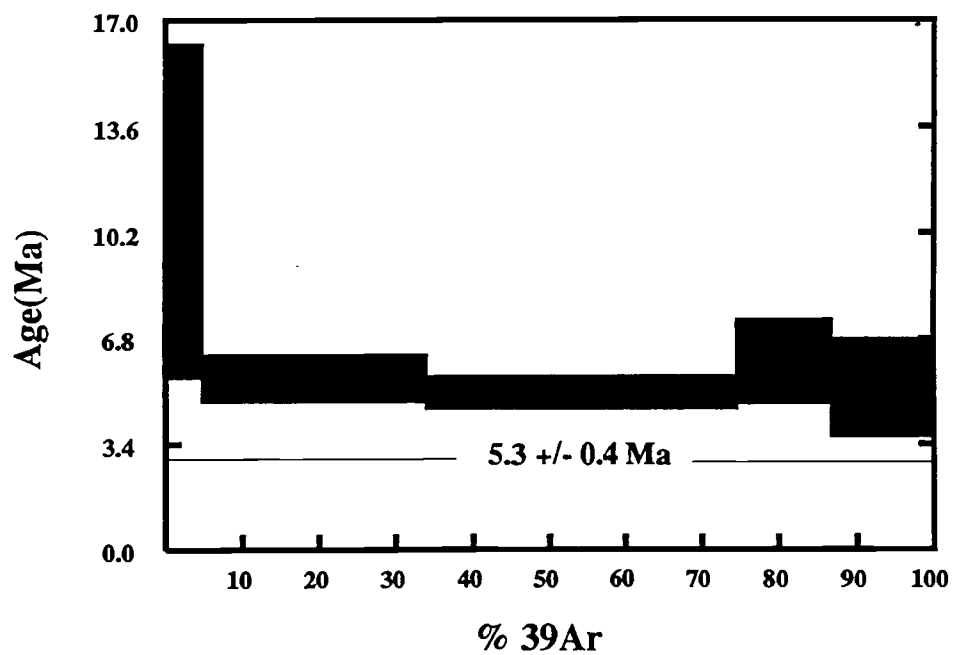
## Galapagos basalt PL11-2



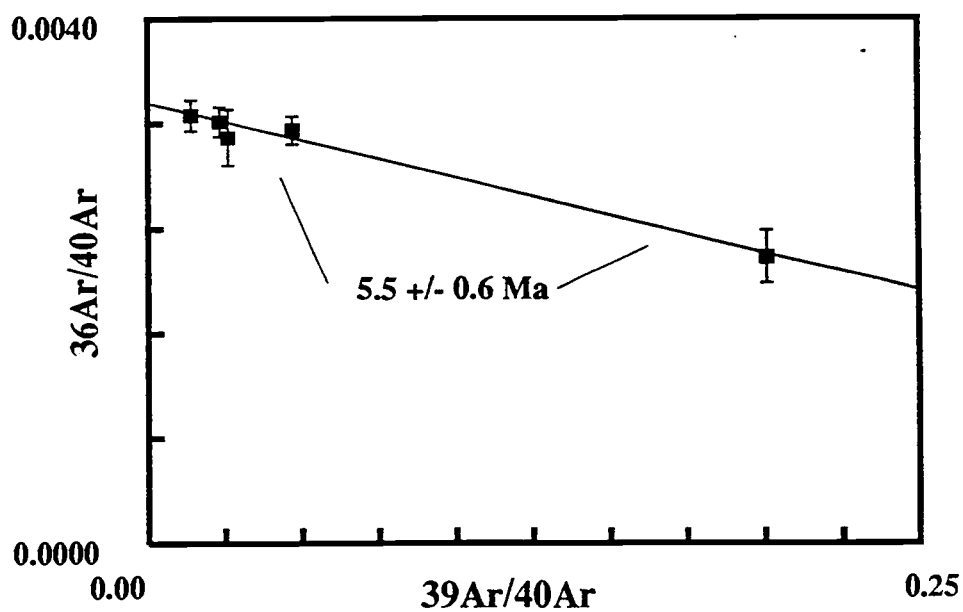
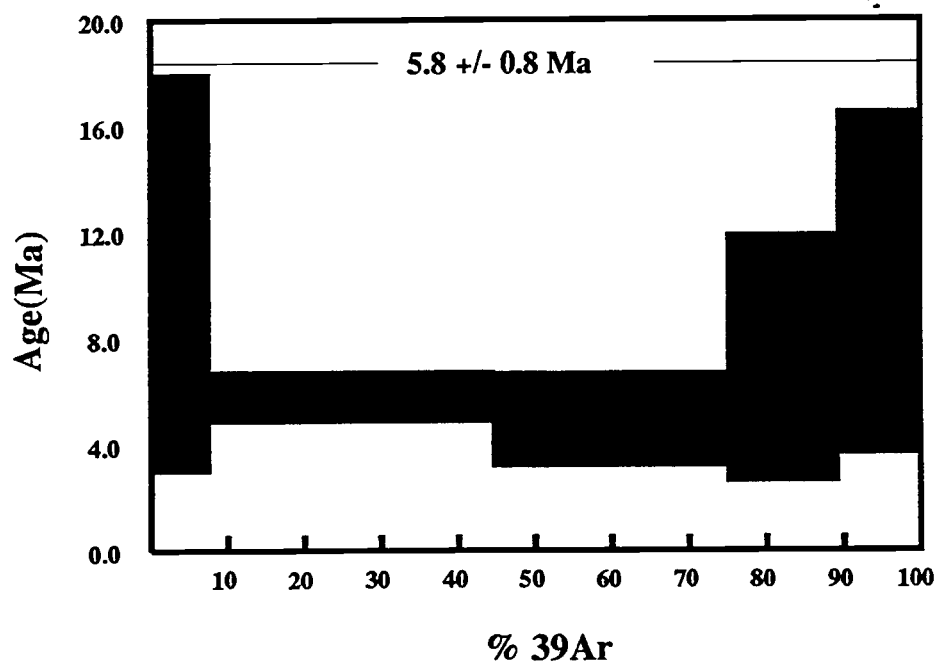
## Galapagos basalt PL16-3



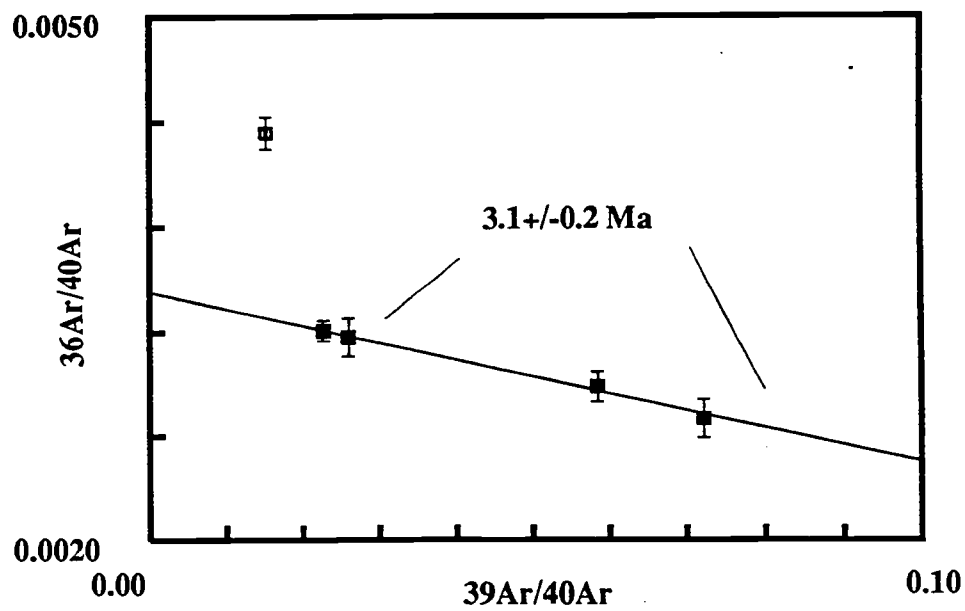
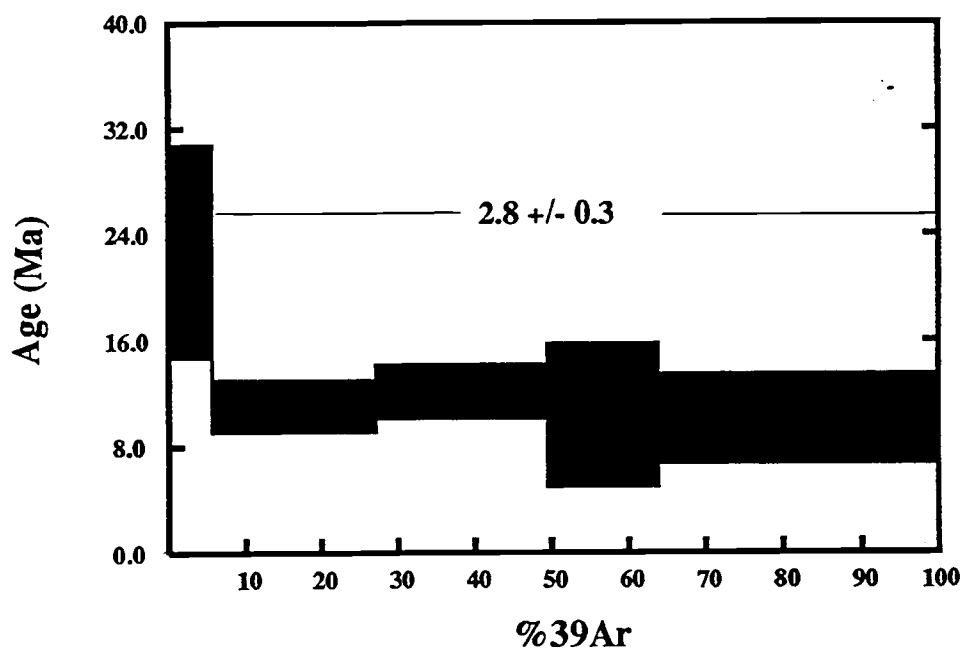
## Galapagos basalt PL17-1



### Galapagos basalt PL17-4



## Galapagos basalt PL20-2





**APPENDIX 2: Major Element Data from PL13-12 Inclusions and Minerals**

Each inclusion composition in the following table represents a single point analysis from one inclusion. Each mineral composition represents a single point analysis. Analyses were performed on the Camebax SX50 microprobe at Oregon State University. The beam had an acceleration voltage of 15 kV and a current of 30 nA. Counting times for the inclusion analyses were as follows:  $\text{TiO}_2$ ,  $\text{MnO}$ ,  $\text{P}_2\text{O}_5$ ,  $\text{K}_2\text{O}$  - 30 sec;  $\text{MgO}$ ,  $\text{Na}_2\text{O}$  - 15 sec;  $\text{SiO}_2$ ,  $\text{Al}_2\text{O}_3$ ,  $\text{FeO}$ ,  $\text{CaO}$  - 20 sec. For the mineral analyses, counting times for each element was 10 sec.

## Microprobe data from PL13-12 inclusions

<u>SiO2</u>	<u>TiO2</u>	<u>Al2O3</u>	<u>FeO</u>	<u>MnO</u>	<u>MgO</u>	<u>CaO</u>	<u>Na2O</u>	<u>K2O</u>	<u>P2O5</u>	<u>Total</u>
<b>1240° inclusions</b>										
49.73	0.83	16.18	8.70	0.20	9.85	12.83	1.80	0.06	0.04	100.21
50.73	0.36	16.25	8.21	0.12	9.32	12.56	2.16	0.03	0.00	99.74
50.00	0.59	16.51	8.03	0.14	9.19	12.74	2.40	0.03	0.03	99.65
50.65	0.62	16.64	8.16	0.19	9.22	12.67	2.33	0.03	0.00	100.52
49.07	0.83	16.27	9.00	0.26	9.83	13.22	1.76	0.13	0.09	100.47
49.07	0.66	16.41	8.83	0.21	9.13	12.76	2.30	0.04	0.03	99.44
48.55	0.76	16.49	8.72	0.19	9.34	13.04	2.23	0.02	0.04	99.38
48.90	0.74	16.39	8.83	0.17	9.39	12.97	2.17	0.04	0.04	99.63
48.91	0.68	16.27	8.99	0.14	9.12	13.12	2.10	0.05	0.04	99.42
48.95	0.73	16.56	8.88	0.17	9.25	12.87	2.20	0.04	0.05	99.70
48.91	0.76	16.43	8.91	0.15	9.24	12.94	2.17	0.03	0.05	99.59
48.99	0.73	16.48	8.66	0.14	9.18	12.91	2.17	0.03	0.05	99.35
48.68	0.73	16.50	8.69	0.20	9.17	12.97	2.19	0.03	0.00	99.17
48.87	0.76	16.45	8.63	0.19	9.23	13.01	2.13	0.04	0.00	99.31
48.75	0.71	16.65	8.62	0.18	9.19	12.97	2.20	0.04	0.06	99.36
48.93	0.77	16.44	9.09	0.20	9.23	12.88	2.27	0.03	0.01	99.85
48.88	0.75	16.37	8.61	0.18	9.14	12.76	2.14	0.03	0.04	98.92
49.22	0.58	16.51	8.51	0.16	9.10	12.59	2.32	0.03	0.02	99.05
<b>1250° inclusions</b>										
49.51	0.52	16.46	8.57	0.15	9.73	13.04	1.74	0.09	0.10	99.90
49.57	0.49	16.66	8.25	0.16	10.12	12.89	1.84	0.15	0.04	100.17
48.12	0.58	16.16	9.23	0.13	9.52	12.83	2.03	0.17	0.04	98.79
48.13	0.55	16.81	8.14	0.10	10.22	12.63	1.92	0.12	0.05	98.67
48.54	0.55	17.00	8.06	0.15	10.19	12.63	1.81	0.11	0.08	99.11
47.91	0.57	17.14	8.19	0.17	10.39	12.54	1.78	0.27	0.07	99.01
48.27	0.52	17.03	8.02	0.12	9.86	12.61	2.30	0.04	0.01	98.77
48.29	0.55	16.88	8.23	0.11	10.07	12.23	2.18	0.05	0.01	98.59
<b>1260° inclusions</b>										
48.69	0.41	17.71	7.61	0.14	10.50	12.68	2.27	0.02	0.00	100.01
48.55	0.33	17.70	7.30	0.15	10.80	12.72	2.13	0.03	0.04	99.75
48.09	0.25	17.74	7.03	0.14	10.54	13.12	2.21	0.01	0.03	99.16
48.29	0.26	17.44	7.22	0.16	10.84	12.69	1.95	0.03	0.01	98.89
47.25	0.59	17.20	7.27	0.16	10.52	13.14	2.04	0.03	0.01	98.20
48.27	0.47	17.20	7.29	0.11	10.11	13.30	2.11	0.08	0.04	98.99
47.99	0.30	17.41	7.85	0.13	10.37	12.86	2.11	0.02	0.02	99.05
47.77	0.32	17.37	8.05	0.11	9.90	12.96	2.25	0.03	0.00	98.76
47.41	0.55	17.33	7.98	0.16	10.01	12.94	2.10	0.05	0.03	98.56
48.13	0.39	17.46	8.00	0.17	10.08	12.75	2.16	0.03	0.00	99.17
48.28	0.29	17.39	8.09	0.16	10.24	12.72	2.07	0.02	0.01	99.27

<u>SiO<sub>2</sub></u>	<u>TiO<sub>2</sub></u>	<u>Al<sub>2</sub>O<sub>3</sub></u>	<u>FeO</u>	<u>MnO</u>	<u>MgO</u>	<u>CaO</u>	<u>Na<sub>2</sub>O</u>	<u>K<sub>2</sub>O</u>	<u>P<sub>2</sub>O<sub>5</sub></u>	<u>Total</u>
48.72	0.32	17.66	7.71	0.14	10.21	12.70	2.14	0.03	0.00	99.63
48.17	0.30	17.25	7.66	0.13	10.70	12.88	2.13	0.02	0.02	99.25
48.86	0.32	17.65	7.90	0.15	10.00	12.77	2.18	0.03	0.02	99.89
49.08	0.25	17.66	7.75	0.15	10.14	12.77	2.16	0.03	0.04	100.01
49.07	0.30	18.13	7.61	0.13	10.33	12.69	2.16	0.03	0.02	100.46
48.99	0.37	17.83	7.78	0.15	10.58	12.72	2.08	0.02	0.01	100.53
49.15	0.25	18.17	7.52	0.14	10.44	12.75	2.14	0.01	0.00	100.58
49.32	0.29	18.22	7.24	0.12	10.35	12.74	2.13	0.04	0.02	100.47
49.48	0.27	18.00	7.49	0.12	10.29	12.71	2.07	0.02	0.01	100.47
49.66	0.40	17.72	8.00	0.14	10.24	12.50	1.88	0.03	0.02	100.59
49.41	0.27	17.89	7.80	0.13	10.06	12.72	2.19	0.02	0.02	100.52
49.08	0.25	17.93	7.87	0.12	10.31	12.88	2.11	0.02	0.02	100.59
49.18	0.45	18.02	7.93	0.11	10.05	12.88	2.09	0.03	0.02	100.77
48.92	0.35	18.04	7.97	0.12	9.89	12.88	2.23	0.05	0.02	100.46
48.61	0.49	17.92	7.88	0.13	10.03	12.87	2.11	0.03	0.02	100.09
48.69	0.37	17.89	7.93	0.11	10.09	12.86	2.04	0.02	0.00	100.01
48.57	0.56	18.02	8.01	0.13	9.90	12.87	2.25	0.02	0.05	100.38
48.78	0.40	17.81	7.98	0.12	9.74	12.93	2.23	0.03	0.03	100.05
48.88	0.47	17.96	7.91	0.10	10.19	12.88	2.24	0.03	0.03	100.69
49.89	0.39	18.32	7.79	0.12	10.45	12.66	1.91	0.03	0.03	101.59
49.71	0.42	17.80	7.52	0.18	10.09	12.91	2.16	0.06	0.04	100.89
49.29	0.27	17.92	7.18	0.13	10.39	12.90	2.09	0.04	0.02	100.22
49.18	0.41	17.89	7.27	0.09	10.30	13.06	2.05	0.03	0.04	100.31
48.60	0.59	17.79	7.29	0.08	10.64	12.83	1.95	0.02	0.02	99.80
<b>1270° inclusions</b>										
48.64	0.44	17.98	7.72	0.16	10.29	12.75	2.15	0.04	0.04	100.20
48.36	0.46	18.02	7.59	0.15	10.23	12.68	2.19	0.03	0.05	99.76
48.82	0.46	18.10	7.66	0.16	10.21	12.66	2.18	0.02	0.01	100.28
47.97	0.70	18.06	7.09	0.13	10.62	12.97	2.07	0.02	0.06	99.68
47.94	0.70	18.02	7.14	0.15	10.60	12.92	2.09	0.02	0.06	99.63
48.06	0.69	18.04	7.14	0.13	10.63	12.88	2.05	0.03	0.04	99.68
48.08	0.69	18.09	7.24	0.15	10.55	12.93	2.07	0.02	0.07	99.89
48.09	0.69	18.12	7.01	0.13	10.59	12.94	2.17	0.02	0.06	99.81
47.44	0.68	18.03	7.00	0.14	10.32	12.79	2.07	0.03	0.05	98.53
48.39	0.71	18.34	7.06	0.16	9.97	13.03	2.12	0.02	0.06	99.87
48.09	0.71	18.31	7.12	0.16	9.97	13.30	2.15	0.03	0.07	99.90
47.76	0.70	18.24	7.07	0.14	10.37	12.97	2.01	0.03	0.05	99.32
47.95	0.68	18.01	7.04	0.15	10.67	13.05	2.07	0.02	0.05	99.69
48.01	0.69	18.06	7.13	0.17	10.53	12.87	2.12	0.03	0.08	99.69
47.90	0.69	18.13	6.96	0.15	10.53	12.76	2.18	0.02	0.05	99.36
48.02	0.57	18.02	6.95	0.13	10.50	13.02	2.14	0.02	0.06	99.41
48.43	0.64	18.20	7.11	0.18	10.49	12.88	2.09	0.01	0.04	100.07
49.00	0.33	18.16	7.14	0.17	10.47	12.42	2.22	0.01	0.00	99.93
49.07	0.33	18.20	7.03	0.16	10.48	12.46	2.19	0.02	0.02	99.95

<u>SiO2</u>	<u>TiO2</u>	<u>Al2O3</u>	<u>FeO</u>	<u>MnO</u>	<u>MgO</u>	<u>CaO</u>	<u>Na2O</u>	<u>K2O</u>	<u>P2O5</u>	<u>Total</u>
49.08	0.45	18.18	7.01	0.10	10.60	12.48	2.22	0.02	0.02	100.16
49.11	0.39	18.10	7.17	0.12	10.42	12.31	2.43	0.02	0.02	100.10
48.85	0.62	18.29	7.05	0.14	10.39	12.85	2.16	0.02	0.03	100.40
48.50	0.57	18.21	7.48	0.16	10.26	12.46	2.33	0.04	0.02	100.03
48.58	0.29	17.67	7.81	0.11	10.55	12.34	2.33	0.04	0.01	99.73
48.79	0.37	17.99	7.58	0.10	10.18	12.34	2.35	0.03	0.01	99.72
48.78	0.43	18.02	7.58	0.13	10.18	12.39	2.27	0.03	0.02	99.83
49.09	0.43	18.33	7.17	0.15	10.33	12.28	2.24	0.16	0.06	100.23
48.82	0.61	18.21	7.64	0.17	10.43	12.42	2.15	0.04	0.02	100.49
49.39	0.34	18.35	7.05	0.13	10.41	12.58	2.31	0.01	0.02	100.58
48.80	0.23	18.12	7.11	0.13	10.34	12.67	2.24	0.01	0.01	99.66
48.93	0.40	18.20	7.18	0.14	10.49	12.47	2.25	0.01	0.02	100.09

**1280° inclusions**

47.35	0.57	18.59	7.91	0.13	9.86	12.78	2.17	0.03	0.03	99.42
47.40	0.67	18.20	7.38	0.14	9.47	12.83	2.53	0.04	0.03	98.68
47.81	0.65	18.30	7.51	0.15	9.46	12.65	2.41	0.03	0.01	98.98
47.47	0.59	18.31	7.40	0.13	9.37	12.63	2.30	0.04	0.02	98.25
47.99	0.51	18.30	7.43	0.14	9.60	12.69	2.48	0.04	0.03	99.21
48.17	0.48	18.33	7.34	0.14	9.63	12.59	2.35	0.03	0.02	99.08
48.14	0.29	18.64	7.51	0.11	9.51	12.36	2.54	0.03	0.03	99.15

**Spinel in glass inclusion at 1280°**

	<u>FeO</u>	<u>TiO2</u>	<u>MnO</u>	<u>SiO2</u>	<u>Al2O3</u>	<u>MgO</u>	<u>Cr2O3</u>	<u>V2O5</u>	<u>Fe2O3</u>	<u>Total</u>
core	8.57	0.16	0.10	0.09	46.29	19.79	19.04	0.12	4.53	98.67
core	8.40	0.16	0.13	0.11	46.11	20.04	19.47	0.11	5.01	99.53
core	8.57	0.16	0.13	0.10	46.56	19.83	18.80	0.13	4.60	98.87
core	7.95	0.15	0.12	0.13	46.56	20.39	19.20	0.15	5.00	99.64
avg.	8.37	0.16	0.12	0.11	46.38	20.01	19.13	0.12	4.78	99.18
stdev.	0.29	0.00	0.02	0.02	0.22	0.27	0.28	0.02	0.26	0.48

**Olivine in inclusion at 1260°**

	<u>MgO</u>	<u>Al2O3</u>	<u>SiO2</u>	<u>CaO</u>	<u>MnO</u>	<u>NiO</u>	<u>FeO</u>	<u>Total</u>	<u>%Fo</u>
core	48.33	0.42	40.52	0.53	0.14	0.27	8.95	99.16	91.10

**Representative traverse of PL 13-12 anorthite**

	<u>Na2O</u>	<u>MgO</u>	<u>Al2O3</u>	<u>SiO2</u>	<u>K2O</u>	<u>CaO</u>	<u>FeO</u>	<u>BaO</u>	<u>Total</u>	<u>%An</u>
incl rim	2.69	0.33	31.80	49.41	0.01	15.64	0.47	0.01	100.37	76.20
core	1.10	0.16	35.03	45.49	0.00	18.67	0.30	0.00	100.76	90.34
core	1.03	0.17	35.14	45.35	0.02	18.48	0.35	0.00	100.54	90.72
core	1.01	0.14	35.13	45.58	0.01	18.74	0.35	0.02	100.97	91.04
core	1.05	0.15	35.07	45.35	0.01	18.50	0.26	0.00	100.37	90.66
core	1.12	0.16	34.99	45.72	0.01	18.37	0.26	0.01	100.63	90.02
core	1.08	0.17	35.16	45.84	0.01	18.40	0.27	0.02	100.95	90.34
core	0.97	0.15	35.32	45.14	0.01	18.60	0.33	0.00	100.52	91.28
rim	2.52	0.27	32.08	48.63	0.02	15.82	0.68	0.03	100.05	77.54

### **APPENDIX 3: Major Element Data from PLUME2 Pillow-rim Glass**

Each analysis in the following table is an average of five microprobe analyses of a single glass chip mounted in epoxy. All analyses were normalized to the BASL standard, which was run as an unknown after every fifth sample. Analyses were performed on the Camebax SX50 microprobe at Oregon State University. The beam had an approximate diameter of 30  $\mu$ , acceleration voltage of 15 kV and a current of 30 nA. Counting times for each element were 10 seconds. Many of the chips were analyzed more than once. Given multiple analyses, those with totals < 98% or >101% were rejected, as well as those displaying any obvious anomalies. After this screening, multiple analyses from a single sample were averaged.

## Microprobe Results of PLUME2 pillow-rim glass

<u>Sample</u>	<u>SiO2</u>	<u>TiO2</u>	<u>Al2O3</u>	<u>FeO</u>	<u>MnO</u>	<u>MgO</u>	<u>CaO</u>	<u>Na2O</u>	<u>K2O</u>	<u>P2O5</u>	<u>Total</u>
PL 09-04	47.19	1.01	17.89	8.92	0.14	9.96	12.42	2.55	0.03	0.05	100.15
PL 09-06	47.36	0.99	17.91	8.93	0.13	10.00	12.41	2.51	0.03	0.07	100.34
PL 09-12	47.50	1.01	17.96	8.90	0.11	10.08	12.37	2.56	0.03	0.06	100.59
PL 09-14	47.47	1.03	17.97	9.08	0.11	10.03	12.57	2.50	0.02	0.04	100.82
PL 09-15	47.49	0.93	17.93	9.11	0.14	10.12	12.56	2.51	0.02	0.07	100.89
PL 09-16	47.46	1.14	17.83	9.06	0.11	9.37	12.39	2.58	0.03	0.07	100.02
PL 09-17	47.21	1.00	18.02	8.77	0.14	9.79	12.40	2.48	0.03	0.05	99.88
PL 09-18	47.23	1.00	17.81	8.83	0.12	9.89	12.24	2.48	0.03	0.07	99.71
PL 09-19	47.53	1.12	18.02	8.75	0.11	10.00	12.61	2.50	0.01	0.07	100.75
PL 09-20	47.40	1.02	18.00	8.98	0.14	10.18	12.56	2.51	0.03	0.06	100.85
PL 09-22	47.60	0.98	17.91	9.04	0.11	10.02	12.51	2.49	0.02	0.06	100.74
PL 09-23	47.63	1.02	17.87	9.02	0.12	9.93	12.51	2.51	0.02	0.05	100.70
PL 09-24	47.63	1.01	17.92	9.05	0.13	10.04	12.42	2.40	0.03	0.05	100.68
PL 09-26	47.50	1.04	17.77	8.87	0.12	10.04	12.39	2.44	0.01	0.02	100.19
PL 09-27	47.66	1.02	17.88	8.93	0.11	9.62	12.64	2.52	0.02	0.08	100.48
PL 09-29	47.50	0.83	17.70	9.09	0.10	10.13	12.38	2.40	0.02	0.07	100.21
PL 09-30	47.57	1.14	17.69	9.20	0.15	9.56	12.51	2.51	0.03	0.11	100.45
PL 09-31	47.70	1.15	17.86	8.85	0.14	9.97	12.68	2.51	0.02	0.08	100.96
PL 09-32	47.38	1.00	17.76	9.03	0.13	10.19	12.50	2.38	0.02	0.05	100.45
PL 09-33	47.17	0.99	17.70	8.99	0.15	9.85	12.24	2.52	0.02	0.09	99.72
PL 09-34	48.69	1.80	14.82	11.58	0.16	6.83	12.11	3.15	0.31	0.17	99.61
PL 09-35	49.17	1.54	15.86	10.05	0.15	7.54	12.43	2.96	0.19	0.14	100.03
PL 09-36	49.00	1.54	15.78	10.14	0.17	7.71	12.45	2.94	0.20	0.15	100.07
PL 09-37	47.61	1.22	17.62	9.13	0.14	9.50	12.64	2.63	0.02	0.08	100.58
PL 09-38	47.28	1.13	17.83	9.08	0.12	9.56	12.33	2.64	0.03	0.09	100.09
PL 09-39	47.57	1.05	17.76	8.92	0.07	10.12	12.60	2.48	0.01	0.07	100.66
PL 09-42	47.49	0.97	17.96	8.87	0.16	9.69	12.55	2.41	0.03	0.06	100.20
PL 09-43	46.70	0.99	17.70	8.83	0.16	9.91	12.42	2.34	0.02	0.09	99.15
PL 09-44	47.27	0.99	17.77	8.86	0.13	10.06	12.52	2.44	0.02	0.10	100.15
PL 09-46	47.55	1.04	17.87	8.79	0.16	10.12	12.51	2.40	0.03	0.06	100.53
PL 09-47	47.34	1.09	17.73	8.81	0.11	10.00	12.50	2.51	0.02	0.05	100.15
PL 09-48	47.57	0.99	17.86	8.92	0.12	9.96	12.51	2.48	0.02	0.05	100.49
PL 09-49	47.95	1.02	18.02	8.88	0.11	9.75	12.63	2.45	0.02	0.06	100.88
PL 09-50	48.72	1.93	14.87	11.44	0.16	6.74	12.00	3.17	0.30	0.16	99.50
PL 09-51	47.28	1.06	17.79	8.88	0.11	10.01	12.48	2.40	0.03	0.05	100.09
PL 09-52	47.44	1.04	17.98	9.07	0.12	10.00	12.55	2.38	0.02	0.06	100.65
PL 09-53	47.17	1.12	17.86	9.06	0.12	9.55	12.35	2.63	0.02	0.06	99.94
PL 09-58	48.35	1.86	14.85	11.40	0.15	6.69	11.97	3.22	0.32	0.19	99.01
PL 09-65	48.56	1.53	15.76	10.11	0.13	7.70	12.31	3.00	0.22	0.11	99.43
PL 09-83	48.42	1.56	15.69	10.16	0.14	7.73	12.31	3.05	0.20	0.14	99.41
PL 10-07	49.53	1.48	14.88	10.08	0.13	7.89	12.81	2.85	0.12	0.11	99.87
PL 10-08	49.49	1.51	14.92	10.00	0.14	7.76	12.87	2.87	0.11	0.09	99.77

## Microprobe Results of PLUME2 pillow-rim glass

<u>Sample</u>	<u>SiO2</u>	<u>TiO2</u>	<u>Al2O3</u>	<u>FeO</u>	<u>MnO</u>	<u>MgO</u>	<u>CaO</u>	<u>Na2O</u>	<u>K2O</u>	<u>P2O5</u>	<u>Total</u>
PL 10-09	49.93	1.47	14.92	10.10	0.12	7.97	12.88	2.78	0.11	0.12	100.41
PL 11 misc	49.24	2.15	14.55	11.61	0.15	6.31	11.55	3.66	0.38	0.23	99.83
PL 11-04	49.08	2.19	14.63	11.57	0.17	6.22	11.57	3.60	0.37	0.22	99.63
PL 11-08	48.87	2.18	14.49	11.60	0.15	6.24	11.48	3.67	0.37	0.23	99.29
PL 11-10	48.79	2.21	14.58	11.65	0.17	6.28	11.51	3.66	0.37	0.25	99.46
PL 11-12	48.83	2.19	14.55	11.57	0.16	6.24	11.48	3.60	0.37	0.22	99.21
PL 12-01	49.24	1.82	14.70	11.28	0.14	7.45	12.70	2.78	0.07	0.10	100.27
PL 12-02	48.29	1.05	16.68	8.85	0.12	9.24	12.76	2.43	0.03	0.07	99.52
PL 12-03	48.44	1.05	16.95	8.62	0.12	9.25	12.81	2.53	0.05	0.06	99.89
PL 12-04	49.19	1.09	17.02	8.90	0.14	9.28	12.78	2.48	0.04	0.09	101.02
PL 12-05	49.17	1.49	14.51	10.74	0.15	7.58	12.54	2.77	0.11	0.11	99.17
PL 12-06	49.44	0.98	16.99	8.89	0.11	9.23	12.79	2.46	0.06	0.09	101.04
PL 12-09	48.31	1.04	16.88	8.88	0.11	9.26	12.68	2.45	0.02	0.05	99.68
PL 12-10	49.50	1.00	17.19	8.57	0.15	9.23	12.74	2.52	0.04	0.05	100.99
PL 12-11	48.02	1.03	16.90	8.82	0.14	9.35	12.71	2.46	0.03	0.08	99.55
PL 13-12	47.94	0.83	17.15	8.36	0.11	9.99	12.91	2.17	0.00	0.04	99.51
PL 13-17	50.36	1.11	15.81	9.55	0.13	8.56	13.06	2.51	0.06	0.09	101.24
PL 13-18	49.93	1.02	16.20	9.25	0.10	8.89	12.74	2.44	0.04	0.08	100.69
PL 13-19	50.06	1.00	16.12	9.13	0.11	8.81	12.91	2.44	0.04	0.06	100.69
PL 13-20	49.64	1.01	15.69	9.29	0.11	8.70	12.95	2.44	0.03	0.07	99.93
PL 13-21	47.90	0.81	17.28	8.29	0.12	10.10	12.85	2.10	0.01	0.06	99.52
PL 13-22	50.22	1.00	16.00	9.55	0.12	8.74	12.82	2.45	0.03	0.05	100.98
PL 13-23	49.98	1.18	15.35	9.83	0.11	8.23	12.91	2.55	0.04	0.04	100.22
PL 13-24	49.42	1.07	16.15	9.42	0.12	8.96	12.97	2.48	0.03	0.06	100.67
PL 13-25	49.73	0.99	15.95	9.52	0.12	8.95	12.69	2.45	0.04	0.07	100.51
PL 13-26	50.01	1.13	15.38	10.06	0.12	8.22	12.96	2.54	0.04	0.07	100.53
PL 13-27	48.91	1.00	15.81	8.96	0.10	8.70	12.53	2.32	0.04	0.06	98.42
PL 13-28	49.57	1.14	15.69	9.58	0.12	8.63	12.94	2.33	0.03	0.07	100.08
PL 13-29	49.31	1.03	16.12	9.20	0.14	8.90	12.61	2.40	0.02	0.06	99.80
PL 13-30	48.47	0.87	17.08	8.53	0.10	9.83	12.94	2.22	0.01	0.05	100.10
PL 13-31	48.14	0.84	17.29	8.36	0.10	9.73	12.95	2.17	0.02	0.06	99.66
PL 14-02	47.62	1.21	17.29	8.95	0.13	9.44	12.74	2.67	0.03	0.07	100.15
PL 14-03	47.75	1.18	17.25	9.08	0.12	9.40	12.69	2.58	0.02	0.06	100.14



## Microprobe Results of PLUME2 pillow-rim glass

Sample	SiO <sub>2</sub>	TiO <sub>2</sub>	Al <sub>2</sub> O <sub>3</sub>	FeO	MnO	MgO	CaO	Na <sub>2</sub> O	K <sub>2</sub> O	P <sub>2</sub> O <sub>5</sub>	Total
PL 14-04	47.75	1.38	16.79	9.32	0.13	9.57	12.24	2.64	0.04	0.09	99.96
PL 14-05	47.45	1.36	16.72	9.03	0.13	9.37	12.25	2.65	0.04	0.09	99.09
PL 14-06	47.86	1.18	17.36	9.01	0.11	9.26	12.57	2.62	0.02	0.07	100.05
PL 14-07	47.79	1.36	16.72	9.38	0.11	9.69	12.23	2.63	0.04	0.08	100.02
PL 14-08	47.97	1.19	17.28	8.94	0.12	9.33	12.50	2.56	0.02	0.08	99.99
PL 14-09	48.18	1.23	17.41	8.96	0.10	9.40	12.81	2.63	0.02	0.05	100.79
PL 14-14	47.83	1.20	17.17	8.84	0.11	9.37	12.62	2.61	0.02	0.07	99.83
PL 14-15	48.01	1.27	17.14	8.98	0.11	9.31	12.57	2.62	0.03	0.07	100.12
PL 14-16	48.07	1.19	17.15	9.08	0.13	9.36	12.72	2.73	0.02	0.08	100.54
PL 14-17	47.95	1.13	17.34	9.00	0.11	9.35	12.76	2.76	0.02	0.08	100.50
PL 14-18	47.79	0.90	17.65	9.30	0.15	9.94	12.47	2.49	0.01	0.05	100.75
PL 14-19	48.01	1.23	17.47	8.91	0.15	9.33	12.79	2.71	0.01	0.08	100.69
PL 14-20	47.77	0.86	17.66	9.26	0.12	9.83	12.54	2.48	0.03	0.06	100.60
PL 14-21	48.27	1.18	17.32	9.05	0.12	9.33	12.77	2.70	0.02	0.09	100.86
PL 14-22	48.41	1.21	17.31	8.92	0.12	9.32	12.73	2.68	0.02	0.09	100.81
PL 14-23	47.09	0.95	17.38	9.22	0.15	9.71	12.40	2.35	0.02	0.05	99.32
PL 24-02	48.17	3.03	13.83	11.89	0.15	6.34	11.04	2.81	0.45	0.29	98.00
PL 24-05	48.63	3.06	13.99	11.98	0.17	5.91	10.32	2.89	0.51	0.29	97.76
PL 24-07	48.96	2.88	14.04	11.92	0.14	6.41	11.22	3.06	0.47	0.31	99.41
PL 24-08	48.77	3.00	13.64	11.83	0.16	6.35	10.91	2.83	0.47	0.26	98.22
PL 24-09	49.44	3.34	13.76	12.22	0.16	6.13	10.72	3.02	0.55	0.32	99.66
PL 24-10	49.18	2.92	13.88	11.90	0.16	6.36	11.21	2.91	0.46	0.29	99.28
PL 24-11	48.99	2.89	13.91	11.91	0.15	6.37	11.24	2.95	0.47	0.24	99.13
PL 24-12	49.18	3.02	13.92	12.02	0.15	6.46	11.27	2.85	0.45	0.25	99.57
PL 24-13	49.07	2.88	13.86	11.98	0.17	6.48	11.26	2.88	0.46	0.23	99.26
PL 24-14	49.16	3.07	13.88	11.81	0.14	6.44	11.08	2.87	0.47	0.24	99.17
PL 24-15	48.69	3.11	13.61	11.75	0.14	6.37	11.02	2.87	0.46	0.26	98.28
PL 24-16	48.74	3.17	13.56	12.03	0.12	6.31	10.95	2.86	0.45	0.27	98.45
PL 24-17	48.75	2.94	13.79	11.73	0.12	6.35	11.02	2.92	0.47	0.27	98.37
PL 24-18	49.14	2.97	13.86	12.03	0.14	6.50	11.10	2.88	0.47	0.23	99.31
PL 24-19	48.54	2.97	13.66	11.77	0.16	6.26	11.14	2.81	0.45	0.25	98.01
PL 24-20	48.66	2.94	13.77	11.91	0.13	6.41	11.06	2.84	0.46	0.24	98.42
PL 24-21	48.85	2.95	13.72	11.56	0.15	6.30	11.09	2.85	0.46	0.24	98.17
PL 24-22	48.90	3.04	13.80	12.02	0.14	6.41	11.08	2.94	0.48	0.24	99.05
PL 24-24	48.60	2.85	13.79	11.86	0.17	6.32	10.94	2.89	0.43	0.21	98.06
PL 24-25	48.87	3.01	13.61	11.82	0.17	6.28	11.07	2.85	0.47	0.25	98.40
PL 24-26	48.91	3.05	13.89	11.89	0.14	6.46	11.07	2.86	0.46	0.26	99.00
PL 24-27	48.58	3.01	13.56	11.78	0.13	6.36	11.04	2.87	0.47	0.25	98.05
PL 24-28	48.74	3.03	13.73	11.95	0.14	6.45	11.12	2.86	0.47	0.25	98.75
PL 24-29	48.82	3.06	13.94	12.05	0.13	6.41	11.24	2.79	0.45	0.25	99.15
PL 24-30	48.51	3.09	13.79	11.91	0.13	6.32	11.17	2.84	0.48	0.24	98.48

## Microprobe Results of PLUME2 pillow-rim glass

Sample	SiO <sub>2</sub>	TiO <sub>2</sub>	Al <sub>2</sub> O <sub>3</sub>	FeO	MnO	MgO	CaO	Na <sub>2</sub> O	K <sub>2</sub> O	P <sub>2</sub> O <sub>5</sub>	Total
PL 24-31	48.73	3.01	13.85	12.11	0.12	6.18	11.00	2.84	0.46	0.25	98.55
PL 24-32	49.20	3.17	13.81	12.28	0.14	6.30	11.06	2.91	0.48	0.24	99.58
PL 24-33	49.24	3.04	13.72	11.86	0.13	6.48	11.21	2.84	0.46	0.27	99.26
PL 24-34	48.42	3.09	13.68	11.75	0.17	6.44	11.21	2.83	0.46	0.24	98.28
PL 24-35	48.51	3.02	13.77	11.86	0.15	6.28	11.07	2.74	0.46	0.27	98.13
PL 24-36	49.38	2.99	13.88	12.06	0.13	6.47	11.24	2.82	0.47	0.23	99.67
PL 24-37	48.53	3.11	14.10	11.35	0.13	6.53	11.22	2.85	0.47	0.27	98.55
PL 25-01	46.71	3.72	15.31	12.25	0.15	5.15	9.64	4.04	1.20	0.56	98.73
PL 25-02	47.24	3.70	15.48	12.46	0.14	5.11	9.65	4.01	1.16	0.57	99.52
PL 25-03	47.38	3.65	15.45	12.45	0.16	5.07	9.64	3.93	1.17	0.55	99.46
PL 25-04	48.14	3.25	14.53	11.64	0.15	6.61	11.07	3.04	0.47	0.34	99.24
PL 25-05	47.21	3.80	15.51	12.32	0.16	5.14	9.70	4.04	1.18	0.60	99.65
PL 25-06	47.27	3.72	15.53	12.63	0.16	5.05	9.61	4.15	1.19	0.64	99.95
PL 25-07	46.87	3.65	15.72	12.21	0.17	5.13	9.52	3.85	1.15	0.60	98.87
PL 26-01	47.90	1.91	15.66	9.73	0.12	7.90	12.09	2.93	0.22	0.13	98.60
PL 26-02	48.69	1.88	15.56	9.96	0.12	7.93	12.05	3.05	0.23	0.15	99.63
PL 26-03	48.83	1.93	15.77	10.14	0.11	7.85	12.07	3.03	0.25	0.17	100.14
PL 26-04	48.36	1.99	15.77	10.06	0.12	7.91	12.16	2.77	0.26	0.18	99.57
PL 26-05	48.64	1.84	15.74	9.95	0.10	7.94	11.99	3.07	0.24	0.14	99.65
PL 26-06	48.71	1.92	15.64	10.07	0.14	7.86	11.94	3.01	0.25	0.21	99.76
PL 26-07	48.61	1.92	15.57	9.99	0.13	7.81	11.93	3.01	0.24	0.17	99.37
PL 26-08	48.11	1.90	15.64	10.02	0.14	7.81	12.00	2.99	0.24	0.13	98.99
PL 26-10	48.18	1.86	15.42	9.94	0.13	8.03	11.95	3.00	0.24	0.16	98.91
PL 26-11	48.81	1.86	15.81	10.07	0.14	7.95	11.95	3.00	0.22	0.13	99.94
PL 26-12	48.30	1.90	15.49	9.93	0.13	7.83	12.07	3.00	0.24	0.16	99.04
PL 26-13	48.18	1.90	15.58	9.95	0.13	7.86	12.03	3.12	0.25	0.18	99.19
PL 26-14	48.36	1.92	15.62	9.87	0.13	7.86	12.01	3.11	0.25	0.19	99.32
PL 26-15	48.79	1.89	15.54	9.62	0.13	7.96	12.09	3.06	0.25	0.17	99.51
PL 26-16	48.51	1.92	15.61	10.13	0.13	7.81	12.02	2.99	0.24	0.15	99.51
PL 26-17	48.40	1.91	15.61	9.96	0.13	7.95	12.08	2.99	0.24	0.16	99.42
PL 26-18	48.41	1.87	15.57	10.02	0.13	7.92	12.07	3.06	0.24	0.15	99.44
PL 26-19	48.92	1.87	15.63	9.86	0.13	8.04	12.04	3.01	0.24	0.15	99.90
PL 26-20	48.23	1.91	15.52	9.97	0.13	7.98	12.00	2.99	0.25	0.16	99.15
PL 26-21	48.22	1.87	15.64	9.96	0.13	7.92	12.08	2.98	0.23	0.18	99.21
PL 26-22	48.20	1.89	15.64	9.88	0.15	7.80	12.15	2.99	0.25	0.16	99.11
PL 26-23	48.14	1.96	15.20	10.22	0.14	7.43	12.10	3.08	0.25	0.16	98.67
PL 26-23	48.14	1.96	15.20	10.22	0.14	7.43	12.10	3.08	0.25	0.16	98.67
PL 26-23	48.14	1.96	15.20	10.22	0.14	7.43	12.10	3.08	0.25	0.16	98.67

## Microprobe Results of PLUME2 pillow-rim glass

Sample	SiO <sub>2</sub>	TiO <sub>2</sub>	Al <sub>2</sub> O <sub>3</sub>	FeO	MnO	MgO	CaO	Na <sub>2</sub> O	K <sub>2</sub> O	P <sub>2</sub> O <sub>5</sub>	Total
PL 26-24	48.47	1.87	15.61	9.95	0.15	7.81	12.03	3.02	0.23	0.13	99.28
PL 26-25	48.02	1.83	15.50	11.01	0.15	7.63	11.82	3.15	0.08	0.10	99.29
PL 26-26	48.68	1.85	15.71	9.87	0.13	7.97	11.86	3.00	0.22	0.16	99.44
PL 26-27	48.47	1.88	15.73	9.88	0.13	7.99	11.88	3.00	0.23	0.15	99.33
PL 26-28	48.39	1.84	15.72	9.82	0.16	7.90	11.87	3.02	0.24	0.14	99.11
PL 27-01	47.88	1.81	15.41	11.12	0.16	7.59	11.93	3.17	0.08	0.10	99.27
PL 27-02	47.86	1.85	15.46	11.05	0.15	7.28	11.98	3.17	0.08	0.14	99.03
PL 27-03	48.59	1.80	15.71	11.05	0.14	7.54	12.00	2.94	0.08	0.13	99.98
PL 27-04	47.68	1.81	15.55	10.99	0.13	7.90	11.93	3.00	0.07	0.16	99.24
PL 27-05	48.32	1.76	15.68	11.13	0.13	7.75	11.84	3.02	0.07	0.11	99.80
PL 27-07	47.84	1.84	15.68	11.33	0.15	7.51	12.13	3.09	0.08	0.10	99.76
PL 27-08	47.96	1.87	15.55	11.13	0.13	7.20	12.18	3.07	0.07	0.11	99.25
PL 27-09	48.05	1.64	15.77	10.90	0.16	7.53	11.92	3.08	0.08	0.09	99.23
PL 27-10	47.73	1.84	15.61	11.10	0.14	7.65	11.87	3.09	0.08	0.09	99.19
PL 27-11	48.28	1.81	15.48	11.15	0.14	7.76	11.84	3.06	0.07	0.12	99.72
PL 27-12	48.26	1.53	15.78	10.98	0.15	7.85	12.09	3.19	0.07	0.12	100.03
PL 27-13	48.40	1.81	15.68	10.92	0.13	7.82	11.87	3.09	0.07	0.12	99.92
PL 27-14	48.47	1.86	15.51	11.22	0.14	7.41	11.93	3.05	0.07	0.13	99.78
PL 27-15	48.60	1.78	15.70	11.03	0.11	7.90	11.95	3.09	0.09	0.15	100.40
PL 27-16	48.48	1.77	15.73	11.09	0.14	7.76	11.98	3.12	0.08	0.10	100.23
PL 27-18	48.43	1.74	15.72	11.07	0.16	7.82	11.94	3.17	0.08	0.15	100.29
PL 27-19	47.36	1.81	15.24	11.04	0.15	7.47	11.80	3.17	0.08	0.10	98.22
PL 27-20	48.20	1.84	15.70	10.94	0.16	7.10	11.92	3.20	0.07	0.13	99.27
PL 27-21	48.46	1.87	15.73	10.84	0.12	7.85	11.88	3.06	0.07	0.11	100.00
PL 27-22	48.09	1.86	15.47	11.21	0.14	7.33	11.80	3.09	0.08	0.14	99.22
PL 27-23	48.31	1.84	15.63	11.20	0.15	7.32	11.88	3.20	0.06	0.13	99.72
PL 27-24	47.61	1.84	15.44	11.30	0.13	7.87	11.74	3.02	0.08	0.10	99.14
PL 27-25	48.09	1.79	15.68	11.10	0.13	7.40	11.86	3.12	0.07	0.12	99.36
PL 27-26	48.31	1.80	15.68	11.23	0.15	7.44	11.57	2.98	0.08	0.11	99.35
PL 27-27	48.49	1.98	15.75	11.12	0.17	7.29	12.04	3.13	0.07	0.11	100.15
PL 27-33	47.95	1.96	15.38	11.09	0.13	7.29	11.95	3.13	0.08	0.11	99.07
PL 28-01	47.42	1.86	16.87	9.61	0.13	8.48	11.71	2.97	0.20	0.13	99.38
PL 28-02	47.39	1.85	16.73	9.59	0.13	8.33	11.67	2.85	0.19	0.14	98.88
PL 28-03	47.69	1.88	16.89	9.58	0.12	8.35	11.75	2.93	0.19	0.15	99.53
PL 28-04	47.98	1.85	16.94	9.54	0.12	8.31	11.79	2.90	0.18	0.17	99.78
PL 28-05	48.23	1.87	16.80	9.46	0.12	8.40	11.87	2.99	0.19	0.13	100.06
PL 28-06	47.91	1.80	16.82	9.64	0.12	8.42	11.69	2.88	0.19	0.16	99.63

## Microprobe Results of PLUME2 pillow-rim glass

Sample	SiO <sub>2</sub>	TiO <sub>2</sub>	Al <sub>2</sub> O <sub>3</sub>	FeO	MnO	MgO	CaO	Na <sub>2</sub> O	K <sub>2</sub> O	P <sub>2</sub> O <sub>5</sub>	Total
PL 28-07	48.39	1.86	16.98	9.34	0.13	8.34	11.84	2.96	0.18	0.19	100.19
PL 28-08	47.95	1.88	16.79	9.77	0.11	8.31	11.76	2.97	0.20	0.18	99.92
PL 28-09	47.74	1.83	16.80	9.81	0.12	8.39	11.81	2.94	0.19	0.15	99.77
PL 28-09	47.77	1.80	16.71	9.67	0.12	8.27	11.63	2.84	0.19	0.13	99.12
PL 28-10	47.59	1.56	16.84	9.62	0.12	8.38	11.74	2.95	0.19	0.16	99.15
PL 28-11	47.53	1.74	16.53	9.67	0.12	8.12	11.61	2.85	0.17	0.15	98.51
PL 28-12	47.88	1.77	16.69	9.78	0.12	8.08	11.63	2.77	0.18	0.14	99.04
PL 28-13	47.76	1.80	16.71	9.69	0.12	8.38	11.63	2.91	0.18	0.17	99.35
PL 28-14	48.14	1.77	16.78	9.76	0.12	8.38	11.67	2.89	0.19	0.17	99.86
PL 28-15	48.20	1.82	16.71	9.82	0.12	8.07	11.67	2.92	0.18	0.16	99.68
PL 28-16	47.84	1.76	16.88	9.75	0.10	8.58	11.63	3.03	0.16	0.14	99.88
PL 28-17	47.67	1.78	16.71	9.72	0.12	8.32	11.65	2.97	0.19	0.16	99.29
PL 28-18	47.75	1.80	16.86	9.74	0.13	8.38	11.69	2.94	0.17	0.18	99.64
PL 28-19	48.17	1.77	16.90	9.84	0.12	8.39	11.68	2.93	0.19	0.14	100.14
PL 28-20	48.12	1.79	16.85	9.80	0.12	8.34	11.55	2.92	0.18	0.13	99.80
PL 28-23	47.97	1.77	16.71	9.67	0.11	8.36	11.54	2.88	0.18	0.14	99.33
PL 28-24	47.32	1.79	16.68	9.61	0.12	8.35	11.57	2.95	0.18	0.20	98.76
PL 28-25	47.96	1.77	16.78	9.77	0.12	8.42	11.51	2.91	0.18	0.16	99.56
PL 28-26	47.61	1.83	16.68	9.42	0.12	8.36	11.59	2.94	0.18	0.15	98.88
PL 28-28	47.95	1.79	16.77	9.63	0.12	8.14	11.55	2.85	0.19	0.18	99.17

PL 29-01	50.33	1.33	14.60	10.47	0.15	7.62	12.55	2.52	0.14	0.12	99.81
PL 29-02	50.15	1.38	14.58	10.30	0.15	7.76	12.52	2.52	0.16	0.08	99.59
PL 29-03	50.35	1.35	14.62	10.41	0.16	7.67	12.56	2.49	0.17	0.10	99.89
PL 29-04	49.39	1.32	14.43	10.18	0.13	7.80	12.54	2.28	0.17	0.08	98.31
PL 29-05	50.56	1.33	14.64	10.49	0.15	7.59	12.65	2.48	0.15	0.09	100.13
PL 29-06	50.28	1.33	14.53	10.33	0.13	7.68	12.58	2.53	0.14	0.10	99.63
PL 29-07	50.36	1.33	14.62	10.23	0.12	7.68	12.50	2.45	0.16	0.09	99.54
PL 29-08	50.75	1.32	14.65	10.47	0.16	7.61	12.57	2.47	0.16	0.11	100.26
PL 29-09	49.61	1.44	14.32	10.64	0.14	7.65	12.46	2.45	0.17	0.14	99.03
PL 29-11	50.05	1.33	14.66	10.35	0.16	7.84	12.37	2.47	0.17	0.12	99.52
PL 29-12	49.26	1.41	14.40	10.49	0.14	7.66	12.52	2.54	0.16	0.10	98.68
PL 29-13	50.26	1.41	14.57	10.17	0.13	7.88	12.55	2.51	0.17	0.12	99.59
PL 29-14	49.78	1.35	14.50	10.31	0.13	7.89	12.51	2.54	0.15	0.11	99.26
PL 29-15	50.79	1.35	14.69	10.06	0.13	7.97	12.51	2.46	0.16	0.12	100.24
PL 29-16	49.85	1.36	14.49	10.34	0.16	7.84	12.51	2.52	0.15	0.11	99.34
PL 29-17	50.07	1.35	14.63	10.37	0.15	7.88	12.59	2.54	0.14	0.12	99.85
PL 29-18	50.18	1.27	14.52	10.51	0.15	7.80	12.54	2.52	0.17	0.13	99.78
PL 29-19	50.68	1.37	14.62	10.05	0.14	7.97	12.59	2.46	0.15	0.08	100.10
PL 29-20	50.79	1.35	14.58	10.04	0.14	8.00	12.47	2.44	0.16	0.11	100.07

## Microprobe Results of PLUME2 pillow-rim glass

<u>Sample</u>	<u>SiO2</u>	<u>TiO2</u>	<u>Al2O3</u>	<u>FeO</u>	<u>MnO</u>	<u>MgO</u>	<u>CaO</u>	<u>Na2O</u>	<u>K2O</u>	<u>P2O5</u>	<u>Total</u>
PL 29-21A	50.25	1.36	14.76	10.36	0.16	7.86	12.90	2.46	0.15	0.16	100.42
PL 29-21B	50.32	1.34	14.51	10.37	0.14	7.95	12.60	2.46	0.15	0.11	99.94
PL 29-22	50.00	1.38	14.42	10.70	0.16	7.82	12.68	2.53	0.16	0.10	99.96
PL 29-23	49.58	1.41	14.64	10.58	0.13	7.87	12.60	2.56	0.16	0.11	99.63
PL 29-24	48.69	1.48	14.31	10.39	0.16	7.89	12.61	2.57	0.16	0.09	98.36
PL 29-25	49.78	1.31	14.53	10.50	0.13	7.82	12.64	2.45	0.15	0.11	99.43
PL 29-26	49.85	1.44	14.44	10.40	0.14	7.96	12.70	2.51	0.15	0.08	99.66
PL 29-27	50.78	1.39	14.86	10.45	0.14	7.82	12.68	2.57	0.15	0.11	100.94
PL 29-28	49.58	1.47	14.61	10.50	0.13	7.74	12.69	2.54	0.16	0.10	99.53
PL 29-29	49.23	1.60	15.71	10.07	0.15	8.16	12.17	2.71	0.17	0.12	100.10
PL 29-30	50.23	1.45	14.62	10.54	0.14	7.81	12.63	2.56	0.16	0.12	100.25
PL 29-31	49.89	1.34	14.56	10.42	0.14	7.83	12.64	2.53	0.16	0.09	99.59
PL 29-32	49.73	1.41	14.71	10.20	0.15	7.91	12.74	2.49	0.17	0.10	99.61
PL 29-33	49.84	1.41	14.74	10.42	0.13	7.73	12.69	2.62	0.16	0.16	99.90
PL 29-34	50.39	1.43	14.63	10.26	0.14	7.94	12.68	2.62	0.16	0.11	100.36
PL 29-35	49.73	1.38	14.65	10.59	0.13	7.62	12.59	2.75	0.13	0.12	99.71
PL 29-36	50.27	1.39	14.64	10.32	0.11	7.65	12.70	2.58	0.15	0.11	99.92
PL 29-37	49.74	1.40	14.39	10.38	0.14	7.80	12.61	2.61	0.15	0.11	99.34
PL 29-38	49.47	1.30	14.54	10.15	0.12	7.90	12.67	2.71	0.16	0.13	99.15
PL 29-39	49.69	1.36	14.41	10.33	0.13	7.76	12.60	2.56	0.16	0.10	99.11
PL 29-41	50.24	1.42	14.66	10.34	0.14	7.76	12.69	2.52	0.16	0.11	100.04
PL 29-42	49.84	1.36	14.63	10.56	0.14	7.55	12.84	2.60	0.13	0.14	99.78
PL 29-49	49.85	1.39	14.59	10.25	0.14	7.86	12.59	2.63	0.16	0.13	99.59
PL 29-49	49.89	1.35	14.58	10.31	0.13	7.80	12.57	2.43	0.15	0.13	99.33
PL 29-49	49.87	1.37	14.59	10.28	0.14	7.83	12.58	2.53	0.16	0.13	99.46
PL 30-01	48.67	1.56	16.58	9.37	0.12	8.32	12.25	2.59	0.36	0.17	100.00

#### APPENDIX 4: Microprobe Data from PLUME2 Minerals

The following tables list the major element analyses for minerals from some of the PLUME2 dredge sites. Minerals were from either polished thin sections or within the pillow-rim glass pieces mounted in epoxy. In thin section, plagioclase megacrysts were usually analyzed by a line of analyses from core to rim. Each swath across a crystal can be identified by sequential point numbers. Megacrysts are generally <5mm and are prismatic. Microcrysts are smaller than 5mm and are prismatic. Groundmass plagioclase are lath-shaped. Analyses were performed on the Camebax SX50 microprobe at Oregon State University. The beam had an acceleration voltage of 15 kV and a current of 30 nA. Counting times for each element were 10 seconds.

# Microprobe analyses of minerals from Galapagos Platform -Dredge 9

samples from mounted glass

## Olivine

Mount#	Sample	Mg	Al	Si	Ca	Mn	Ni	Fe	Total	Fo%
14	PL09-04	46.73	0.22	39.65	0.43	0.16	0.24	12.10	99.52	87.67
14	PL09-04	46.60	0.10	39.74	0.36	0.15	0.35	11.32	98.61	88.31
14	PL09-06	46.66	0.20	39.85	0.39	0.15	0.24	11.39	98.88	88.28
14	PL09-06	46.24	0.17	39.59	0.38	0.16	0.28	11.97	98.79	87.62
14	PL09-06	46.53	0.10	39.68	0.41	0.18	0.32	11.69	98.90	87.97
14	PL09-16	46.67	0.23	39.45	0.42	0.17	0.22	11.25	98.42	88.43
14	PL09-16	48.56	0.13	39.16	0.39	0.14	0.23	10.97	99.59	89.07
14	PL09-16	46.45	0.13	38.98	0.35	0.17	0.25	11.68	98.00	87.89
14	PL09-17	46.56	0.22	39.20	0.36	0.18	0.32	11.28	98.10	88.30
14	PL09-17	47.04	0.13	39.48	0.39	0.15	0.30	11.15	98.64	88.58

## Plagioclase

		Na	Mg	Al	Si	K	Ca	Fe	Ba	Total	An%
14	PL09-16 lath	2.36	0.25	32.49	47.60	0.00	15.96	0.63	0.01	99.30	78.86
14	PL09-16 lath	2.34	0.23	32.35	48.35	0.02	15.87	0.68	0.00	99.84	78.84
14	PL09-16 lath	2.45	0.30	32.04	47.24	0.00	15.76	0.74	0.00	98.53	78.01
14	PL09-35 lath	3.15	0.27	30.76	49.83	0.05	14.48	0.88	0.01	99.41	71.54
14	PL09-35 lath	3.09	0.21	31.01	49.95	0.06	14.26	0.70	0.04	99.32	71.58
14	PL09-35 lath	3.23	0.22	30.67	49.90	0.04	14.26	0.80	0.00	99.11	70.79

# Microprobe analyses of minerals from Galapagos Platform -Dredge 10

## Data from thin section - PL10- 3

### Olivine

date	point #		Mg	Al	Si	Ca	Mn	Ni	Fe	Total	Fo%
9/9/91	19	rim	46.82	0.08	39.96	0.30	0.18	0.32	10.51	98.17	89.01
9/9/91	20	core	47.22	0.10	40.03	0.28	0.17	0.30	10.74	98.84	88.86

### Spinel

			Na	Mg	Al	Si	Ti	V	Cr	Mn	FeO	Ni	Zn	Fe2o3	Total
9/9/91	1	core	0.00	21.22	48.57	0.13	0.20	0.13	16.77	0.07	6.73	0.26	0.01	4.67	98.76
9/9/91	2	core	0.00	21.22	48.25	0.12	0.21	0.11	16.49	0.10	6.49	0.27	0.05	4.98	98.27
9/9/91	3	core	0.00	21.10	48.09	0.12	0.21	0.10	16.56	0.10	6.57	0.22	0.00	4.87	97.93
9/9/91	4	core	0.00	22.13	46.13	0.19	0.20	0.08	16.75	0.12	4.40	0.28	0.00	7.06	97.35
9/9/91	5	core	0.00	20.74	47.87	0.13	0.21	0.08	16.56	0.11	6.81	0.29	0.06	4.34	97.19
9/9/91	6	rim	0.00	21.17	48.06	0.14	0.21	0.09	16.42	0.10	6.46	0.27	0.03	5.04	97.98

### Plagioclase

			Na	Mg	Al	Si	K	Ca	Fe	Ba	Total	An%
		megacrysts										
9/9/91	1	core	1.25	0.15	34.52	44.66	0.00	17.99	0.36	0.00	98.93	88.84
9/9/91	2	core	1.30	0.17	34.37	44.20	0.00	17.96	0.29	0.00	98.28	88.45
9/9/91	3	core	1.28	0.18	34.64	45.36	0.01	17.84	0.27	0.00	99.57	88.50
9/9/91	4	rim	1.06	0.12	35.01	44.48	0.00	18.27	0.42	0.00	99.35	90.53
9/9/91	14	rim	1.84	0.19	33.52	46.25	0.00	17.12	0.45	0.00	99.36	83.73
9/9/91	15	core	1.18	0.15	34.42	44.61	0.01	18.13	0.26	0.00	98.75	89.47
9/9/91	16	core	1.31	0.16	34.05	44.79	0.01	17.78	0.30	0.00	98.40	88.18
9/9/91	11	core	1.12	0.17	34.44	44.43	0.02	18.22	0.27	0.00	98.67	89.88
9/9/91	11	core	1.05	0.13	34.71	44.37	0.03	18.41	0.38	0.01	99.09	90.53
9/9/91	11	core	1.40	0.15	34.09	45.18	0.00	17.82	0.30	0.00	98.93	87.58
9/9/91	12	core	1.39	0.16	34.13	44.87	0.00	17.91	0.30	0.00	98.75	87.70
9/9/91	13	rim	1.04	0.14	34.95	44.45	0.00	18.02	0.33	0.00	98.92	90.55



**Microprobe analyses of minerals from Galapagos Platform -Dredge 10**

			Na	Mg	Al	Si	K	Ca	Fe	Ba	Total	An%
		<b>microphenocryst</b>										
9/9/91	5	micro-rim	1.97	0.23	32.97	47.15	0.00	16.77	0.54	0.00	99.64	82.44
9/9/91	6	micro-core	2.16	0.21	32.73	47.29	0.01	16.54	0.42	0.00	99.36	80.85
9/9/91	7	micro-rim	2.43	0.34	32.32	47.99	0.02	16.00	0.66	0.00	99.76	78.35
		<b>groundmass</b>										
9/9/91	17	gmass	2.19	0.22	33.03	47.18	0.02	16.45	0.58	0.00	99.67	80.50
9/9/91	18	gmass	2.25	0.16	32.63	47.25	0.01	16.18	0.51	0.00	99.00	79.80
9/9/91	8	gmass	2.52	0.39	31.73	48.02	0.07	15.70	1.09	0.00	99.50	77.21
9/9/91	9	gmass	2.39	0.34	31.90	47.43	0.01	16.01	0.78	0.00	98.87	78.68
9/9/91	10	gmass	2.28	0.34	31.89	47.28	0.01	16.21	0.78	0.00	98.79	79.66

**samples from mounted glass**

**Olivine**

Mount#	Sample	Mg	Al	Si	Ca	Mn	Ni	Fe	Total	Fo
14	PL 10-08	43.93	0.07	38.94	0.39	0.24	0.11	14.36	98.04	84.74
14	PL 10-08	43.61	0.05	38.88	0.44	0.22	0.08	14.41	97.68	84.68

**Plagioclase**

		Na	Mg	Al	Si	K	Ca	Fe	Ba	Total	An%
14	PL 10-08 micro	3.01	0.29	30.72	49.47	0.04	14.71	0.80	0.00	99.04	72.82
14	PL 10-08 micro	3.08	0.24	31.08	49.29	0.04	14.51	0.67	0.00	98.91	72.08
14	PL 10-08 micro	3.11	0.25	30.99	49.67	0.04	14.53	0.86	0.00	99.46	71.90

Microprobe analyses of minerals from Galapagos Platform -Dredge 11

			Na	Mg	Al	Si	K	Ca	Fe	Ba	Total	An %
		high An micro										
9/9/91	5	micro-rim	2.18	0.15	33.16	47.99	0.01	16.59	0.55	0.00	100.63	80.78
9/9/91	36	core	1.23	0.12	34.67	44.95	0.00	18.05	0.43	0.00	99.44	89.02
9/9/91	1	core	1.08	0.09	34.87	44.62	0.01	18.27	0.36	0.00	99.31	90.25
9/9/91	2	core	1.30	0.10	34.59	44.99	0.00	17.90	0.37	0.00	99.26	88.40
9/9/91	3	core	1.27	0.09	34.57	45.15	0.00	18.21	0.49	0.00	99.78	88.79
9/9/91	1	micro-rim	3.25	0.21	31.20	49.57	0.03	14.48	0.50	0.00	99.24	70.99
9/9/91	2	core	1.94	0.12	33.37	46.42	0.01	16.77	0.42	0.01	99.05	82.62
9/9/91	3	micro-rim	3.47	0.18	31.09	50.38	0.03	14.38	0.54	0.00	100.07	69.51
		<u>Groundmass</u>										
9/9/91	25	gmass	3.94	1.42	26.61	51.68	0.03	13.47	2.19	0.00	99.35	65.27
9/9/91	26	gmass	3.90	0.43	29.24	50.65	0.04	13.40	0.95	0.00	98.61	65.37
9/9/91	35	gmass	3.61	0.25	30.90	51.10	0.02	13.93	0.88	0.00	100.69	68.00
9/9/91	6	gmass	4.70	0.34	28.11	52.71	0.05	11.83	1.19	0.00	98.94	58.00
9/9/91	7	gmass	4.10	0.26	29.34	51.64	0.02	13.06	0.85	0.00	99.27	63.68
9/9/91	7	gmass	4.50	0.28	28.78	52.86	0.03	12.12	0.97	0.00	99.55	59.70

samples from mounted glass

Plagioclase

Mount#	Sample		Na	Mg	Al	Si	K	Ca	Fe	Ba	Total	An%
15	PL 11-12	micro	3.73	0.15	30.30	51.20	0.09	13.42	0.71	0.00	99.60	66.21
15	PL 11-12	micro	3.83	0.14	30.06	50.89	0.09	13.47	0.90	0.00	99.38	65.68

Olivine

Mount#	Sample	Mg	Al	Si	Ca	Mn	Ni	Fe	Total	Fo
15	PL 11-12	41.03	0.05	38.20	0.39	0.25	0.08	17.37	97.36	81.02
15	PL 11-12	41.41	0.05	38.15	0.36	0.32	0.10	17.72	98.10	80.76

# Microprobe analyses of minerals from Galapagos Platform -Dredge 11

## Thin section PL11-7

### Olivine

date	point #		Mg	Al	Si	Ca	Mn	Ni	Fe	Total	Fo%
9/9/91	28	olivine - rim	41.99	0.05	38.09	0.41	0.28	0.16	17.12	98.09	81.60
9/9/91	29	olivine - core	42.20	0.05	38.46	0.38	0.26	0.16	17.03	98.54	81.75
9/9/91	33	olivine - rim	41.58	0.05	39.11	0.42	0.31	0.18	17.07	98.72	81.47
9/9/91	34	olivine - core	42.13	0.04	39.04	0.37	0.25	0.09	17.26	99.17	81.51
9/9/91	37	olivine - core	42.05	0.04	39.14	0.39	0.26	0.13	17.63	99.63	81.17

### Plagioclase

#### Megacrysts

			Na	Mg	Al	Si	K	Ca	Fe	Ba	Total	An%
9/9/91	20	rim	2.25	0.16	32.63	47.25	0.01	16.18	0.51	0.00	99.00	79.80
9/9/91	21	core	1.11	0.13	34.78	44.41	0.03	18.24	0.37	0.00	99.05	89.98
9/9/91	22	core	1.34	0.11	34.18	44.72	0.02	17.81	0.40	0.00	98.58	87.87
9/9/91	23	core	1.21	0.11	34.18	44.37	0.02	18.21	0.36	0.00	98.46	89.18
9/9/91	24	rim	3.23	0.20	31.12	49.67	0.02	14.35	0.52	0.00	99.13	70.96
9/9/91	29	rim	2.79	0.17	32.00	49.35	0.01	15.35	0.47	0.04	100.18	75.21
9/9/91	30	core	1.77	0.13	33.59	46.49	0.01	16.90	0.44	0.03	99.35	84.04
9/9/91	31	core	2.59	0.16	32.01	47.90	0.01	15.84	0.44	0.03	98.97	77.15
9/9/91	4	rim	2.32	0.16	33.13	48.17	0.00	16.03	0.46	0.00	100.27	79.22
9/9/91	5	core	1.22	0.12	34.54	44.83	0.00	18.05	0.32	0.00	99.09	89.13
9/9/91	6	core	1.33	0.15	34.32	45.29	0.00	17.91	0.25	0.00	99.24	88.17

#### Microphenocrysts

9/9/91	32	core	3.65	0.18	30.23	51.09	0.02	13.84	0.55	0.03	99.59	67.62
--------	----	------	------	------	-------	-------	------	-------	------	------	-------	-------

# Microprobe analyses of minerals from Galapagos Platform -Dredge 12

## Thin section PL12-5

### Olivine

date	point #		Mg	Al	Si	Ca	Mn	Ni	Fe	Total	Fo%
9/9/91	1	micro-core	43.57	0.06	38.92	0.33	0.23	0.17	15.43	98.71	83.60
9/9/91	2	micro	42.51	0.06	38.73	0.37	0.27	0.12	16.54	98.60	82.26
9/9/91	3	micro-rim	40.74	0.05	38.31	0.40	0.33	0.10	18.27	98.18	80.06
9/9/91	12	micro-core	43.58	0.06	38.97	0.34	0.22	0.18	15.37	98.72	83.67
9/9/91	13	micro-core	42.98	0.04	38.93	0.34	0.25	0.16	15.73	98.44	83.13
9/9/91	18	micro	43.01	0.06	39.46	0.38	0.30	0.11	15.65	98.96	83.21
9/9/91	19	micro	42.87	0.05	39.28	0.36	0.26	0.14	15.69	98.65	83.14
9/9/91	20	micro	42.66	0.05	39.14	0.37	0.34	0.15	16.26	98.97	82.50

### Plagioclase

		<u>Megacrysts</u>	Na	Mg	Al	Si	K	Ca	Fe	Ba	Total	An %
9/9/91	4	mega-rim	3.04	0.18	31.28	49.48	0.02	14.58	0.53	0.00	0.27	72.51
9/9/91	5	mega	1.69	0.18	33.71	45.80	0.00	17.21	0.31	0.01	0.15	84.88
9/9/91	6	mega	1.51	0.17	33.90	45.34	0.02	17.37	0.28	0.00	0.14	86.27
9/9/91	7	mega	1.50	0.15	33.93	45.31	0.01	17.73	0.27	0.00	0.14	86.66
		<u>Microcrysts</u>										
9/9/91	14	micro-rim	3.60	0.20	30.27	50.72	0.02	13.93	0.67	0.01	0.32	68.08
9/9/91	15	micro	1.99	0.16	33.18	46.93	0.00	16.70	0.42	0.00	0.18	82.23
9/9/91	16	micro	1.92	0.14	33.53	47.02	0.00	16.88	0.38	0.00	0.17	82.92
9/9/91	17	micro	1.96	0.16	33.66	46.84	0.01	16.69	0.38	0.01	0.18	82.48
		<u>Groundmass</u>										
9/9/91	8	gmass	3.45	0.26	30.30	50.11	0.02	14.27	0.69	0.01	0.31	69.47
9/9/91	9	gmass	3.39	0.23	29.80	48.70	0.03	13.91	0.91	0.00	0.31	69.29
9/9/91	10	gmass	3.35	0.16	30.72	50.04	0.02	13.95	0.47	0.01	0.30	69.64
9/9/91	11	gmass	3.28	0.19	30.42	49.11	0.03	14.05	0.69	0.01	0.30	70.16
9/9/91	21	gmass	3.38	0.18	30.76	50.27	0.01	14.19	0.46	0.00	0.30	69.81
9/9/91	22	gmass	3.47	0.24	30.08	50.66	0.02	13.75	0.93	0.00	0.31	68.61
9/9/91	23	gmass	3.40	0.21	30.73	50.23	0.02	14.38	0.77	0.02	0.30	69.97

# Microprobe analyses of minerals from Galapagos Platform -Dredge 12

## Samples from mounted glass

Mount	Plagioclase	Na	Mg	Al	Si	K	Ca	Fe	Ba	Total	An%
16	PL 12-02 micro	2.53	0.21	31.88	48.32	0.01	15.46	0.61	0.00	99.01	77.14
16	PL 12-02 micro	2.54	0.22	31.98	48.32	0.01	15.62	0.69	0.00	99.37	77.25
16	PL 12-02 micro	2.70	0.20	31.56	48.13	0.04	15.16	0.66	0.00	98.45	75.49
16	PL 12-02 micro	2.27	0.24	32.27	47.98	0.03	15.93	0.59	0.00	99.31	79.36
16	PL 12-02 micro	2.94	0.20	30.87	49.13	0.01	14.50	0.82	0.00	98.45	73.12
16	PL 12-02 micro	3.01	0.19	31.07	49.88	0.01	14.62	0.61	0.00	99.38	72.84
15	PL 12-02 micro	2.46	1.32	30.99	48.11	0.02	15.04	1.19	0.00	99.13	77.06
15	PL 12-02 micro	2.39	0.17	32.00	47.81	0.01	15.95	0.51	0.00	98.85	78.58
15	PL 12-02 micro	2.41	0.21	31.59	47.50	0.02	15.66	0.62	0.01	98.02	78.12
15	PL 12-02 micro	2.73	1.20	29.62	49.34	0.02	14.89	1.30	0.00	99.10	74.99
15	PL 12-02 micro	2.21	0.23	32.69	47.81	0.02	15.89	0.50	0.00	99.35	79.78
15	PL 12-02 micro	2.20	0.20	32.57	47.66	0.01	16.05	0.52	0.00	99.21	80.07

	Olivine	Mg	Al	Si	Ca	Mn	Ni	Fe	Total	Fo%
16	PL 12-02	46.95	0.07	39.25	0.37	0.18	0.22	11.30	98.33	
16	PL 12-02	44.85	0.08	38.26	0.34	0.21	0.16	13.00	96.89	
16	PL 12-05	43.94	0.04	38.59	0.34	0.28	0.15	14.99	98.34	
16	PL 12-05	43.48	0.04	38.58	0.33	0.29	0.15	15.51	98.39	
16	PL 12-05	44.29	0.07	38.49	0.31	0.26	0.17	14.62	98.21	
16	PL 12-05	43.62	0.04	37.65	0.45	0.31	0.13	16.18	98.38	
15	PL 12-09	46.73	0.08	39.45	0.28	0.16	0.23	10.92	97.86	88.59
15	PL 12-09	46.34	0.07	39.55	0.28	0.17	0.19	10.75	97.35	88.66
15	PL 12-09	45.80	0.07	39.15	0.33	0.19	0.19	11.51	97.24	87.87
15	PL 12-11	45.99	0.10	39.72	0.37	0.15	0.17	11.28	97.77	88.21
15	PL 12-11	46.03	0.08	39.53	0.39	0.17	0.16	11.58	97.94	87.95

# Microprobe analyses of minerals from Galapagos Platform -Dredge 13

## Thin section PL13-23

### Olivine

date	point #		Mg	Al	Si	Ca	Mn	Ni	Fe	Total	Fo%
9/10/91	23	gmass	42.79	0.08	38.40	0.47	0.25	0.12	16.15	98.25	82.84
9/10/91	20	gmass	42.84	0.09	38.24	0.50	0.23	0.07	16.67	98.65	82.44
9/10/91	21	gmass	45.12	0.08	38.94	0.41	0.23	0.07	14.49	99.34	85.00

### Plagioclase

### Megacrysts

			Na	Mg	Al	Si	K	Ca	Fe	Ba	Total	An%
9/10/91	1	rim	3.27	0.32	30.94	50.23	0.01	14.56	0.80	0.01	100.14	71.08
9/10/91	2	core	1.09	0.16	34.73	44.86	0.00	18.53	0.34	0.02	99.73	90.38
9/10/91	3	core	0.92	0.14	35.19	44.63	0.00	18.54	0.33	0.02	99.75	91.76
9/10/91	4	core	1.08	0.16	34.38	44.68	0.02	18.16	0.47	0.00	98.95	90.21
9/10/91	5	core	0.68	0.08	35.84	44.11	0.01	18.97	0.27	0.00	99.97	93.85
9/10/91	15	rim	1.90	0.20	33.19	46.91	0.00	16.91	0.55	0.01	99.66	83.11
9/10/91	16	core	1.62	0.20	33.81	45.95	0.02	17.37	0.38	0.01	99.35	85.41
9/10/91	17	core	1.39	0.18	34.33	45.27	0.00	17.90	0.33	0.00	99.39	87.71
9/10/91	18	rim	3.84	1.94	22.24	50.98	0.02	13.06	5.55	0.00	97.63	65.21
9/10/91	19	rim	2.25	0.22	32.66	48.15	0.01	16.14	0.54	0.00	99.97	79.83
9/10/91	20	core	1.52	0.18	34.17	45.90	0.01	17.61	0.40	0.00	99.78	86.46
9/10/91	21	core	1.86	0.19	33.43	46.81	0.00	17.00	0.36	0.00	99.65	83.45
9/10/91	1	core	0.80	0.10	35.21	43.49	0.00	19.08	0.32	0.01	99.01	92.92
9/10/91	2	core	0.98	0.10	35.27	44.53	0.00	18.62	0.29	0.00	99.78	91.33
9/10/91	3	rim	3.41	0.27	30.79	50.47	0.00	14.38	0.73	0.00	100.05	69.98
9/10/91	6	rim	3.48	0.27	30.21	50.97	0.00	14.13	0.83	0.00	99.89	69.17
9/10/91	7	core	1.72	0.16	33.67	46.52	0.00	17.34	0.37	0.00	99.78	84.78
9/10/91	8	core	1.22	0.11	34.50	44.92	0.00	18.22	0.30	0.00	99.28	89.16
9/10/91	9	core	1.62	0.12	33.88	46.01	0.00	17.50	0.32	0.00	99.46	85.62
9/10/91	10	rim	2.40	0.25	32.12	47.19	0.00	16.27	0.59	0.00	98.80	78.95
9/10/91	11	core	1.70	0.17	33.41	45.62	0.00	17.35	0.39	0.00	98.64	84.94
9/10/91	12	core	1.39	0.12	34.11	45.23	0.00	17.81	0.36	0.00	99.01	87.62
9/10/91	13	core	2.06	0.19	32.77	46.74	0.00	16.44	0.39	0.00	98.59	81.51

Microprobe analyses of minerals from Galapagos Platform -Dredge 13

			Na	Mg	Al	Si	K	Ca	Fe	Ba	Total	An%
9/10/91	14	core	1.47	0.14	34.07	45.85	0.00	17.55	0.35	0.00	99.44	86.86
9/10/91	15	rim	3.45	0.24	30.27	50.36	0.00	14.08	0.69	0.00	99.08	69.26
9/10/91	16	rim	2.11	0.19	33.10	47.01	0.00	16.81	0.50	0.02	99.72	81.52
9/10/91	17	core	1.82	0.17	33.72	46.54	0.00	17.19	0.32	0.01	99.78	83.91
9/10/91	18	core	1.37	0.12	34.30	45.18	0.00	18.05	0.30	0.00	99.32	87.93
		<u>Microcrysts</u>										
9/10/91	9	micro-rim	2.84	0.31	31.82	49.33	0.00	15.17	0.66	0.00	100.12	74.71
9/10/91	10	micro-core	1.79	0.21	33.57	46.88	0.00	17.01	0.42	0.03	99.91	83.97
9/10/91	13	micro-core	1.47	0.16	33.86	45.52	0.00	17.62	0.47	0.00	99.10	86.86
9/10/91	14	micro-core	1.99	0.21	33.28	46.83	0.02	16.93	0.38	0.00	99.63	82.39
9/10/91	4	micro-rim	3.59	0.39	29.87	50.59	0.00	14.08	0.82	0.00	99.33	68.42
9/10/91	5	micro-core	1.76	0.16	34.07	47.02	0.00	17.12	0.43	0.00	100.56	84.30
9/10/91	19	micro-core	1.90	0.16	33.28	46.79	0.00	16.91	0.40	0.00	99.43	83.07
		<u>Groundmass</u>										
9/10/91	6	gmass	3.15	0.28	30.96	50.04	0.01	14.58	0.73	0.04	99.79	71.85
9/10/91	7	gmass	3.27	0.36	30.81	50.23	0.01	14.64	0.93	0.02	100.26	71.20
9/10/91	8	gmass	4.22	0.37	28.80	52.16	0.04	12.88	1.15	0.00	99.61	62.63
9/10/91	22	gmass	3.38	0.25	30.43	50.49	0.01	14.28	0.82	0.00	99.65	69.98

Samples from mounted glass

Mount		Plagioclase	Na	Mg	Al	Si	K	Ca	Fe	Ba	Total	An%
19	PL13-12	megacryst	1.26	0.14	33.92	45.16	0.00	17.41	0.27	0.00	98.16	88.40
19	PL13-12	megacryst	1.29	0.16	33.83	45.28	0.00	17.51	0.30	0.01	98.37	88.27
19	PL13-12	megacryst	1.21	0.15	34.21	45.05	0.01	17.67	0.32	0.02	98.65	88.89
19	PL13-12	megacryst	1.12	0.15	34.19	45.06	0.01	17.74	0.28	0.00	98.56	89.72
19	PL13-12	megacryst	0.92	0.11	34.06	44.83	0.00	17.81	0.28	0.00	98.00	91.47
19	PL13-31	megacryst	1.13	0.13	34.49	44.93	0.00	17.86	0.34	0.00	98.88	89.70
19	PL13-31	megacryst	1.12	0.13	34.20	44.87	0.00	17.86	0.24	0.00	98.42	89.76
19	PL13-31	megacryst	1.15	0.15	34.47	44.95	0.02	17.89	0.32	0.01	98.96	89.50
19	PL13-31	megacryst	1.13	0.13	34.14	44.51	0.01	17.57	0.24	0.01	97.74	89.51

Microprobe analyses of minerals from Galapagos Platform -Dredge 13

			Na	Mg	Al	Si	K	Ca	Fe	Ba	Total	An%
19	PL13-31	megacryst	1.21	0.17	34.06	44.70	0.00	17.75	0.28	0.03	98.19	89.05
19	PL13-32	megacryst	1.34	0.17	33.67	45.15	0.00	17.46	0.32	0.00	98.10	87.81
19	PL13-32	megacryst	1.18	0.15	34.00	44.62	0.00	17.64	0.28	0.01	97.87	89.19
19	PL13-32	megacryst	1.24	0.16	34.00	44.51	0.00	17.86	0.26	0.02	98.05	88.84
19	PL13-32	megacryst	1.18	0.13	34.17	45.18	0.02	17.79	0.29	0.01	98.77	89.16
19	PL13-32	megacryst	1.20	0.17	34.11	45.13	0.01	17.65	0.28	0.00	98.54	89.03
19	PL13-32	megacryst	1.27	0.15	33.97	45.09	0.00	17.59	0.30	0.00	98.37	88.45
19	PL13-32	megacryst	1.30	0.16	33.93	45.11	0.00	17.65	0.29	0.02	98.46	88.27
19	PL13-33	megacryst	1.14	0.12	34.29	45.17	0.02	17.84	0.27	0.00	98.85	89.53
19	PL13-33	megacryst	1.09	0.14	34.23	44.96	0.01	17.93	0.29	0.00	98.65	90.02
19	PL13-33	megacryst	1.14	0.12	34.33	44.69	0.00	17.95	0.23	0.00	98.45	89.70
19	PL13-33	megacryst	1.05	0.13	34.38	44.56	0.00	17.92	0.25	0.02	98.32	90.36
19	PL13-33	megacryst	1.08	0.13	34.31	44.53	0.01	17.97	0.28	0.01	98.33	90.12
16	PL13-28	lath	2.67	0.28	30.98	48.62	0.00	15.33	0.75	0.00	98.63	76.01
16	PL13-28	lath	2.37	0.22	31.84	47.92	0.00	15.81	0.62	0.00	98.80	78.61
16	PL13-28	lath	2.53	0.24	31.92	48.89	0.01	15.38	0.70	0.00	99.67	77.05
16	PL13-29	lath	3.09	0.23	30.76	49.83	0.01	14.38	0.87	0.00	99.16	71.97
16	PL13-29	lath	2.55	0.26	31.55	48.59	0.00	15.44	0.74	0.00	99.13	76.96
15	PL13-30	lath	2.53	0.49	31.15	48.46	0.02	15.39	0.87	0.00	98.92	76.93
15	PL13-30	lath	2.07	0.25	32.47	47.30	0.03	16.18	0.65	0.00	98.95	81.04
19	PL13-31	lath	2.36	2.16	27.76	48.10	0.00	14.70	2.22	0.03	97.33	77.45
19	PL13-31	lath	2.33	1.25	29.87	48.09	0.00	15.20	1.51	0.01	98.26	78.26

	Olivine	Mg	Al	Si	Ca	Mn	Ni	Fe	Total	Fo%
16	RD 13-28	44.86	0.09	38.75	0.39	0.16	0.11	12.66	97.02	
16	RD 13-29	46.07	0.10	39.01	0.33	0.18	0.14	12.19	98.03	
16	RD 13-29	45.37	0.11	39.72	0.38	0.16	0.14	12.28	98.15	
16	RD 13-29	46.50	0.07	39.17	0.33	0.18	0.14	12.07	98.46	
15	RD 13-30	46.31	0.08	39.69	0.35	0.18	0.28	10.86	98.46	88.64
15	RD 13-30	45.73	0.12	39.46	0.38	0.19	0.20	11.52	97.74	87.90



Microprobe analyses of minerals from Galapagos Platform -Dredge 14

Thin section PL14-17

Olivine

date	point #		Mg	Al	Si	Ca	Mn	Ni	Fe	Total	Fo%
9/10/91	22	megacryst-rim	49.51	0.08	40.64	0.33	0.13	0.34	8.89	99.91	91.12
9/10/91	23	core	49.03	0.09	39.69	0.31	0.12	0.36	9.35	98.95	90.60
9/10/91	24	core	48.00	0.09	39.95	0.30	0.14	0.37	9.84	98.68	89.92
9/10/91	25	core	44.11	0.22	41.50	0.34	0.13	0.35	8.86	95.49	90.18
9/10/91	26	core	49.36	0.11	40.20	0.32	0.15	0.30	8.88	99.30	91.07
9/10/91	27	megacryst-rim	48.50	0.10	40.15	0.30	0.16	0.34	10.46	99.99	89.41
9/10/91	31	micro-core	46.69	0.09	39.41	0.31	0.20	0.26	11.73	98.69	87.84
9/10/91	32	micro-core	46.28	0.09	39.39	0.32	0.19	0.20	12.87	99.35	86.70
9/10/91	43	megacryst-rim	46.67	0.05	39.54	0.35	0.18	0.30	11.41	98.48	88.18
9/10/91	44	core	47.26	0.07	39.61	0.29	0.18	0.20	11.17	98.78	88.46
9/10/91	45	core	47.59	0.06	39.58	0.30	0.16	0.26	11.13	99.08	88.61
9/10/91	46	core	47.43	0.06	39.86	0.30	0.14	0.20	11.34	99.32	88.40
9/10/91	49	micro-core	45.99	0.06	39.65	0.32	0.19	0.23	11.98	98.42	87.45

Plagioclase

Megacrysts

			Na	Mg	Al	Si	K	Ca	Fe	Ba	Total	An%
9/10/91	35	rim	2.13	0.21	32.65	47.18	0.01	16.25	0.56	0.01	98.98	80.80
9/10/91	36	core	1.89	0.16	33.51	46.39	0.02	16.74	0.35	0.05	99.09	82.98
9/10/91	37	core	1.88	0.18	33.46	46.59	0.03	16.75	0.35	0.02	99.26	83.01
9/10/91	38	core	1.94	0.16	33.26	46.78	0.02	16.76	0.39	0.05	99.35	82.61
9/10/91	39	core	1.56	0.15	33.99	45.91	0.02	17.38	0.33	0.01	99.36	85.90
9/10/91	40	core	1.68	0.16	33.86	46.09	0.01	17.16	0.34	0.01	99.31	84.92
9/10/91	41	core	1.96	0.17	33.24	46.71	0.01	16.92	0.34	0.02	99.36	82.66
9/10/91	42	rim	1.86	0.15	33.66	46.29	0.01	17.05	0.46	0.00	99.50	83.45

Microcrysts

9/10/91	33	core	2.60	0.21	32.12	48.35	0.01	15.75	0.55	0.00	99.58	76.96
9/10/91	47	core	2.56	0.22	32.26	48.12	0.00	15.87	0.49	0.00	99.52	77.38
9/10/91	48	core	2.18	0.20	32.84	47.81	0.00	16.25	0.55	0.00	99.82	80.46

**Microprobe analyses of minerals from Galapagos Platform -Dredge 14**

		<u>Groundmass</u>	Na	Mg	Al	Si	K	Ca	Fe	Ba	Total	An%
9/10/91	28	gmass	2.36	0.17	32.47	47.85	0.00	16.02	0.66	0.00	99.53	78.95
9/10/91	29	gmass	2.55	0.21	32.15	48.38	0.00	15.74	0.52	0.00	99.55	77.32
9/10/91	30	gmass	2.37	0.19	32.63	47.78	0.01	16.14	0.56	0.00	99.67	78.95
9/10/91	50	gmass	3.28	6.92	23.69	48.54	0.02	11.48	4.33	0.03	98.29	65.85

**samples from mounted glass**

**Olivine**

Mount#	Sample	Mg	Al	Si	Ca	Mn	Ni	Fe	Total	Fo
15	PL14-23	46.58	0.05	39.66	0.30	0.17	0.22	10.83	97.81	88.66
15	PL14-23	46.86	0.06	39.45	0.32	0.20	0.25	10.88	98.02	88.66
15	PL14-23	46.42	0.08	39.78	0.32	0.18	0.26	11.13	98.15	88.36

Microprobe analyses of minerals from Galapagos Platform -Dredge 16  
Thin section PL16-1

Plagioclase

Megacrysts

			Na	Mg	Al	Si	K	Ca	Fe	Ba	Total	An %
9/9/91	24	rim	4.04	0.12	29.34	51.22	0.15	12.82	1.02	0.01	98.70	63.16
9/9/91	25	core	1.47	0.06	33.64	45.51	0.05	17.28	0.50	0.00	98.49	86.46
9/9/91	26	core	1.75	0.06	33.29	46.33	0.05	17.13	0.50	0.00	99.11	84.18
9/9/91	27	rim	3.94	0.12	29.75	50.58	0.13	13.36	0.83	0.00	98.70	64.68
9/9/91	41	rim	3.33	0.14	30.41	49.68	0.11	13.99	0.81	0.05	98.51	69.46
9/9/91	42	core	1.84	0.09	33.22	46.27	0.04	16.84	0.50	0.04	98.83	83.32
9/9/91	43	core	2.02	0.10	33.03	46.86	0.03	16.41	0.50	0.02	98.97	81.61

Microphenocrysts

9/9/91	33	rim	3.64	0.10	29.79	50.39	0.11	13.35	0.85	0.00	98.22	66.56
9/9/91	34	core	2.75	0.09	31.70	48.41	0.09	15.08	0.69	0.00	98.81	74.81
9/9/91	35	core	2.79	0.09	31.48	48.43	0.07	15.14	0.66	0.01	98.66	74.69
9/9/91	36	zoned micro-rim	4.90	0.12	27.94	52.54	0.21	11.44	0.88	0.00	98.03	55.63
9/9/91	37	core	3.51	0.11	30.16	49.61	0.11	14.00	0.65	0.01	98.16	68.40
9/9/91	38	core	2.75	0.09	31.37	48.22	0.09	15.10	0.69	0.00	98.30	74.82

Groundmass

9/9/91	28	gmass	5.05	0.12	27.81	53.63	0.27	10.96	1.11	0.03	98.98	53.67
9/9/91	29	gmass	4.98	0.08	28.13	53.69	0.25	11.07	1.02	0.02	99.24	54.33
9/9/91	44	gmass	4.89	0.11	27.61	52.81	0.25	11.00	0.89	0.02	97.57	54.60
9/9/91	45	gmass	4.95	0.12	28.32	53.93	0.24	11.09	1.13	0.05	99.82	54.54

Microprobe analyses of minerals from Galapagos Platform -Dredge 24  
samples from mounted glass

Olivine

Mount#	Sample	Mg	Al	Si	Ca	Mn	Ni	Fe	Total	Fo%
	PL24-05	39.35	0.07	37.61	0.33	0.31	0.07	19.84	97.58	78.04
	PL24-05	39.46	0.04	37.77	0.34	0.30	0.13	19.33	97.37	78.55
	PL24-05	40.17	0.06	37.73	0.30	0.28	0.13	18.04	96.69	79.96

Plagioclase

	Na	Mg	Al	Si	K	Ca	Fe	Ba	Total	An%
PL24-05	3.73	0.14	29.93	50.69	0.11	12.82	0.97	0.00	98.39	65.05
PL24-05	3.76	0.46	28.93	50.55	0.13	12.99	1.65	0.00	98.47	65.12

Microprobe analyses of minerals from Galapagos Platform -Dredge 25

Thin section PL25-3

Plagioclase

<u>Phenocrysts</u>			Na	Mg	Al	Si	K	Ca	Fe	Ba	Total	An%
date	point #											
5/22/91	1	rim	3.52	0.09	30.53	51.22	0.20	13.77	0.73	0.020	100.08	67.62
5/22/91	2	core	4.75	0.04	29.03	53.84	0.29	11.39	0.36	0.018	99.73	56.02
5/22/91	3	core	4.81	0.04	28.96	53.81	0.32	11.29	0.33	0.012	99.56	55.41
5/22/91	4	core	4.74	0.04	29.25	53.85	0.31	11.55	0.35	0.024	100.11	56.36
5/22/91	5	core	4.68	0.03	29.25	53.78	0.30	11.48	0.42	0.000	99.94	56.54
5/22/91	6	core	4.78	0.04	29.27	53.84	0.31	11.45	0.38	0.005	100.06	55.96
5/22/91	7	core	4.70	0.04	29.01	53.92	0.32	11.52	0.40	0.029	99.93	56.46
5/22/91	8	core	4.82	0.05	29.13	54.06	0.32	11.43	0.33	0.040	100.17	55.65
5/22/91	9	core	4.78	0.03	29.13	54.20	0.34	11.21	0.37	0.040	100.11	55.30
5/22/91	10	core	4.83	0.03	29.36	53.85	0.31	11.52	0.36	0.022	100.27	55.85
5/22/91	11	core	4.70	0.04	29.40	53.86	0.31	11.54	0.42	0.013	100.28	56.53
5/22/91	12	rim	4.04	0.14	29.93	51.96	0.21	13.13	0.84	0.017	100.25	63.44

<u>Groundmass</u>			Na	Mg	Al	Si	K	Ca	Fe	Ba	Total	An%
5/22/91	13	gmass	3.87	0.13	30.23	51.62	0.22	13.55	0.76	0.034	100.40	65.13
5/22/91	14	gmass	3.72	0.06	30.88	51.77	0.18	13.67	0.62	0.018	100.91	66.34

# Microprobe analyses of minerals from Galapagos Platform -Dredge 26

Sample 26-25

## Plagioclase

### Megacrysts

			Na	Mg	Al	Si	K	Ca	Fe	Ba	Total	An%
7/15/91	36	core	2.08	0.00	33.27	47.75	0.02	16.31	0.31	0.00	99.74	81.13
7/15/91	37	core	2.22	0.00	33.32	48.28	0.03	16.06	0.41	0.00	100.31	79.85
7/15/91	38	core	1.87	0.00	31.26	44.71	0.02	14.74	0.41	0.00	93.02	81.25
7/15/91	39	core	2.14	0.00	33.52	48.50	0.04	16.48	0.41	0.00	101.08	80.80
7/15/91	40	rim	3.41	0.04	31.28	51.00	0.04	14.20	0.51	0.00	100.48	69.54
7/15/91	44	incl. rim	3.40	0.21	30.82	51.41	0.05	14.06	0.68	0.01	100.63	69.32
7/15/91	45	core	2.23	0.15	33.03	48.52	0.04	16.19	0.44	0.00	100.59	79.89
7/15/91	46	core	2.22	0.15	33.09	48.29	0.03	15.93	0.45	0.00	100.14	79.74

## samples from mounted glass

### Plagioclase

Mount#	Sample		Na	Mg	Al	Si	K	Ca	Fe	Ba	Total	An%
16	PL 26-19	lath	3.22	0.33	30.37	49.99	0.04	14.30	0.96	0.00	99.21	70.89
16	PL 26-19	lath	3.47	0.26	29.82	50.46	0.06	13.77	0.88	0.00	98.72	68.46
16	PL 26-25	lath	2.93	0.17	31.13	49.59	0.01	14.45	0.80	0.00	99.07	73.12
16	PL 26-25	lath	3.25	0.23	30.49	50.18	0.02	14.18	0.94	0.00	99.28	70.64

### Olivine

Mount#	Sample	Mg	Al	Si	Ca	Mn	Ni	Fe	Total
16	PL 26-19	44.41	0.09	38.33	0.38	0.22	0.15	14.61	98.19
16	PL 26-25	43.02	0.08	38.40	0.41	0.25	0.16	15.82	98.14
16	PL 26-25	42.77	0.08	38.78	0.41	0.26	0.18	15.52	97.99

Microprobe analyses of minerals from Galapagos Platform -Dredge 27  
samples from mounted glass

Olivine

Mount#	Sample	Mg	Al	Si	Ca	Mn	Ni	Fe	Total
16	PL27-22	43.15	0.08	38.38	0.40	0.22	0.18	15.69	98.11
16	PL27-22	43.08	0.07	38.11	0.39	0.23	0.20	16.20	98.27
16	PL27-22	42.85	0.14	38.68	0.42	0.21	0.17	15.34	97.81

Plagioclase

Mount#	Sample	Na	Mg	Al	Si	K	Ca	Fe	Ba	Total	An%
16	PL27-22 lath	3.08	0.24	30.89	50.06	0.04	14.45	0.91	0.02	99.68	71.99
16	PL27-22 lath	3.21	0.24	30.56	50.46	0.03	14.05	1.03	0.03	99.62	70.59
18	PL27-19 lath	3.35	0.45	29.85	50.27	0.02	13.72	1.23	0.00	98.89	69.28
18	PL27-19 lath	3.14	0.23	30.58	49.86	0.03	14.24	0.96	0.00	99.01	71.38

Microprobe analyses of minerals from Galapagos Platform -Dredge 28

Thin section PL28-22

Plagioclase

			<u>Megacrysts</u>									
date	point #		Na	Mg	Al	Si	K	Ca	Fe	Ba	Total	An%
5/22/91	1	core	1.98	0.13	33.14	47.34	0.01	16.78	0.36	0.000	99.74	82.36
5/22/91	2	core	2.03	0.15	33.14	47.43	0.02	16.62	0.40	0.000	99.78	81.80
5/22/91	3	core	2.03	0.14	33.16	47.56	0.03	16.52	0.35	0.000	99.79	81.67
5/22/91	4	core	1.89	0.15	33.39	47.32	0.02	16.92	0.36	0.000	100.06	83.06
5/22/91	5	core	2.00	0.11	33.46	47.14	0.02	16.78	0.36	0.000	99.88	82.13
5/22/91	6	core	2.24	0.14	33.36	47.12	0.04	16.81	0.35	0.000	100.07	80.35
5/22/91	7	core	2.04	0.14	33.32	47.46	0.02	16.86	0.42	0.000	100.25	81.94
5/22/91	8	core	2.01	0.15	33.39	47.41	0.02	16.96	0.35	0.000	100.29	82.28
5/22/91	9	core	1.92	0.13	33.51	47.30	0.02	16.98	0.34	0.000	100.19	82.94
5/22/91	10	rim	2.60	0.25	31.64	48.66	0.04	15.86	0.82	0.000	99.86	76.96
5/22/91	17	rim	3.05	3.07	9.65	48.31	0.74	15.86	13.16	0.000	93.83	71.28
5/22/91	18	core	2.13	0.10	33.65	48.13	0.02	16.73	0.26	0.000	101.01	81.20
5/22/91	19	core	2.35	0.11	33.39	48.24	0.02	16.43	0.29	0.000	100.83	79.33
5/22/91	20	core	2.24	0.11	33.46	48.10	0.02	16.78	0.28	0.000	100.98	80.43
5/22/91	21	core	2.16	0.11	33.54	48.00	0.02	16.56	0.30	0.000	100.68	80.84
5/22/91	22	core	2.34	0.10	33.52	48.52	0.03	16.42	0.32	0.000	101.25	79.36
5/22/91	23	core	2.26	0.11	33.48	48.15	0.03	16.43	0.30	0.000	100.77	79.92
5/22/91	24	core	1.99	0.10	33.77	47.80	0.01	17.10	0.28	0.000	101.04	82.56
5/22/91	25	core	2.11	0.10	33.78	47.80	0.01	16.70	0.29	0.000	100.79	81.33
5/22/91	26	rim	2.33	0.13	33.18	49.03	0.02	16.21	0.43	0.000	101.33	79.23
5/22/91	2	core	1.86	0.13	33.70	47.57	0.05	17.31	0.39	0.016	101.02	83.48
5/22/91	3	core	2.10	0.11	33.55	47.87	0.04	16.89	0.34	0.002	100.90	81.44
5/22/91	4	core	2.15	0.11	33.35	47.86	0.03	16.80	0.40	0.000	100.69	81.08



Microprobe analyses of minerals from Galapagos Platform -Dredge 28

			Na	Mg	Al	Si	K	Ca	Fe	Ba	Total	An%
5/22/91	5	core	2.06	0.11	33.38	48.04	0.02	16.70	0.41	0.011	100.71	81.68
5/22/91	6	core	2.16	0.10	33.27	47.82	0.04	16.76	0.39	0.000	100.53	80.90
5/22/91	7	core	1.99	0.13	33.59	47.52	0.02	16.86	0.31	0.000	100.42	82.26
5/22/91	8	core	1.93	0.11	33.57	47.36	0.02	17.16	0.40	0.000	100.56	82.96
5/22/91	9	core	1.91	0.11	33.54	47.55	0.02	17.19	0.37	0.002	100.69	83.18
5/22/91	10	core	1.93	0.11	33.51	47.53	0.02	17.06	0.40	0.004	100.57	82.93
5/22/91	11	core	1.99	0.11	33.47	47.77	0.02	16.87	0.37	0.000	100.60	82.32

Groundmass

5/22/91	11	gmass	3.28	0.28	30.72	50.66	0.04	14.57	0.89	0.000	100.42	70.91
5/22/91	12	gmass	3.56	0.36	29.82	50.88	0.07	14.02	1.19	0.000	99.89	68.25

Thin section PL28-26

Megacrysts \* the first three xtals are from a single glomerocryst

7/15/91	1	core	2.21	0.16	32.73	47.88	0.02	16.34	0.39	0.00	99.73	80.25
7/15/91	2	core	2.23	0.14	33.23	47.73	0.01	16.03	0.43	0.00	99.79	79.79
7/15/91	3	core	2.23	0.13	33.02	47.85	0.04	16.13	0.42	0.00	99.80	79.83
7/15/91	4	core	2.32	0.16	32.89	47.74	0.02	15.92	0.38	0.00	99.43	79.06
7/15/91	5	core	2.04	0.15	33.28	47.57	0.03	16.40	0.42	0.00	99.88	81.47
7/15/91	6	core	2.09	0.12	33.23	47.56	0.02	16.49	0.36	0.00	99.86	81.29
7/15/91	7	rim	2.09	0.18	31.59	44.88	0.03	16.26	0.46	0.00	95.49	80.98
7/15/91	8	core	2.18	0.14	33.03	47.91	0.02	16.10	0.44	0.00	99.81	80.21
7/15/91	9	core	2.33	0.13	33.05	47.98	0.02	16.27	0.44	0.03	100.24	79.34
7/15/91	10	core	2.31	0.15	32.83	48.17	0.01	16.25	0.49	0.00	100.21	79.45
7/15/91	11	core	2.26	0.14	32.79	48.10	0.01	16.14	0.49	0.00	99.92	79.77
7/15/91	12	core	2.37	0.15	32.18	47.91	0.01	15.84	0.61	0.00	99.06	78.64
7/15/91	13	incl. rim	2.56	5.72	20.58	49.39	0.08	12.68	7.11	0.00	98.12	72.84

Microprobe analyses of minerals from Galapagos Platform -Dredge 28

			Na	Mg	Al	Si	K	Ca	Fe	Ba	Total	An%
7/15/91	1	rim	2.15	0.15	33.21	48.11	0.04	16.31	0.46	0.02	100.44	80.55
7/15/91	2	core	2.06	0.14	33.26	47.77	0.02	16.50	0.41	0.01	100.16	81.48
7/15/91	3	core	2.14	0.13	33.47	47.67	0.02	16.28	0.44	0.02	100.17	80.67
7/15/91	4	core	2.15	0.14	33.26	47.90	0.03	16.32	0.38	0.01	100.18	80.66
7/15/91	5	incl. rim	3.08	0.52	30.99	49.53	0.02	14.90	0.76	0.01	99.82	72.68
7/15/91	6	incl. rim	1.97	0.12	33.48	47.12	0.03	16.77	0.43	0.02	99.93	82.33
7/15/91	7	core	2.01	0.15	32.68	46.16	0.04	16.59	0.33	0.04	98.01	81.77
7/15/91	8	core	2.04	0.13	33.40	47.40	0.04	16.62	0.36	0.03	100.02	81.62
7/15/91	9	core	1.91	0.13	33.49	46.59	0.03	16.70	0.36	0.03	99.24	82.71
7/15/91	10	rim	1.88	0.11	33.91	47.28	0.04	16.80	0.33	0.03	100.38	83.02
7/15/91	14	rim	2.85	8.73	16.61	45.97	0.19	11.55	9.84	0.00	95.74	68.23
7/15/91	15	core	2.33	0.00	33.10	47.91	0.02	16.17	0.42	0.00	99.95	79.23
7/15/91	16	core	1.99	0.00	33.57	47.45	0.02	16.64	0.30	0.00	99.96	82.14
7/15/91	17	core	2.00	0.00	33.60	47.70	0.01	16.49	0.31	0.00	100.11	81.95
7/15/91	18	core	2.09	0.00	33.63	47.95	0.03	16.38	0.35	0.00	100.42	81.10
7/15/91	19	core	2.00	0.00	34.03	49.13	0.01	16.01	0.31	0.00	101.48	81.48
7/15/91	20	core	1.92	0.00	33.54	47.01	0.02	16.39	0.33	0.00	99.21	82.41
7/15/91	21	core	1.95	0.00	33.66	47.38	0.01	16.71	0.29	0.00	99.99	82.51
7/15/91	22	core	1.93	0.00	33.52	47.23	0.02	16.78	0.38	0.00	99.84	82.69
7/15/91	23	rim	1.93	0.00	33.69	47.45	0.02	16.61	0.32	0.00	100.01	82.55
7/15/91	24	rim	2.77	0.15	31.60	48.90	0.04	15.00	0.61	0.00	99.07	74.77
7/15/91	25	core	1.97	0.00	33.53	47.09	0.01	16.60	0.30	0.00	99.49	82.29
7/15/91	26	core	1.93	0.00	33.49	46.20	0.02	16.60	0.26	0.00	98.50	82.56
7/15/91	27	core	1.93	0.00	29.25	40.87	0.02	14.37	0.30	0.00	86.74	80.33
7/15/91	28	core	2.01	0.00	33.34	47.53	0.02	16.56	0.35	0.00	99.81	81.89

Microprobe analyses of minerals from Galapagos Platform -Dredge 28

			Na	Mg	Al	Si	K	Ca	Fe	Ba	Total	An%
7/15/91	29	core	2.00	0.00	33.32	47.31	0.02	16.30	0.33	0.00	99.28	81.70
7/15/91	30	core	1.98	0.00	33.06	46.98	0.01	16.25	0.33	0.00	98.62	81.86
7/15/91	31	core	0.46	0.00	6.05	8.02	0.00	3.15	0.01	0.00	17.70	78.97
7/15/91	32	core	0.00	0.00	3.75	9.62	0.10	0.81	1.83	0.00	16.10	87.56
7/15/91	33	core	2.07	0.00	33.48	47.28	0.01	16.38	0.42	0.00	99.64	81.32
7/15/91	34	core	1.69	0.00	30.54	41.59	0.03	15.44	0.31	0.00	89.59	83.33
7/15/91	35	rim	1.92	0.00	33.60	46.92	0.02	16.64	0.36	0.00	99.46	82.64

analyses of vitric core of melt inclusion in PL28-26

			Na	Mg	Al	Si	P	K	Ca	Ti	Mn	Fe	Total
7/15/91	11		1.24	8.04	17.08	50.15	0.183	0.35	12.07	1.46	0.17	9.496	100.23
7/15/91	12		2.23	7.95	16.58	48.64	0.064	0.16	12.08	1.42	0.20	9.279	98.60
7/15/91	13		1.72	7.98	16.68	49.75	0.165	0.32	11.82	1.47	0.15	9.406	99.46
	avg		1.73	7.99	16.78	49.51	0.14	0.28	11.99	1.45	0.17	9.39	99.43

samples from mounted glass

Plagioclase

mount #	sample		Na	Mg	Al	Si	K	Ca	Fe	Ba	Total	An%
18	PL28-19	megacryst	1.95	0.13	33.04	46.75	0.02	16.42	0.39	0.02	98.71	82.22
18	PL28-19	megacryst	1.94	0.13	33.29	47.01	0.02	16.42	0.36	0.00	99.16	82.34
18	PL28-19	megacryst	1.90	0.14	33.21	46.49	0.03	16.45	0.43	0.02	98.66	82.58
18	PL28-20	megacryst	2.21	0.15	32.53	47.42	0.03	15.83	0.41	0.00	98.58	79.74
18	PL28-20	megacryst	2.15	0.15	32.61	47.38	0.03	15.94	0.40	0.01	98.67	80.22
18	PL28-23	megacryst	2.23	0.13	32.30	47.47	0.02	15.71	0.36	0.00	98.21	79.46
18	PL28-23	megacryst	2.20	0.13	32.57	47.30	0.01	15.84	0.34	0.00	98.40	79.88
18	PL28-23	megacryst	2.25	0.16	32.63	47.29	0.00	15.95	0.39	0.00	98.67	79.66
18	PL28-24	megacryst	1.81	0.11	33.04	46.65	0.03	16.54	0.43	0.00	98.61	83.32
18	PL28-24	megacryst	2.17	0.13	32.33	47.19	0.02	15.94	0.41	0.00	98.18	80.20
16	PL28-10	lath	3.03	0.23	31.44	49.07	0.05	14.74	0.79	0.03	99.37	72.66
16	PL28-10	lath	2.95	0.64	30.56	49.66	0.05	14.23	1.14	0.02	99.24	72.50

**Microprobe analyses of minerals from Galapagos Platform -Dredge 28**

mount #	sample		Na	Mg	Al	Si	K	Ca	Fe	Ba	Total	An %
18	PL28-17	lath	2.99	0.24	30.74	49.45	0.04	14.19	0.89	0.03	98.56	72.20
18	PL28-17	lath	2.87	0.30	30.75	49.47	0.05	14.42	0.92	0.04	98.82	73.34
18	PL28-24	lath	2.94	0.16	31.38	49.08	0.04	14.44	0.81	0.00	98.85	72.93
18	PL28-24	lath	2.74	0.20	31.53	49.22	0.04	14.51	0.75	0.00	98.99	74.39
18	PL28-24	lath	3.14	0.28	29.98	50.32	0.03	14.07	0.99	0.01	98.80	71.13
18	PL28-24	lath	3.19	0.60	29.48	50.62	0.03	14.09	1.11	0.01	99.12	70.83
18	PL28-24	lath	3.25	0.36	29.92	50.52	0.04	14.00	0.93	0.00	99.02	70.21

**Olivine**

Mount#	Sample	Mg	Al	Si	Ca	Mn	Ni	Fe	Total	Fo
16	PL28-10	44.42	0.25	38.60	0.39	0.23	0.27	13.71	97.87	85.23
16	PL28-10	45.10	0.12	38.84	0.40	0.26	0.27	13.32	98.31	85.78
16	PL28-10	45.43	0.14	38.35	0.36	0.20	0.27	13.40	98.15	85.80

## **APPENDIX 5: Analyses of the BASL Standard**

The following table presents the results of analyzing the BASL basalt glass standard as an unknown during analysis of the PLUME2 pillow-rim glasses. Each analyses represents an average of five point analyses. Beam conditions are the same as those reported in Appendix 3.

<u>Date</u>	<u>SiO2</u>	<u>TiO2</u>	<u>Al2O3</u>	<u>FeO</u>	<u>MnO</u>	<u>MgO</u>	<u>CaO</u>	<u>Na2O</u>	<u>K2O</u>	<u>P2O5</u>	<u>Total</u>
3/2/90	50.94	4.06	12.49	13.30	0.15	5.08	9.30	2.66	0.82	0.38	99.18
3/2/90	51.03	4.04	12.34	13.27	0.19	5.07	9.25	2.61	0.88	0.45	99.11
3/2/90	50.90	4.12	12.34	13.23	0.22	5.07	9.20	2.56	0.89	0.46	98.99
3/2/90	51.02	4.34	12.39	13.49	0.17	5.12	9.29	2.61	0.87	0.46	99.76
3/2/90	51.13	4.48	12.44	13.56	0.17	5.10	9.24	2.60	0.89	0.52	100.13
3/2/90	50.89	4.40	12.40	13.53	0.20	5.04	9.35	2.62	0.87	0.48	99.78
3/2/90	51.01	4.04	12.57	13.56	0.21	5.10	9.40	2.59	0.88	0.43	99.90
3/6/90	50.83	4.06	12.59	14.04	0.21	5.09	9.36	2.60	0.88	0.47	100.13
3/6/90	51.06	4.12	12.66	14.16	0.25	5.01	9.37	2.55	0.88	0.44	100.49
3/6/90	49.43	4.31	12.43	14.01	0.19	5.07	9.32	2.57	0.86	0.44	98.62
3/6/90	51.33	4.04	12.55	14.25	0.18	5.05	9.35	2.60	0.89	0.45	100.68
3/6/90	50.95	4.09	12.48	13.75	0.21	5.08	9.39	2.64	0.85	0.42	99.85
3/6/90	50.75	4.15	12.46	13.81	0.19	5.02	9.29	2.61	0.87	0.46	99.61
3/21/90	51.06	4.06	12.45	13.13	0.21	5.01	9.35	2.63	0.84	0.45	99.17
3/21/90	50.82	3.92	12.43	13.15	0.21	5.03	9.38	2.59	0.83	0.50	98.86
3/21/90	50.90	3.97	12.56	13.16	0.22	5.05	9.38	2.59	0.84	0.44	99.11
3/22/90	50.82	3.99	12.55	13.03	0.19	5.01	9.34	2.57	0.85	0.41	98.76
3/22/90	51.09	4.00	12.47	13.07	0.20	4.95	9.25	2.51	0.82	0.45	98.80
3/22/90	50.87	3.97	12.59	13.06	0.19	5.03	9.37	2.64	0.84	0.49	99.05
3/22/90	51.08	4.01	12.51	12.95	0.20	5.04	9.38	2.60	0.83	0.45	99.06
3/22/90	51.08	4.05	12.56	13.04	0.22	5.02	9.38	2.63	0.82	0.43	99.22
3/22/90	50.99	4.01	12.51	13.00	0.19	5.02	9.33	2.63	0.85	0.43	99.05
3/22/90	51.12	3.94	12.51	13.12	0.22	5.04	9.29	2.64	0.83	0.48	99.20
3/22/90	51.06	3.93	12.46	13.00	0.20	5.03	9.25	2.56	0.83	0.46	98.78
3/22/90	50.76	3.93	12.45	13.06	0.20	5.01	9.31	2.62	0.85	0.46	98.65
3/22/90	51.14	3.90	12.61	13.05	0.23	4.94	9.29	2.61	0.82	0.48	99.07
3/22/90	50.95	3.85	12.42	13.08	0.18	5.05	9.33	2.68	0.86	0.51	98.91
3/22/90	50.33	3.88	12.45	13.21	0.22	5.01	9.20	2.63	0.83	0.46	98.23
3/22/90	51.09	3.89	12.43	13.05	0.19	5.11	9.28	2.59	0.84	0.45	98.93
3/22/90	51.09	3.90	12.49	13.01	0.22	5.00	9.33	2.62	0.81	0.44	98.92
3/22/90	50.88	3.94	12.41	12.98	0.19	5.11	9.26	2.66	0.86	0.42	98.72
3/22/90	50.98	4.25	12.48	13.12	0.22	5.06	9.27	2.59	0.84	0.45	99.26
3/22/90	51.01	3.94	12.46	12.95	0.21	5.04	9.30	2.57	0.83	0.49	98.80
3/23/90	50.98	4.11	12.54	12.97	0.20	5.02	9.43	2.57	0.83	0.44	99.09
3/23/90	50.67	4.02	12.58	13.30	0.23	4.96	9.35	2.56	0.84	0.45	98.95
3/23/90	50.23	4.10	12.48	13.10	0.20	4.87	9.41	2.59	0.83	0.45	98.26
3/23/90	50.01	4.03	12.64	12.86	0.22	4.81	9.36	2.63	0.84	0.48	97.87
3/23/90	50.73	3.93	12.55	12.74	0.21	4.93	9.37	2.55	0.83	0.43	98.26
3/23/90	49.86	3.84	12.34	12.96	0.20	4.77	9.42	2.60	0.85	0.49	97.32
3/23/90	50.58	4.03	12.50	12.92	0.20	4.93	9.37	2.60	0.84	0.45	98.41
3/23/90	50.12	3.91	12.48	13.00	0.22	4.91	9.38	2.56	0.84	0.46	97.88
3/23/90	50.40	3.98	12.49	13.07	0.24	4.93	9.37	2.56	0.82	0.45	98.31
3/23/90	49.39	3.92	12.41	13.12	0.24	4.88	9.41	2.58	0.82	0.45	97.22
3/23/90	50.62	3.85	12.60	12.89	0.20	5.00	9.36	2.45	0.81	0.41	98.19
3/23/90	49.33	3.99	12.48	13.19	0.20	4.89	9.34	2.61	0.84	0.43	97.30
3/23/90	50.33	3.91	12.57	12.92	0.21	4.87	9.43	2.53	0.82	0.44	98.03
7/10/90	50.89	4.07	12.43	13.37	0.21	5.03	9.31	2.66	0.85	0.45	99.27
7/10/90	50.94	4.06	12.49	13.08	0.21	5.02	9.29	2.62	0.82	0.47	99.01

<u>Date</u>	<u>SiO2</u>	<u>TiO2</u>	<u>Al2O3</u>	<u>FeO</u>	<u>MnO</u>	<u>MgO</u>	<u>CaO</u>	<u>Na2O</u>	<u>K2O</u>	<u>P2O5</u>	<u>Total</u>
7/10/90	50.87	4.01	12.45	13.27	0.21	5.03	9.40	2.58	0.81	0.49	99.12
7/10/90	50.99	4.06	12.39	13.06	0.21	5.01	9.37	2.62	0.84	0.43	98.96
7/17/90	50.96	3.99	12.50	13.37	0.17	5.14	9.13	2.59	0.84	0.43	99.10
7/17/90	50.60	3.97	12.45	13.38	0.19	5.05	9.20	2.72	0.83	0.43	98.82
7/17/90	50.95	4.02	12.51	13.29	0.17	5.03	9.25	2.62	0.81	0.44	99.08
7/17/90	50.87	3.97	12.50	13.33	0.20	5.03	9.28	2.64	0.86	0.46	99.13
7/17/90	50.69	4.05	12.44	13.24	0.17	5.03	9.27	2.61	0.83	0.46	98.78
7/17/90	50.91	4.07	12.46	13.17	0.19	5.02	9.15	2.66	0.80	0.48	98.92
7/17/90	50.82	3.93	12.41	13.10	0.18	5.02	9.27	2.63	0.79	0.47	98.62
7/17/90	51.02	3.99	12.48	13.24	0.18	5.09	9.20	2.63	0.80	0.47	99.10
9/19/90	50.88	3.92	12.63	13.14	0.21	5.1	9.04	2.7	0.86	0.42	98.89
9/19/90	50.84	4.04	12.47	13.26	0.2	5.06	9.29	2.62	0.87	0.42	99.05
9/19/90	51.04	3.91	12.57	13.34	0.17	5.13	8.98	2.63	0.82	0.46	99.05
9/19/90	50.87	3.89	12.51	13.26	0.19	5.09	8.95	2.69	0.87	0.50	98.82
9/19/90	50.61	3.90	12.54	13.34	0.19	5.11	9.40	2.60	0.85	0.49	99.03
9/19/90	50.72	3.89	12.57	13.23	0.22	5.12	9.33	2.67	0.86	0.44	99.05
9/19/90	49.46	3.93	12.48	13.27	0.17	5.11	9.44	2.63	0.84	0.52	97.85
9/19/90	49.82	3.96	12.49	13.22	0.20	5.14	9.45	2.67	0.85	0.45	98.25
9/20/90	50.79	4.05	12.45	13.20	0.18	5.12	9.31	2.67	0.84	0.49	99.09
9/20/90	51.01	4.08	12.42	13.31	0.19	5.07	9.29	2.66	0.85	0.48	99.36
9/20/90	51.02	4.08	12.49	13.45	0.20	5.01	9.32	2.64	0.86	0.42	99.49
9/20/90	50.61	4.02	12.42	13.40	0.20	4.99	9.30	2.66	0.84	0.46	98.89
9/20/90	51.04	4.05	12.47	13.45	0.20	5.11	9.30	2.48	0.86	0.47	99.42
9/20/90	50.89	4.10	12.43	13.47	0.19	5.06	9.31	2.67	0.85	0.49	99.45
9/20/90	50.98	4.05	12.40	13.35	0.21	5.04	9.31	2.73	0.85	0.46	99.39
9/20/90	51.03	4.07	12.60	13.41	0.19	5.03	9.32	2.64	0.84	0.42	99.57